PERTURBATIVE CALCULATIONS AND THEIR APPLICATION TO HIGGS PHYSICS

TOM J.E. ZIRKE

Dissertation zur Erlangung des Grades Dr. rer. nat.
vorgelegt von Dipl.-Phys. Tom J.E. Zirke

September 2014

Erster Gutachter:	Prof. Dr. Robert Harlander (Bergische Universität Wuppertal)
Zweiter Gutachter:	Prof. Dr. Stefan Dittmaier (Albert-Ludwigs-Universität Freiburg)

CONTENTS

LIST OF FIGURES

LISTINGS

ACRONYMS

BSM	beyond the Standard Model
CL	confidence level
DM	Dark Matter
DR	Dimensional Regularization
EW	electroweak
FDR	Four-Dimensional Regularization
HEP	High Energy Physics
IR	infrared
LEP	Large Electron-Positron Collider
LHC	Large Hadron Collider
LO	leading order
$\overline{\text{MS}}$	modified minimal subtraction
MSSM	Minmal Supersymmetric Standard Model
NLO	next-to-leading order
NNLO	next-to-next-to-leading order
N^3LO	next-to-next-to-next-to-leading order
NP	new physics
PDF	parton distribution function
QCD	Quantum Chromodynamics
QED	Quantum Electrodynamics

QFT	Quantum Field Theory
RGE	renormalization group equation
SM	Standard Model
SSB	spontaneous symmetry breaking
SUSY	Supersymmetry
UV	ultraviolet
2HDM	Two-Higgs-Doublet Model
VEV	vacuum expectation value

Part I

INTRODUCTION: THE HIGGS, THE LHC, AND THE TOOL BOX

In this introductory part we will briefly discuss motivations for studying Higgs Physics in general and more particularly at the Large Hadron Collider, as well as some theoretical concepts and tools needed to make predictions for observables in this context.

1 HIGGS PHYSICS

All known fundamental forces of nature — except for gravity — are described with remarkable precision by the Standard Model (SM) of particle physics:[1] the strong force, described by QCD based on the gauge group $SU(3)$, as well as the electromagnetic and the weak force, incorporated in a common electroweak theory [3] with initial $SU(2) \times U(1)$ gauge symmetry. Among these three forces the weak force has unique and especially interesting properties, which are highlighted in the first section.

1.1 PROPERTIES OF THE WEAK INTERACTION

Since the weak force is mediated by massive W and Z bosons, the corresponding generators of the gauge transformation must be broken at the scale of $M_Z \approx 91$ GeV. Explicit breaking would result in a non-renormalizable and, which is even more severe, unitarity-violating theory. As it is well known, this is solved in the SM by using spontaneous symmetry breaking (SSB) via the Higgs mechanism, where the gauge symmetry is not a symmetry of the vacuum state of the Higgs field. This brings along the prediction of the Higgs boson as a new massive, fundamental scalar particle, whose mass is however not predicted. Whether this mechanism was realized in nature was unclear until the discovery of a boson with a mass of about 125 GeV at the Large Hadron Collider (LHC)[2] that seems to have the properties of the Higgs boson within the current experimental limits.

Another unique feature of the weak interaction is inherent to its coupling to fermions. As opposed to the strong and electromagnetic interaction it is chiral, i.e. left and right-chiral fermions couple differently to W and Z bosons. As a consequence, fermion masses would break the gauge symmetry, too, so that also the chiral symmetry must be broken spontaneously by the Higgs field rather than explicitly. Thus each massive fermion should interact with the Higgs boson with the strength being proportional to its mass.

[1] It is assumed that the reader is familiar with the SM and the basics of Quantum Field Theory (QFT). For pedagogical introductions to the former see Ref. [1] and to the latter Ref. [2], for example.

[2] The LHC, located at the CERN site near Geneva, Switzerland, in a tunnel with a circumference of about 27 kilometers, is the largest particle collider in the world. During its first major run from 2010 to 2012, proton-proton collisions were studied at record-breaking 3.5 TeV and later 4 TeV per beam at the two multi-purpose detectors ATLAS and CMS. Currently, the LHC is shut down for maintenance and is scheduled to start operating at presumably 6.5 TeV per beam in 2015.

A closer look at the Yukawa couplings of the Higgs H to fermions fields ψ_i, given by

$$\mathcal{L}_{SM} \ni Y_{ij}\bar{\psi}_i\psi_j H, \tag{1.1}$$

reveals that it is not only the origin of the fermion masses but also of the mixing between the three generations, which shows up in charged-current interactions mediated by W bosons, and is therefore the basis for Flavor Physics, i.e. the description of phenomena where flavor quantum numbers are not conserved. Besides, this provides the only known source of CP violation in the SM.[3]

1.2 THE HIGGS AT THE LHC

Having pointed out the important theoretical role of the Higgs boson, let us now discuss its phenomenological properties with special regard to searches at the LHC. After a few general remarks on cross sections at hadron colliders, the main results for Higgs boson production and decay rates within the SM will be reviewed shortly, followed by a discussion of observations by the LHC experiments, both from the time of the discovery of the new boson in July 2012 and more recent results.

1.2.1 *Interlude: Hadronic Processes*

The basic quantities in High Energy Physics (HEP) experiments are count rates of particles, measured either as total rates or as functions of additional observables like energy, momentum, or charge of the detected particles. Such a rate can be written as

$$\frac{dN}{dt} = L \cdot \sigma, \tag{1.2}$$

where technical parameters of the experiment like the intensity of the beams are absorbed in the luminosity L and the physical properties of the system are contained in the cross section σ.

If the colliding particles are hadrons made up of partons, i.e. quarks and gluons, the calculation of the cross section is only possible using several steps of approximation. The first step consists in separating the soft physics that takes place at low energy and determines the structure of the hadron from the hard interaction that is responsible for the production of heavy particles. This is expressed in the factorization formula for hadronic cross sections,[4] which reads for the

[3] There is also the possibility of CP violation in the strong interaction (induced by the so-called θ term proportional to the contraction of the gluonic field-strength tensor and its dual), which has however not been observed yet. The puzzle why this term is absent or highly suppressed is known as the strong CP problem.

[4] For further reading see Chapter 7 of Ref. [4], for example.

production of a heavy particle C in the collision of hadrons of type A and B plus any hadronic final state X:

$$\sigma_{AB\to C+X}\left(\frac{M^2}{s}\right) = \sum_{i,j\in\{q,\bar{q},g\}} \int_0^1 dx_1 \int_0^1 dx_2\, f_{i/A}(x_1) f_{j/B}(x_2) \cdot \sum_{n\geqslant 0} \hat{\sigma}_{ij\to C+n\text{ partons}}\left(\frac{M^2}{\hat{s}}\right)\Bigg|_{\hat{s}=x_1x_2s}, \quad (1.3)$$

where $\sqrt{s}$ is the center-of-mass energy and M the mass of particle C, which is required to be much larger than Λ_{QCD}, the scale where the strong coupling α_S becomes of order one. The functions $f_{i/A}(x)$ are known as parton distribution functions (PDFs) and describe the probability density to find a parton i with a momentum fraction x within the hadron A. $\hat{\sigma}$ denotes the hard cross section on the parton level, which can be calculated in perturbation theory, i.e. as a series in powers of α_S, which is small only at sufficiently high scales. The PDFs have to be determined by fits to experimental data. Since in practice one can calculate only a finite number of terms in the perturbative expansion, this is another approximation.[5] Note that the center-of-mass energy relevant for the partonic process, given by $\sqrt{\hat{s}} = \sqrt{x_1x_2s}$, varies between M and $\sqrt{s}$. Thus hadron colliders actually probe a large spectrum of energies and are ideal for the discovery of new particles. Since the probability densities for the parton momentum fraction decrease rapidly, high partonic energies are strongly suppressed, however.

In fact, Eq. (1.3) still does not cover all the features of hadronic interactions. In reality also the final state involves hadrons instead of partons. Color-charged particles in the final state lose their energy by successively radiating off partons and finally form hadrons. This final-state radiation, and similarly initial-state radiation as well, can be taken into account by parton showers. They apply in an intermediate range, where perturbation theory is in principle still applicable, but truncating the series at a fixed order is no longer a good approximation.[6] The formation of hadrons is dominated by non-perturbative effects and can be described only by phenomenological models. Hard scattered partons show up in detectors as more or less localized bunches of hadrons, known as jets. Within perturbation theory one can at least specify the number of jets and roughly their kinematics, using so-called jet functions. In this thesis however, we restrict ourselves to inclusive quantities, where simply any additional hadronic final state is accepted.

[5] How one arrives at a series expansion for the hadronic cross section will be explained in the next chapter.

[6] For details see Ref. [5], for example.

1.2.2 *Higgs Production and Decay in the Standard Model*

In the following the most important results for Higgs boson production and decay rates within the SM are discussed.[7]

1.2.2.1 *Higgs Production*

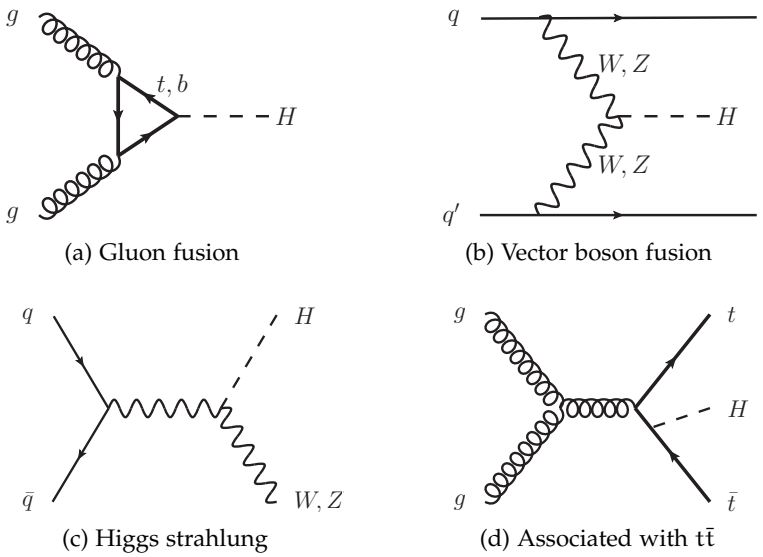

(a) Gluon fusion

(b) Vector boson fusion

(c) Higgs strahlung

(d) Associated with $t\bar{t}$

Figure 1: Important Higgs production channels at hadron colliders in the SM.

The most important production modes of a SM Higgs at hadron colliders are shown in Fig. 1 for the LHC at its latest center-of-mass energy of $\sqrt{s} = 8$ TeV. Since the strength of the interaction of a particle with the Higgs boson is proportional to its mass, all of these production channels involve heavy quarks or vector bosons, either solely as virtual particles or on their mass shell. In the so-called gluon-fusion mode shown in Fig. 1a, the Higgs couples to two initial gluons via a virtual heavy quark loop, where the largest contribution is from the top quark. The vector boson fusion and Higgs strahlung channels (see Figs. 1b and 1c, respectively) involve the Higgs coupling to vector bosons. In the former channel, the Higgs is radiated off a virtual vector boson exchanged between two incoming quarks, and in the latter off a vector boson produced by an annihilating quark-anti-quark pair. Associated production with a top-anti-top-quark pair is somewhat similar to gluon fusion, except that the top-quark line does not form a closed loop but is part of the final state.

In case of the LHC it turns out that the gluon fusion production mode has by far the largest cross section, as illustrated in Fig. 2. Al-

[7] For a detailed discussion of state-of-the-art results see Ref. [6].

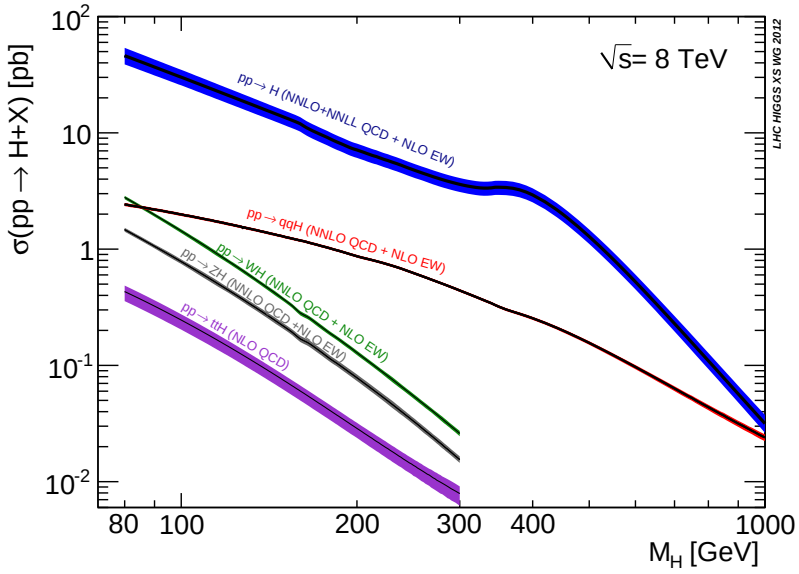

Figure 2: Production cross sections of the SM Higgs at the LHC with a center-of-mass energy of 8 TeV; from Ref. [7].

most over the complete mass range it is at least one order of magnitude larger than the vector boson fusion channel. At low values of M_H, Higgs strahlung is at the same order of magnitude as vector boson fusion, but decreases faster with increasing mass, so it is relevant for low to moderate Higgs masses only. The same is true for the associated production with a $t\bar{t}$ pair, whose cross section is almost another magnitude smaller than the one of Higgs strahlung.

1.2.2.2 *Higgs Decays*

Significant for the experimental sensitivity is the combination of the production and the subsequent decay of the Higgs. If the decay width Γ_H is small compared to the mass, it can be calculated simply as

$$\sigma_{pp\to H\to X} = \sigma_{pp\to H} \cdot BR_{H\to X} + \mathcal{O}\left(\frac{\Gamma_H}{M_H}\right), \tag{1.4}$$

where the branching ratio is defined in terms of the partial and total decay widths as

$$BR_{H\to X} := \frac{\Gamma_{H\to X}}{\Gamma_H}. \tag{1.5}$$

This is known as the narrow-width approximation.

In Fig. 3a the branching ratios for the individual decay channels for the Higgs boson are plotted as a function of M_H. The low mass range is dominated by the decay into a $b\bar{b}$ pair with a fraction of up to around 80%. At about 135 GeV $H \to WW^{(*)}$ takes the lead and reaches a fraction of almost 1 between $160 - 180$ GeV. It remains

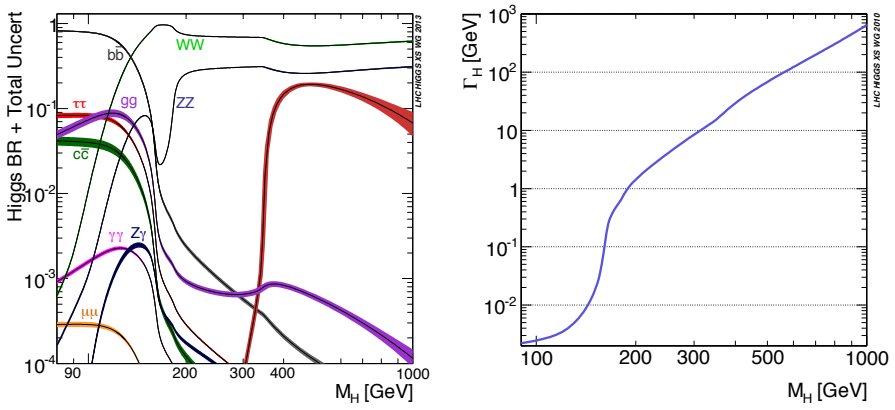

(a) (b)

Figure 3: Branching ratio (left) and total width (right) of the SM Higgs; from Ref. [7].

dominant in the high mass range, where the sub-leading channels $H \to ZZ$ and $H \to t\bar{t}$ reach fractions at the order of 10% each. The total decay width is shown in Fig. 3b. As a function of M_H it increases over several orders of magnitude as more and more channels open up. While for low masses $M_H \lesssim 150$ GeV it is below 10^{-2} GeV, it is at the order of M_H for high masses $M_H \gtrsim 500$ GeV.

1.2.3 *Higgs Search and Discovery*

Before the launch of the LHC the Higgs boson had escaped discovery for over 40 years since the postulation of the Higgs mechanism in 1964 [8, 9, 10, 11]. The experiments at LEP[8] had been able to set a lower limit on the Higgs mass of $M_H > 114.4$ GeV at 95% confidence level (CL) [12], and the Tevatron[9] was only beginning to become sensitive to signals of the Higgs. Thus the discovery of the Higgs was one of the main goals of the LHC.

As described above, the Higgs boson has a variety of production and decay modes. Deciding on which channel is the most sensitive, not only the branching ratio of a certain decay is important but also how well it can be distinguished from the background. Since the LHC is a hadron collider, hadronic final states usually suffer from large backgrounds. In addition, as already mentioned, these states show up

[8] The Large Electron-Positron Collider (LEP) was a particle collider at the CERN site located in the tunnel where today is the LHC. It was operated from 1989 to 2000, reaching a maximum center-of-mass energy of 209 GeV, and allowed to study the properties of W and Z bosons with high precision.

[9] The Tevatron was a circular proton-anti-proton accelerator located at Fermilab near Batavia, Illinois, and in operation from 1983 to 2011 with a maximum energy of about 1 TeV per beam. A great success was the discovery of the top quark in 1995.

as jets, whose energy cannot be determined to satisfactory precision. In contrast, leptons and photons allow for a better reconstruction of the energy and the momentum of the decayed particles so that cleaner signals can be expected.

For these reasons in the low mass range the obvious channel $H \to b\bar{b}$ is not suitable unless there are additional final state particles to help identify the signal. In the dominant production mode, gluon fusion, there are no such extra particles, so that the most significant channel is $H \to \gamma\gamma$, even though the corresponding branching ratio is at the order of 10^{-3}. The decays into vector bosons, which dominate for larger Higgs masses, can also provide clean signals, if the bosons decay leptonically, i.e $Z \to l^+l^-$ and $W \to l\nu$, where $l \in \{e, \mu\}$. In the case of W bosons, however there is the limitation that neutrinos cannot be detected directly, but only from the fact that the transverse momenta[10] of the other final state particles do not add up to zero, which brings in additional uncertainties.

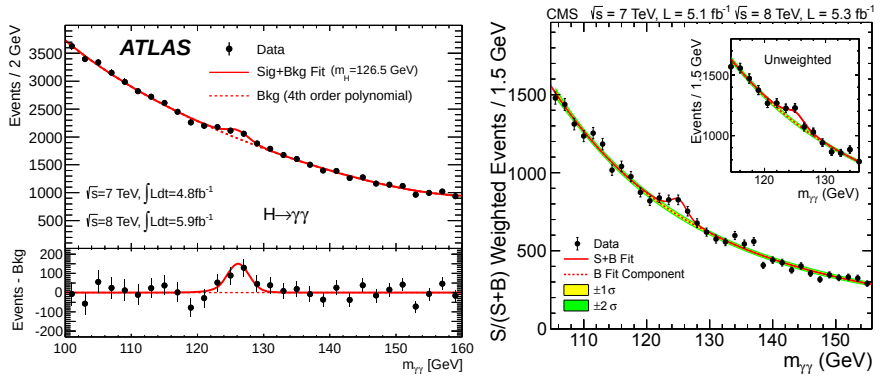

(a) (b)

Figure 4: $\gamma\gamma$ invariant mass spectrum published in July 2012 from ATLAS (left, from Ref. [13]) and CMS (right, from Ref. [14]).

On July 4^{th}, 2012, CERN announced the observation of a new particle, mainly due to a clearly visible resonance in the invariant mass spectrum of $\gamma\gamma$ pairs at about 126 GeV, observed by both ATLAS and CMS (see Fig. 4a and Fig. 4b, respectively). Combined with signals seen in other search channels, mostly from $H \to ZZ$, both experiments reported an excess large enough to claim discovery.

[10] The transverse momentum p_T is the projection of the momentum in the plane perpendicular to the beam axis. This is a useful quantity in collider physics, because the momentum component parallel to beam axis of the underlying partonic system is not known.

1.2.4 *Measuring Higgs properties*

After the discovery of the new boson the natural question to ask is whether it has all the properties of the SM Higgs or whether there are deviations on some level of precision. Its basic quantities fit: the predicted spin-parity of $J^P = 0^+$ is favored by the data [15, 16], and the observed mass of $M_H = 125$ GeV[11] is not too far away from the range around about 100 GeV expected by fits of electroweak precision data [19].

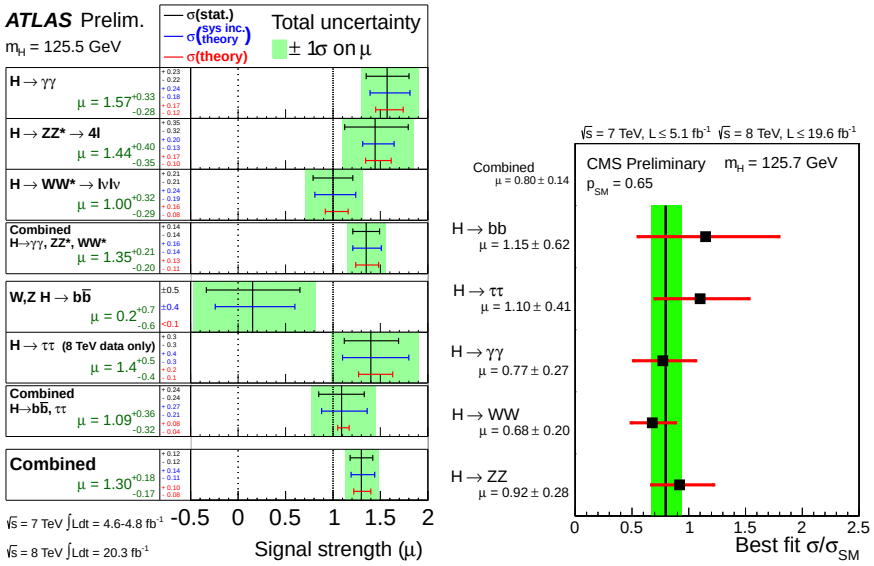

(a) (b)

Figure 5: Higgs signal strength with full 2011 and 2012 data from ATLAS (left, from Ref. [20]) and CMS (right, from Ref. [21]).

The next step is to go more into detail by comparing the observed signal to the SM prediction. Current results for the Higgs signals in various channels normalized to the SM expectation are shown in Fig. 5. Whereas there are mentionable deviations in individual channels the overall picture is consistent with the hypothesis that the new boson is the SM Higgs. On the other hand, there is still plenty room for extensions of the SM that involve a SM-like Higgs. Therefore, besides the ongoing search for further new particles, the investigation of all the available Higgs channels to the highest possible precision will be the top challenge for the next run of the LHC.

[11] The Higgs mass has already been determined with remarkably good precision. Using the channels with the best resolution $H \to \gamma\gamma$ and $H \to ZZ \to 4l$, ATLAS has measured $M_H = 125.36 \pm 0.37 \pm 0.18$ GeV [17] and CMS $M_H = 125.03^{+0.26}_{-0.27}{}^{+0.13}_{-0.15}$ GeV [18], where the former uncertainties are statistical and the latter systematic, respectively.

1.3 THE HIGGS AND NEW PHYSICS

Given the special role of the Higgs field and boson in the understanding of electroweak scale physics it does not come as a surprise that many ideas for beyond the Standard Model (BSM) physics are somehow related to Higgs physics, some of which shall be sketched in this section. This makes it worthwhile to understand the theoretical properties of the Higgs boson precisely — in the SM and beyond — to be able to find possible deviations from the SM when comparing to experimental results.

1.3.1 *Sensitivity to Higher Scales*

Although the SM is a self-consistent QFT (however not up to arbitrary scales, see below), it is clear that it cannot be fundamental from the mere fact that gravity is not included. Hence it makes sense to regard it rather as an effective theory with a limited range of validity up to some scale Λ_{NP}, where one expects new physics (NP) phenomena. Since the SM — extended by right-handed neutrinos — is successful in describing all known phenomena up to the electroweak scale, and effects of quantum gravity should become important at the Planck scale M_P at the latest, it must be $M_Z < \Lambda_{NP} < M_P$.

A well-known reason to believe that NP should exist not far above the electroweak scale is known as the *hierarchy problem* and due to the fact that the Higgs is a fundamental scalar. As is now established experimentally, the Higgs mass is at the electroweak scale. However, quantum corrections should actually drive the Higgs to higher scales because there is — in contrast to fermion and vector boson masses — no reason that these corrections have to be proportional to the mass itself, i.e. $\Delta M_H^2 \propto M_H^2$. If there is any large scale Λ entering the problem, there will be a term proportional to its square, and thus $\Delta M_H^2 \propto \Lambda^2$. This could be a cut-off scale introduced to regulate the ultraviolet (UV) divergencies of the theory[12] or, even if a regularization method without such a scale is used, the mass of a heavy particle that is part of a more complete theory coupling directly or indirectly to the SM particles. In any case, the Higgs mass is highly sensitive to physics at higher scales, which must exist at M_P at the latest, requiring the introduction of a fine-tuned counterterm to keep M_H small.[13]

A well-studied solution is to embed the SM into a *supersymmetric*[14] theory like the Minmal Supersymmetric Standard Model (MSSM), where every fermionic (bosonic) SM particle is related to a bosonic (fermionic) super-partner with – apart from the spin – identical quan-

[12] More on regularization of infinities in Section 2.2.

[13] This is explained well in Ref. [22].

[14] For a pedagogical introduction to Supersymmetry (SUSY) see Refs. [22] and [23], for example.

tum numbers. The corrections of particles and their super-partner to scalar masses (partly) compensate each other so that the quadratic sensitivity is canceled.[15] In other words SUSY can serve as a protective symmetry for the scalar masses as the chiral symmetry does for the fermion and gauge symmetry for vector boson masses.

It is clear that SUSY is not realized exactly in nature but broken at a scale M_{SUSY}, because no equal-mass super-partners of the SM particles are observed. As a consequence, one expects $\Delta M_H^2 \propto M_{SUSY}^2 + \cdots$. Hence M_{SUSY} should not be much larger than M_Z lest the fine-tuning problem reappears. However, no super-partners have been observed until now.

Another at least imaginable way out may be that there is no NP between the electroweak and the Planck scale and the coupling between the Higgs and gravity is such that it does not effect the Higgs mass for some reason we do not understand yet.

The sensitivity of the Higgs boson to higher scales can also have positive aspects. For example we know that there cannot be a fourth generation of the same kind because the production cross section for $gg \to H$ is independent of the quark mass running in the loop in the limit of very large masses[16] and the observed signal strength is in agreement with the three-generation SM.

Another even more speculative hint of a connection of the Higgs to higher scales comes from a very different direction, namely Neutrino Physics. From the observation of neutrino oscillations we know that neutrinos must have small but non-zero masses. This could be incorporated into the SM by simply introducing right-handed neutrino fields and Yukawa terms as for generating the masses of the up-type quarks. However, this does neither explain why neutrino masses are so small, nor is it known whether neutrinos are described accurately as Dirac fermions. Since they are electrically neutral and colorless they might as well be their own antiparticles, so they would have to be understood as Majorana fermions. If this is the case and we still insist that their masses be generated by the Higgs mechanism, we are forced to introduce a dimension-five operator to describe the interaction between the Majorana neutrino N and the Higgs field:

$$\mathcal{L} \ni \frac{y_N}{\Lambda} \bar{N} H H N. \tag{1.6}$$

Since this interaction is non-renormalizable it is valid up to the scale Λ, where it has to be replaced by a deeper theory.

However, as evidence of NP is still lacking, one may wonder what the maximum value for Λ is without running into consistency issues such as vacuum instability when the running quartic self coupling of

[15] For this cancellation it is essential that fermionic loops get a minus sign due to anti-commutation instead of commutation relations whereas bosonic loops do not and that the couplings of the super-partners are related by SUSY.

[16] cf. Section 4.2

the Higgs becomes negative so that the Higgs potential is no longer bounded from below. The answer to this question depends critically on the Higgs and the top quark mass. The larger the Higgs mass is, the larger the initial value for the Higgs self coupling must be and thus the larger is the scale where the vacuum becomes unstable and NP must occur at the latest. Recent next-to-next-to-leading order (NNLO) results [24] show that this coupling becomes negative between $10^8 - 10^{18}$ when the relevant parameters are varied by three standard deviations and that absolute stability up to the Planck scale is excluded for $M_H < 126$ GeV at 98% CL.

On the other hand, if unknown particles existed that couple strongly enough to the Higgs boson and are light enough, they would be visible in exotic decays. Weakly-interacting particles like Dark Matter (DM) candidates could be seen in invisible Higgs decays. Consequently the Higgs can be sensitive to physics below M_Z as well.

1.3.2 *Extended Higgs Sector*

NP could also be connected immediately to Higgs physics. It is well possible that there exists simply more than one Higgs multiplet. The central constraint on a possible extended Higgs sector is given by the ρ parameter [25], which is defined as

$$\rho := \frac{M_W^2}{\cos^2 \theta_w M_Z^2}, \tag{1.7}$$

where θ_w is the weak mixing angle. Since the experimental value is very close to unity,[17] this must be respected by possible extended theories.

It can be shown that only doublets and some exotic higher representations of $SU(2)$ are possible . The minimally possible extension is the Two-Higgs-Doublet Model (2HDM), where the assumed two Higgs doublets lead to five physical Higgs bosons. A phenomenological study of Higgs strahlung in the 2HDM will be given in Chapter 5. In supersymmetric extensions of the SM two Higgs doublets are required. Hence hints of the existence of additional Higgs bosons may be considered first hints that SUSY could be realized in nature.

[17] Deviations to unity can be understood as quantum corrections, which will be the subject of Section 8.3.

2 PERTURBATIVE CALCULATIONS

The goal of this chapter is to outline the basic concepts as well as some useful techniques and tools applied in this thesis in perturbative calculations for observables at hadron colliders. Besides, it also serves the purpose of fixing some notation for the main parts of this thesis.

2.1 MATRIX ELEMENTS FROM FEYNMAN DIAGRAMS

In the following the relation of cross sections to Feynman diagrams will be recapped.[1] To describe scattering processes in the framework of QFT the basis quantity to compute is simply the overlap of the final state f with the initial state i. In experiments the initial and final states are typically characterized only by the four momenta of the colliding and scattered particles and are represented in theory rather by asymptotic states with definite momenta in the distant past and future, respectively. If we consider the scattering of two particles A and B with momenta p_A and p_B to a final state of n particles with momenta $p_1, \cdots, p_n$, we can write

$$\langle f|i\rangle = \langle p_1, \cdots, p_n|\mathcal{S}|p_A, p_B\rangle, \tag{2.1}$$

which defines the so-called $\mathcal{S}$ *matrix*. It can be represented in terms of the interaction part of the Hamiltonian H_I as a Dyson series:

$$\mathcal{S} = T\exp\left[-i\int_{-\infty}^{\infty} dt\, H_I\right], \tag{2.2}$$

where T denotes the time-ordering operator. Using $H_I = -\int d^3x\, \mathcal{L}_I$, where $\mathcal{L}_I$ is the interaction part of the Lagrangian, this can be rewritten in a manifestly Lorentz invariant way:

$$\mathcal{S} = T\exp\left[i\int d^4x\, \mathcal{L}_I\right]. \tag{2.3}$$

We do not need all the information from $\mathcal{S}$. To separate configurations where initial and final states are the same, one introduces the $\mathcal{T}$ matrix, from which, in turn, one can factorize a delta function representing overall momentum conversation:

$$\mathcal{S} = 1 + i\mathcal{T}, \tag{2.4a}$$

$$\langle p_1, \cdots, p_n|i\mathcal{T}|p_A, p_B\rangle = (2\pi)^4\delta^{(4)}\left(p_A + p_B - \sum p_f\right) \cdot i\mathcal{M}(p_A, p_B, \{p_f\}). \tag{2.4b}$$

[1] This section is based on Ref. [2], in particular Chapter 4.

The relevant information on the scattering process is contained in the invariant *matrix element* $\mathcal{M}$.

As already mentioned in Section 1.2.1, the central observable we wish to compute is the cross section σ. Its differential $d\sigma$ is related to the absolute square of $\mathcal{M}$ in the case of n final state particles via

$$d\sigma = \frac{1}{F} |\mathcal{M}(p_A, p_B, \{p_f\})|^2 \, dPS_n(p_A + p_B), \quad \text{where} \tag{2.5a}$$

$$F = 2E_A 2E_B |v_A - v_B|, \tag{2.5b}$$

$E_{A,B}$ and $v_{A,B}$ denote energy and velocity of the colliding particles, respectively, and

$$dPS_n(P) = \left(\prod_f \int \frac{d^3 p_f}{(2\pi)^3} \frac{1}{2E_f} \right) (2\pi)^4 \delta^{(4)} \left(P - \sum_f p_f \right) \tag{2.6}$$

is the Lorentz-invariant n-particle *phase space*. The total cross section can be calculated by integrating over dPS_n:

$$\sigma = \int_n d\sigma \,. \tag{2.7}$$

It can be instructive to perform this integration only partially to obtain kinematical distributions and/or to restrict it to certain kinematical regions in order to increase the comparability to experimental results.

Another observable of interest for HEP is the decay rate Γ of an unstable particle. In analogy to Eq. (2.5) it is given by

$$d\Gamma = \frac{1}{2m_A} |\mathcal{M}(p_A, \{p_f\})|^2 \, dPS_n(p_A) \tag{2.8}$$

for the decay of a particle with mass m_A and momentum p_A into an n-particle final state.

The calculation of $\mathcal{M}$ is a major challenge. In perturbation theory it is obtained as an expansion of the right hand side of Eq. (2.3) in terms of small couplings using free-particle states defined in the unperturbed theory for the external particles in the evaluation of Eq. (2.1). This procedure is equivalent to calculating the corresponding Feynman diagrams based on the Feynman rules.[2] One can write:

$$i\mathcal{M}(p_A, p_B, \{p_f\}) \propto \sum_{\text{connected, amputated}} \begin{pmatrix} \text{Feynman diagrams} \\ \text{in momentum space} \end{pmatrix}. \tag{2.9}$$

Diagrams that are not fully connected contribute to the 1 in Eq. (2.4a), hence they are neglected. Amputating the diagrams means to cut off

[2] Unless stated otherwise, we will use the conventions of Ref. [2] throughout this work.

corrections to the external legs, which should not be regarded as part of the scattering process but rather of the external states transforming from the free to the interacting theory. This is stated precisely in the Lehmann-Symanzik-Zimmermann-reduction formula, which also fixes the constant in Eq. (2.9) as will be taken up later.

In this way one obtains a perturbation series for $\mathcal{M}$ in terms of the coupling constants. As we will calculate solely QCD corrections in this thesis, we will write only the dependence on the strong coupling g_s (or rather $\alpha_S = \frac{g_s^2}{4\pi}$) explicitly:

$$\mathcal{M} = \sum_{l \geqslant 0} \left(\frac{\alpha_{S,0}}{\pi}\right)^l \mathcal{M}^{(l)}. \tag{2.10}$$

The subscript 0 indicates that this is the bare coupling, which still has to be replaced by the measurable renormalized coupling. Accordingly, this yields a series expansion for the cross section, which we write as

$$\sigma = \alpha_{S,0}^k \sum_{l \geqslant 0} \left(\frac{\alpha_{S,0}}{\pi}\right)^l \sigma_0^{(l)}, \quad k \geqslant 0, \tag{2.11}$$

where we have factorized the dependence of the cross section on $\alpha_{S,0}$ at leading order (LO). Going to higher orders in the perturbative expansion increases the number and complexity of the diagrams that have to be evaluated dramatically as more and more closed-loop momenta have to be integrated over.

2.2 REGULARIZATION OF INFINITIES

The integrals over loop and final-state momenta often involve divergencies of different kinds. Loop integrations may exhibit singularities for large loop momenta (UV divergencies), small loop momenta (infrared (IR) divergencies) and integrable singularities at thresholds. Since final state momenta are naturally cut off by the available energy, integrating them can only induce IR divergencies. It is clear that infinities are acceptable only in intermediate terms and should cancel in physical quantities. To this end, they must be regulated in a consistent way to obtain an unambiguous result.

An obvious approach to regulate UV divergencies is to introduce an upper cutoff Λ on the loop momenta. This can be useful for certain considerations, e.g. to classify integrals according to their degree of divergency: If the result behaves like $\ln(\Lambda)$, it is called *logarithmically divergent* and in the case of polynomial behavior $\sim \Lambda^n$ *linearly, quadratically, etc. divergent*.

In practice, however, a different method has turned out to be most useful, namely *Dimensional Regularization (DR)*. It was introduced by 't Hooft and Veltman in 1972 [26] and is based on the observation that integrals can be made convergent if the number of space-time

dimensions is altered. For example, a logarithmically UV-divergent integral would be convergent in less than four dimensions.

On the integrand level, all momenta, or alternatively only loop momenta, are interpreted as d dimensional objects. The Dirac algebra has to be extended to d dimensions as well:

$$\{\gamma^\mu, \gamma^\nu\} = 2g^{\mu\nu}, \quad \mu = 0, \cdots, d-1. \tag{2.12}$$

Of course one cannot expect to find a four-dimensional representation for each d, but nevertheless the trace of the unit matrix is usually kept to be equal to four. Although the d-dimensional integral itself is only well-defined for positive integer d, its result is interpreted as the analytic continuation to arbitrary complex d. Then one can analyze the behavior close to four dimensions. Writing $d = 4 - 2\epsilon$, divergencies show up as poles of the form $\frac{1}{\epsilon^k}$, $k = 1, \cdots, 2L$, where L denotes the number of loops.

A conceptual advantage of DR is the fact that gauge symmetries are in principle respected, which is essential especially in the SM. As a consequence, for instance, it is ensured that Ward identities are valid during all steps of the calculation. A complication arises, however, if axial-vector or pseudoscalar currents are involved. This is because the continuation of γ_5, which is an intrinsically four-dimensional object, is problematic. The original proposition by 't Hooft and Veltman was to use

$$\gamma_5 = i\gamma^0\gamma^1\gamma^2\gamma^3, \tag{2.13}$$

which results in mixed commutation and anti-commutation relations:

$$\{\gamma^\mu, \gamma_5\} = 0 \qquad \mu = 0, 1, 2, 3, \tag{2.14a}$$

$$[\gamma^\mu, \gamma_5] = 0 \qquad \mu = 4, \cdots, d-1. \tag{2.14b}$$

An equivalent and more practical alternative we will pursue throughout this thesis is to write

$$\gamma_5 = \frac{i}{4!}\epsilon_{\mu\nu\rho\sigma}\gamma^\mu\gamma^\nu\gamma^\rho\gamma^\sigma \tag{2.15}$$

and to perform the contraction with the epsilon tensor after a finite result has been obtained so that one can safely return to $d = 4$. A good testing ground for consistency of the definition of γ_5 is the anomalous chiral symmetry breaking known as the ABJ anomaly [27]. While the result is correct at one-loop order, it has to be fixed by hand in multi-loop calculations [28].

The IR divergencies appearing in loop and phase-space integrations can be treated by DR as well. However, here the number of dimensions needs to be larger than four to arrive at a convergent integral. Despite of this, one can use DR for UV and IR divergencies at the same time.

Whereas we will use DR exclusively in the first main part of this thesis, from Chapter 6 on we will switch to Four-Dimensional Regularization (FDR), a recently introduced alternative approach.

2.3 RENORMALIZATION

A problem of quantum field theory is the fact that the relation between observable quantities and their theoretical correspondence is changed by the interaction of the theory itself, which is fixed in the renormalization procedure.[3] If this is possible with a finite number of renormalization parameters, as is the case for the SM, the theory is called renormalizable.

In perturbation theory, these parameters have to fixed be order by order. We write

$$X^{\text{bare}} = Z_X X, \tag{2.16a}$$

$$Z_X = 1 + \sum_{k=1}^{\infty} \left(\frac{\alpha_S}{\pi}\right)^k Z_X^{(k)} \tag{2.16b}$$

for the renormalization of a quantity X.

In QCD calculations, when DR is used, the modified minimal subtraction ($\overline{\text{MS}}$) scheme is common, where only the poles and a universal combination of $\ln(4\pi)$ and Gamma-Euler γ_E are subtracted. In this scheme the renormalization of the strong coupling g_s, for example, reads

$$Z_g = 1 + \frac{\alpha_S}{\pi}\left(\frac{4\pi\mu^2}{e^{\gamma_E}\mu_R^2}\right)^{\epsilon}\left(-\frac{11}{6}C_A + \frac{2}{3}T_R n_f\right)\frac{1}{4\epsilon} + \mathcal{O}\left(\alpha_S^2\right), \tag{2.17}$$

where $T_R = \frac{1}{2}$ and $C_A = 3$ are QCD color factors, and n_f denotes the number of active quark flavors. μ denotes the auxiliary scale introduced in the definition of the loop integrals (as for example in Section A.1.1), and μ_R is the renormalization scale.[4] Since the bare coupling does not depend on μ_R, the renormalized one will. The running of $\alpha_S = \frac{g_s^2}{4\pi}$ is determined by the renormalization group equation (RGE) obtained from evaluating

$$0 = \mu_R \frac{\partial}{\partial \mu_R} Z_g^2 \alpha_S. \tag{2.18}$$

The mass M of a particle is usually defined as the pole of the propagator when the momentum goes on-shell. The corresponding mass is known as the pole mass and for a quark is given by

$$Z_M^{\text{pole}} = 1 - \frac{\alpha_S}{\pi}C_F\left[\frac{3}{4\epsilon} + 1 - \frac{3}{4}\ln\left(\frac{M^2}{\mu^2}\right)\right] + \mathcal{O}\left(\alpha_{S,0}^2\right), \tag{2.19}$$

where $C_F = \frac{4}{3}$. The residue of the pole Z_2 is essential as well and identical to Z_m at this order. By definition the pole mass is independent of

[3] For this section see also Ref. [2].

[4] In the rest of this work we will consistently drop the $\ln(4\pi)$ and γ_E terms .

μ_R if expressed in terms of the renormalized coupling. However, since free quarks do not exist, it is doubtful whether this should be considered an observable quantity, especially for light quarks, or rather a parameter of the theory so that one might as well renormalize it in the $\overline{\text{MS}}$ scheme:

$$Z_M^{\overline{\text{MS}}} = 1 - \frac{\alpha_S}{\pi} C_F \frac{3}{4\epsilon} + \mathcal{O}\left(\alpha_S^2\right). \tag{2.20}$$

Analogously to the running of the coupling the $\overline{\text{MS}}$ mass will be scale dependent.

Gluons and massless quarks are massless to all orders thanks to gauge and chiral symmetry, respectively, so there is no mass parameter to be renormalized. However, the residue of the pole at momentum squared equals zero changes. For the on-shell renormalization of the gluon one has

$$Z_3 = 1 - \sum_q \frac{\alpha_S}{\pi} T_R \left[\frac{1}{3\epsilon} - \frac{1}{3} \ln\left(\frac{M_q^2}{\mu^2}\right)\right] + \mathcal{O}\left(\alpha_S^2\right), \tag{2.21}$$

where the sum is over all massive quarks. Massless quarks do not contribute at this order in α_S because the corresponding one-loop corrections to the gluon propagator are scaleless for vanishing external momentum and thus vanish in DR.[5] For the same reason it is

$$Z_2 = 1 + \mathcal{O}\left(\alpha_S^2\right) \tag{2.22}$$

for massless quarks.

Now we are ready to fix the constant in Eq. (2.9) to relate $\mathcal{M}$ to Feynman diagrams: For each external particle the square root of the residue from the corresponding on-shell renormalization, i.e. $\sqrt{Z_2}$ in case of a quark and $\sqrt{Z_3}$ in case of a gluon, has to be multiplied to the sum of diagrams.

As mentioned in the last section DR does not account for chiral symmetry properly beyond NLO. This can be compensated by a finite renormalization [28]:

$$Z_5^P = 1 - 2\frac{\alpha_S}{\pi} C_F + \mathcal{O}\left(\alpha_S^2\right), \tag{2.23a}$$

$$Z_5^A = 1 - \frac{\alpha_S}{\pi} C_F + \mathcal{O}\left(\alpha_S^2\right), \tag{2.23b}$$

which, if necessary, has to be included in $\mathcal{M}$ for the case of a pseudoscalar or axial-vector, respectively.

For color-charged external particles one should always sum over the color indices of final state particles and average over those of initial state particles. Since we will exclusively consider unpolarized cross sections in this work, we will do the same for the spin degrees

[5] This is a consequence of regulating IR and UV divergencies simultaneously in DR and not distinguishing the corresponding poles in ϵ.

of freedom, and denote the properly summed/averaged matrix element squared by $\overline{|\mathcal{M}|^2}$. Using this notation we arrive at the UV-finite, unpolarized cross section in terms of renormalized parameters as a series of α_S:

$$\begin{aligned}\sigma &= \frac{1}{F}\int \overline{|\mathcal{M}|^2}\mathrm{dPS} \\ &= \alpha_S^k(\mu_R)\sum_{l\geqslant 0}\left(\frac{\alpha_S(\mu_R)}{\pi}\right)^l \sigma^{(l)}(\mu_R).\end{aligned} \tag{2.24}$$

In principle σ is independent of μ_R. If, however, the series is truncated at a certain order N there will be a dependence on the renormalization scale proportional to α_S^{N+1}. Often the influence of higher order terms is estimated by the influence of varying the scale μ_R around a central value.

2.4 INFRARED SINGULARITIES

In general, the cross section (2.24) obtained from squaring the UV-renormalized matrix element can still contain IR divergencies from the integration over loop and phase-space momenta, indicating that it is not yet a proper observable.

For example configurations with and without an additional gluon in the final state cannot be distinguished in the limit where the gluon becomes soft, i.e. its energy vanishes. Such configurations have to be combined to obtain an IR-finite result. The amplitude for the emission of a soft gluon often tends to infinity, i.e. the phase-space integration diverges, which will be canceled by an IR divergency appearing in the integration over a closed loop involving an extra gluon. However, this cancellation is complete only if the gluon is radiated of a final state particle. Initial state radiation causes an additional complication as will be discussed in the following subsection.

Afterwards, we will discuss at the NLO level how the cancellation of IR divergencies between contributions with extra gluon radiation (real corrections) and those with an extra gluon propagator (virtual corrections) can be organized despite the fact that they appear at different stages of the calculation.

2.4.1 *Mass Factorization*

Now we specialize the discussion to hadronic cross sections.[6] Recalling Eq. (1.3), which more precisely reads

$$\begin{aligned}
&\sigma_{AB\to C+X}\left(\frac{M^2}{s}\right)\\
&= \sum_{i,j\in\{q,\bar{q},g\}} \int_0^1 dx_1 \int_0^1 dx_2\, f_{i/A}(x_1,\mu_F) f_{j/B}(x_2,\mu_F)\\
&\quad\cdot \sum_{n\geqslant 0} \hat{\sigma}_{ij\to C+n\text{ partons}}\left(\frac{M^2}{x_1x_2s},\mu_F^2\right),
\end{aligned} \tag{2.25}$$

where $\hat{\sigma}$ describes the hard scattering to produce the final state C of invariant mass $M^2 \ll \Lambda_{QCD}$ and $f_{i/A}(x)$ gives the probability to find a parton i within the hadron A carrying a fraction x of the momentum. Similarly as for the renormalization procedure, the factorization is defined at scale μ_F, the factorization scale, which we have omitted previously. Whereas the dependence on μ_F is given by the Alarelli-Parisi-splitting functions P_{ab} [30], which describe the probability for a parton b to emit or split into a parton a,

$$\mu_F \frac{\partial}{\partial\mu_F} f_{a/A}(x,\mu_F) = \sum_b \int_x^1 dy\, P_{ab}(y,\alpha_S(\mu_F)) f_{b/A}(x/y,\mu_F), \tag{2.26}$$

the initial conditions cannot be calculated from first principles and have to be determined from fits to experimental data.

The partonic cross section $\bar{\sigma}$ that is obtained from Feynman diagrams contains not only this hard scattering we are interested in, but also soft and collinear configurations[7] that cannot be treated in perturbation theory and have to be replaced by the proper low energy behavior. To this end one factorizes the renormalized partonic cross section as well, yielding

$$\begin{aligned}
&\bar{\sigma}_{ab\to C+\text{partons}}\left(\frac{M^2}{s}\right)\\
&= \sum_{i,j\in\{q,\bar{q},g\}} \int_0^1 dx_1 \int_0^1 dx_2\, \Gamma_{i/a}(x_1,\mu_F) \Gamma_{j/b}(x_2,\mu_F)\\
&\quad\cdot \sum_{n\geqslant 0} \hat{\sigma}_{ij\to C+n\text{ partons}}\left(\frac{M^2}{x_1x_2s},\mu_F^2\right),
\end{aligned} \tag{2.27}$$

[6] For this subsection see also Ref. [29].

[7] By soft configuration it meant that the energy of a massless external particle vanishes, and by collinear that the momenta of two such particles become parallel.

where Γ_{ij} are known explicitly in terms of the splitting functions, which in the $\overline{\text{MS}}$ scheme reads[8]

$$\Gamma_{ij}(x) = \delta_{ij}\delta(1-x) - \frac{1}{2\epsilon}\left(\frac{4\pi\mu^2}{e^{\gamma}\mu_F^2}\right)^{\epsilon}\frac{\alpha_S}{\pi}P_{ij}^{(0)}(x) + \mathcal{O}\left(\alpha_S^2\right), \quad (2.28)$$

and absorbs the remaining $\frac{1}{\epsilon}$ poles resulting from IR divergencies in $\bar{\sigma}$. One can solve Eq. (2.27) for the hard scattering cross section $\hat{\sigma}$ order by order in α_S, which yields a finite result that can be inserted in Eq. (2.25) to calculate the hadronic cross section. Whereas at LO $\bar{\sigma}$ and $\hat{\sigma}$ are identical, at higher orders convolutions involving splitting functions have to taken into account. We will not show this explicitly because in this thesis only the NLO cases will be required, which is included in the method discussed in the next subsection.

2.4.2 *Dipole Subtraction*

Up to NLO QCD the hard partonic cross section for an n particle final state can be written as

$$\hat{\sigma} = \hat{\sigma}^{\text{LO}} + \hat{\sigma}^{\text{NLO}}, \quad (2.29a)$$

$$\hat{\sigma}^{\text{LO}} = \int_n d\sigma^B, \quad (2.29b)$$

$$\hat{\sigma}^{\text{NLO}} = \int_n d\sigma^V + \int_{n+1} d\sigma^R + \int_n d\sigma^C, \quad (2.29c)$$

where $d\sigma^B$ denotes the differential Born cross section, proportional to the LO approximation of the matrix element squared for the desired final state, $d\sigma^V$ the virtual correction, obtained from the NLO term of the same (renormalized) quantity, $d\sigma^R$ the real corrections, given by the leading term of the matrix element squared involving an additional parton, and $d\sigma^C$ the collinear counterterm, accounting for the difference between $\hat{\sigma}$ and $\bar{\sigma}$ at NLO.

The idea of the subtraction method is to define a local counterterm $d\sigma^A$ that

- approaches $d\sigma^R$ in the peculiar soft and collinear limits so that $d\sigma^R - d\sigma^A$ is finite and thus integrable in four dimensions,
- can be integrated easily over the phase space of the additional parton so that $\int_1 d\sigma^A$ has born kinematics and explicitly cancels $\frac{1}{\epsilon}$ poles in $d\sigma^V$,
- and, ideally, is universal so that the analytical integration can be performed in full generality.

[8] As for $\overline{\text{MS}}$ renormalization we show the $\ln(4\pi)$ and γ_E terms only this once explicitly.

In formulas, this reads

$$\begin{aligned}\hat{\sigma} &= \int_n d\sigma^V + \int_{n+1} d\sigma^R + \int_n d\sigma^C\,, \\ &= \int_n \left(d\sigma^V + \int_1 d\sigma^A + d\sigma^C \right) \Big|_{\epsilon=0} \\ &\quad + \int_{n+1} \left(d\sigma^R \big|_{\epsilon=0} - d\sigma^A \big|_{\epsilon=0} \right). \end{aligned} \tag{2.30}$$

The remaining phase-space integrals can then be evaluated numerically.

A straight-forward way to find suitable universal counterterms systematically is the Dipole Subtraction method [31], where $d\sigma^A$ is given by

$$d\sigma^A = \sum_{\text{dipoles}} d\sigma^B \otimes dV_{\text{dipoles}}\,, \tag{2.31}$$

where $\otimes$ indicates connection in spin and color space in this case.

In the limit, where two partons i and j become collinear or one of them soft, the singular terms of the matrix element squared are shown to behave like the sum over dipoles

$$|\mathcal{M}_{n+1}|^2 \sim \sum_{k\neq,i,j} \mathcal{D}_{ij,k}, \tag{2.32}$$

where the sum is over all color-charged external particles other than i and j. The dipole $\mathcal{D}_{ij,k}$ is connected to a Born-like matrix element, where i and j are merged to a single parton in the presence of parton k, and a universal splitting operator $V_{ij,k}$. The momenta for this Born-like matrix element are expressed in terms of the $n+1$ original ones in such a way that momentum conservation holds and all transformed partons are on-shell. The counterterm $d\sigma^A$ is then constructed by adding up such dipole sums for every peculiar region of the phase space. Possible restrictions on the phase space have to be implemented separately for $d\sigma^R$ and $d\sigma^A$ in the evaluation of $\int_{n+1} d\sigma^R - d\sigma^A$ because they have to be applied to the transformed momenta in the case of $d\sigma^A$.

The piece that has to be added to the virtual corrections can be expressed as follows:

$$\int_{n+1} d\sigma^A + \int_n d\sigma^C = \int_n d\sigma^B \otimes (I + K + P). \tag{2.33}$$

The insertion operator I is connected to $d\sigma^B$ in spin and color space but has the same kinematics and cancels all the poles of $d\sigma^V$. The K and P terms are the finite remainders of the collinear counterterms and correspond to configurations where the momentum p of an initial state parton is replaced by xp. The momentum fraction x has to be integrated over in addition to the n particle phase-space integration.

2.5 ASYMPTOTIC EXPANSIONS

For multi-scale problems analytic expressions for amplitudes are often very hard to obtain at higher loop orders. In such cases it can be helpful to restrict oneself to certain limits, where for example one scale is larger than all the others. This can be systematically evaluated using the method of asymptotic expansions [32, 33].

We will restrict the discussion to the case of a large mass.[9] Suppose we are interested in the behavior of a Feynman integral in the limit where one internal mass M is larger than any other scale Λ, i.e. we seek for an expansion in $\frac{\Lambda^2}{M^2}$. The question is how one can reproduce this series by an expansion *before* the integration in order to simplify the calculation.

Since loop momenta can take arbitrary values, one generally cannot just expand all the propagators in terms of the large mass. Instead, the region where a loop momentum is smaller than or of the same order of the large mass have to be distinguished. The expansion of the propagators is then only performed with respect to quantities that are small. This does not yield a disjoint separation of the integration region but it can be shown that the remaining integrals combine to scaleless tadpoles that vanish in DR.

The procedure how to find the contributions of the different cases is most easily memorized graphically. Take a subgraph that contains at least all the lines involving the large mass, Taylor-expand the corresponding integral assuming all external momenta of the subgraph to be small, and insert the result into the remaining diagram, which is called co-subgraph and obtained by shrinking the lines of the subgraph to a point. The sum over all pairs of subgraphs and co-subgraphs will reproduce the correct asymptotic behavior in the limit where $\frac{\Lambda^2}{M^2}$ is small.

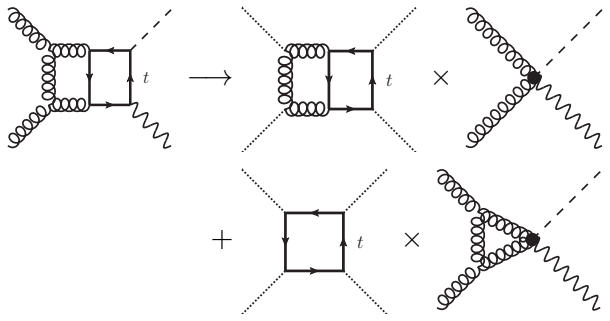

Figure 6: Asymptotic expansion of a double-box integral. The dotted lines indicate that the corresponding external momentum is assumed to be small in the expansion.

[9] For a detailed review see Ref. [34].

As an example Fig. 6 shows the expansion of a diagram we will need to evaluate in Chapter 4. Originally a five-scale problem, the calculation is simplified dramatically by taking the top-quark mass to be the largest scale of the problem. For the first term the complete diagram is taken to be the subgraph, i.e. both loop momenta are not smaller than M_t and only the external momenta are considered small. This results in a two-loop vacuum diagram, which poses only a one-scale problem, and a tree-level diagram. The second contribution is obtained by taking only the top-quark loop as subgraph. Expanding this subgraph in terms of the external as well as the loop momentum running through the gluon arc, leaves us with a one-loop vacuum integral. The corresponding co-subgraph is a massless one-loop diagram that depends on all the external momenta but on M_t.

2.6 PROGRAM SETUP

Performing the methods described in this chapter is complex and requires an efficient combination of suitable programs. In the following the default setup used for calculations throughout this work will be described briefly.

The first step is to find all the Feynman diagrams for a specific problem. For this task we use the program `qgraf` [35], which automatically generates all the (fully connected) diagrams for given in and out states at a certain loop order based on a model, i.e. the particle content and interaction structure of the theory. Further restrictions on the diagrams to be generated can be made, e.g. to eliminate corrections on external legs. Needless to say, this procedure has to be carried out separately for virtual and real corrections and in hadronic collisions for each partonic subchannel.

Next the package `q2e/exp` [36, 37] is run. The program `q2e` serves as an interface between `qgraf` and `exp`. On the one hand it assigns masses to the internal lines completing the topology information[10] on each graph. On the other hand it generates the mathematical expression belonging to each diagram by inserting the Feynman rules.

Then the program `exp` tries to match the diagrams to known topologies. If necessary, asymptotic expansions can be taken into account in order to break diagrams down to pairs of simpler sub- and co-subgraphs. The topologies to be used have to be specified in a specific topology selection file, including the information which topology shall be handled by which integration routine later on.

All subsequent analytic manipulations are performed using the computer algebra program `FORM` [38]. After evaluation of fermion traces, expansion of certain propagators in case of asymptotic expan-

[10] A certain topology is defined by the number of internal and external lines, the number of loops as well as the detailed distribution of masses and momenta.

sions, and possible further steps scheduled by the user, the corresponding integration routine is called depending on the topology.

After performing the asymptotic expansions one is often left with massive vacuum and massless diagrams as was described in the preceding section. The former can be treated with `MATAD` [39] for the case of one non-zero mass up to three loops. The complexity of the latter depends not only on the number of loops but also on the number of the external legs. Massless three-point integrals with one massive external leg up to two loops can be calculated with the program `mint` [40]. For massless one-loop integrals with up to four external legs, one or two of them massive, we have developed the routine `tribox`, which is presented in a bit more detail in Section A.1.4.

Part II

HIGGS STRAHLUNG AT THE LHC: STANDARD MODEL AND BEYOND

This part is about Higgs strahlung at the LHC. After a short introductory chapter, we will focus on two aspects: NLO QCD effects to the gluon-induced sub-channel $gg \to HZ$ and secondly a study of Higgs strahlung in a simple extension of the SM, namely the 2HDM, as an example of how NP could show up in this channel.

3

HIGGS STRAHLUNG AT THE LHC: INTRODUCTION

As pointed out in Chapter 1, after the discovery of a Higgs boson it is essential to learn about this particle as much as possible to understand whether it has all properties of the SM Higgs boson. This applies particularly to the various production and decay channels predicted by the SM, including the associated production of a Higgs boson with a weak gauge boson, i.e. $pp \to HV$, where $V \in \{W^{\pm}, Z\}$. Motivation to study this channel, which is also known as Higgs strahlung, in detail will be given in this chapter, supplemented by an overview of the various contributions to the cross section at higher orders in the strong coupling.

3.1 MOTIVATION

At the Tevatron $p\bar{p} \to HV$ with $H \to b\bar{b}$ was the most promising discovery channel for low Higgs masses.[1] At the LHC Higgs strahlung turns out to be harder to access experimentally because the expected signal-to-background ratio is smaller compared to other channels, however not hopeless. To improve this, it was proposed to consider HV production with a highly boosted Higgs boson [43], i.e. to require the transverse momentum of the Higgs to be large.

The main advantage that Higgs strahlung has to offer is the extra vector boson in the final state, which provides a clean signal if decaying into leptons. This allows searches for Higgs decays that will be impossible to see if the Higgs is produced alone.[2] The most important example is $H \to b\bar{b}$, but also generic BSM searches for exotic Higgs decays into invisible particles [44, 45], such as DM candidates, should be mentioned.

Recalling from Fig. 2 that the cross section for Higgs strahlung drops relatively fast with increasing Higgs mass, the low value of about 125 GeV is fortunate. Clearly SM searches for HV production will mostly use the dominant decay mode for this mass value, namely $H \to b\bar{b}$. Although experiments have only started to become sensitive to this channel,[3] prospects are good that Higgs strahlung may help to

[1] The latest analysis shows evidence for this channel with a local significance of 2.8 standard deviations at $M_H = 125$ GeV [41]. For the latest combination of Higgs searches at the Tevatron see Ref. [42].

[2] To be more precise: in association with soft jets only.

[3] Whereas CMS has already observed an excess of 2.1 standard deviations corresponding to a signal of 1 ± 0.5 times the SM expectation [46], ATLAS has only been able to set an upper limit on the cross section times branching ratio of 1.4 times the SM prediction (at 95% CL) for the $b\bar{b}$ channel [47].

complete the picture of the observed Higgs boson in the future. For this purpose precise knowledge of the cross section is essential. In Chapter 4 we will present a calculation of NLO QCD effects to a particular sub-channel to HZ production, which is intended to increase the reliability of the prediction for the cross section. In addition it is desirable to understand the possible impact of BSM physics. As an example for such NP effects, Chapter 5 will examine the influence of an extended Higgs sector on Higgs strahlung in the framework of the 2HDM.

3.2 CONTRIBUTIONS TO THE CROSS SECTION

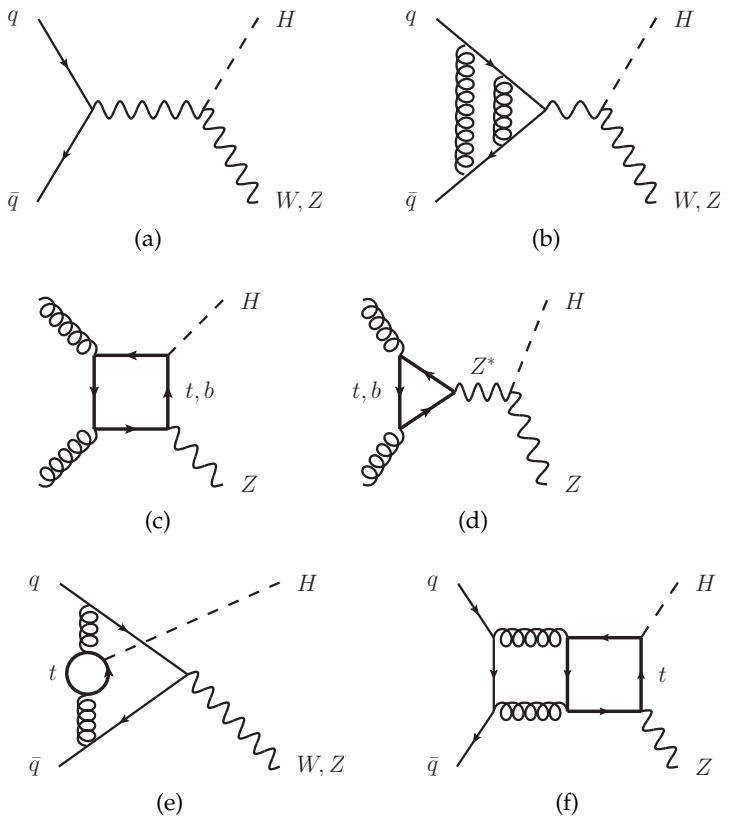

Figure 7: Exemplary Feynman diagrams for different contributions to HV production.

Example diagrams for the different contributions relevant in the SM are shown in Fig. 7. At LO, a quark-antiquark pair annihilates and produces a virtual vector boson, just like in the Drell-Yan process $pp \to V^*$, which then decays into an on-shell vector boson and a Higgs (see Fig. 7a). Since neither the vector nor the Higgs boson are color-charged, QCD corrections from diagrams like in Fig. 7b, for ex-

ample, do not affect the decay $V^* \to HV$ and can thus be reduced to those for the Drell-Yan process. One can write

$$\sigma_{HV,DY} = \int dq^2 \, \frac{d\Gamma_{V^*(q^2)\to HV}}{dq^2} \cdot \sigma_{pp\to V^*(q^2)+X}, \tag{3.1}$$

where q is the momentum of the intermediate vector boson. For this kind of contributions, NLO [48] and later NNLO results [49] (using the results of Ref. [50, 51]) were obtained, amounting to about 30% of the LO prediction for the total cross section.

Up to NLO QCD, only Drell-Yan-like contributions occur, but at NNLO new channels open up. The most important one is initiated by gluons that couple to a Higgs and a Z boson via a virtual heavy quark loop (see Figs. 7c and 7d) and were first studied in Ref. [52] and included in Ref. [49]. As these diagrams have no Drell-Yan correspondence, it is their squared sum which enters the cross section at order α_S^2. This term, denoted as σ_{ggHZ} in the following, contributes around 5% to the total cross section at the LHC, depending on the center-of-mass energy. The perturbative uncertainty induced by the dependence on the renormalization and factorization scale of this channel is relatively large, leading to a higher scale dependence of the total cross section of around 2% than with HW production, where it is below 1% [53]. This is the main motivation to study this particular contribution at NLO QCD [54], which will be presented in the following chapter.

Diagrams containing Yukawa couplings also exist with quarks in the initial state. Consider a quark-antiquark pair that annihilates to produce a vector boson involving a virtual or real gluon line with a quark-loop insertion. If the Higgs is radiated off the quark loop instead of off the vector boson, the diagram will not be Drell-Yan-like, as shown in Fig. 7e, for example. A mentionable effect should be expected from the heaviest quarks only, which is why we will restrict the discussion to top-quark loops in the following. In the case of HZ production, the Z boson, being electrically neutral, can as well be attached to the top-quark loop (see Fig. 7f). The interference of both types of diagrams with the corresponding tree-level Drell-Yan-type diagram yields a contribution to the cross section of order $\lambda_t \alpha_S^2$, which we label $\sigma_{\text{top I}}$ or $\sigma_{\text{top II}}$, respectively. These effects have been studied in Ref. [55] and shown to be at the order of 1-3% with respect to the LO contribution.

This completes the NNLO QCD contributions to Higgs strahlung. However, also NLO electroweak (EW) corrections are numerically important and decrease the total cross section by about 5-10% [56]. At NLO, EW effects can be assumed to factorize from the QCD corrections and written as a correction factor $1 + \delta_{EW}$ acting on the Drell-Yan

term [57]. Summing up all the contributions, the NNLO QCD + NLO EW prediction for the total cross section is given by

$$\sigma_{HV} = (1 + \delta_{EW})\,\sigma_{HV,DY} + \sigma_{\text{top I}} + \delta_{VZ}\left(\sigma_{ggHZ} + \sigma_{\text{top II}}\right), \quad (3.2)$$

as implemented in the public version of the program `vh@nnlo` [49, 58]. Effects of soft gluon resummation have been studied in Ref. [59] and are negligible for the total cross section, reinforcing the excellent behavior of the perturbative series for the Drell-Yan part. Differential results are available at NNLO QCD [60, 61] and NLO EW [62] as well.

3.3 THE HW/HZ RATIO

Having in mind primarily the Drell-Yan-like contributions (see Figs. 7a and 7b) with differences appearing only at NNLO, the following idea may sound surprising: The ratio $R_{WZH} := \frac{\sigma_{HW}}{\sigma_{HZ}}$ is possibly an interesting observable to search for deviations from the SM [63]. Indeed, any modification of the SM couplings that acts uniformly on the HWW and HZZ couplings will simply cancel in the ratio. However, two aspects should be kept in mind.

Firstly, the $gg \to HZ$ channel, which constitutes the major difference between the two sorts of Higgs strahlung, is far from marginal although it is an NNLO contribution. As we will see in Chapter 4, it receives large radiative corrections. Furthermore it is sensitive to quark Yukawa couplings (see Fig. 7c) as well as to the ZZH coupling (Fig. 7d) so that it behaves very differently from the Drell-Yan part in extended theories. We will elaborate on this in Chapter 5, where Higgs strahlung in the 2HDM will be studied and the ratio R_{WZH} will play a central role.

Secondly, the similarity of the HW and HZ channels could in fact turn out to be advantageous as systematic uncertainties cancel in the ratio. On the theoretical side, this should be the case for the uncertainties due to inexact knowledge of the PDFs and α_S. As an example for an experimental source of uncertainty that might be significantly reduced in the ratio one should mention the limited efficiency in the identification of b quarks stemming from the decay $H \to b\bar{b}$.

To sum up, the differences in HW and HZ production are more profound than one may think at first sight and can be quantified in the ratio R_{WZH}, which could turn out to be a valuable probe for deviations from the SM.

4

$gg \to HZ$ AT NEXT-TO-LEADING ORDER

In this chapter a study of NLO QCD effects in gluon-induced Higgs strahlung will be presented.[1] Since the exact determination of the virtual corrections requires the evaluation of massive double-box diagrams, which is hardly possible with current calculational tools, we restrict ourselves to the limit of infinite top-quark and vanishing bottom-quark mass. Technically the calculation in this effective theory is performed using the method of asymptotic expansions.[2] By this means the problem is reduced to the evaluation of one-loop, two-loop vacuum, and massless two-loop triangle diagrams. The latter can even be avoided by a suitable choice of gauge.

After motivating this study in the first section, we will start by discussing the details and consequences of employing the effective theory at LO in Section 4.2. Then we move on to NLO in Section 4.3, showing details of the evaluation of the virtual and real corrections as well as numerical results for the perturbative correction factor. Finally we conclude in Section 4.4.

4.1 MOTIVATION

As already mentioned in the previous chapter, the scale dependence of the $gg \to HZ$ contribution leads to a larger uncertainty on the cross section for HZ production compared to HW production. Since this contribution is separately gauge invariant as well as UV and IR-finite, one can think of it as an independent channel known only to LO accuracy rather than a piece of the NNLO calculation. Hence it makes sense to consider NLO QCD corrections to this channel, which are formally of the same order as next-to-next-to-next-to-leading order (N^3LO) corrections to the Drell-Yan terms, in order to arrive at an equally reliable prediction for HZ production. As discussed in Section 3.1, this is phenomenologically desirable to fully understand the properties of the new Higgs boson once enough data has been collected by the experiments at the LHC.

It is instructive to draw an analogy to the well-studied process $gg \to H$. There the perturbative correction factor (K factor) defined by

$$K^{N^nLO} := \frac{\sigma^{N^nLO}}{\sigma^{LO}}, \quad n = 1, 2, 3, \cdots, \tag{4.1}$$

[1] The ideas and results of this chapter have been published previously in Ref. [54].
[2] cf. Section 2.5

is large ($K^{NLO}_{gg\to H} \approx 2$) [64]. Notably, this is larger than expected from the scale uncertainty of the LO prediction. Only at NNLO the perturbative series stabilizes and the error bands overlap [51]. In view of the close similarity of the two processes,[3] which is manifest in the identical color structure and the fact that both are induced by heavy quark loops, there is thus good reason to believe that the corrections to $gg \to HZ$ may be similarly large, and that the error obtained from scale variation of the LO result may underestimate the effect of missing higher order corrections. Then, following this analogy, the NLO calculation should yield a more reliable result.

4.2 GENERAL STRATEGY AND LEADING-ORDER RESULTS

Since the process $gg \to HZ$ is loop-induced already at LO just as $gg \to H$, higher order calculations are especially challenging. As mentioned previously the calculation is simplified enormously by switching over to an effective theory obtained from taking the limit $M_t \to \infty$ and $M_b \to 0$. In this section we will explore this effective theory for $gg \to HZ$ at LO for a start. After motivating the optimal gauge for this task, we will discuss the behavior of the various contributions in this limit, followed by a numerical analysis of the LO cross section.

4.2.1 *Choice of Gauge*

In the context of electroweak symmetry breaking, one often chooses the physical or unitarity gauge, in which the Goldstone bosons are absorbed by the $W^\pm$ and Z bosons. Whereas this is helpful to understand that the theory indeed describes massive gauge bosons and also to prove the unitarity of the theory, different choices of the gauge can be useful in practical calculations. The Goldstone bosons then appear as virtual particles increasing the number of Feynman diagrams to be calculated. However, choosing a certain gauge may lead to ulterior simplifications. As we will discuss in the following, this is the case for $gg \to HZ$.

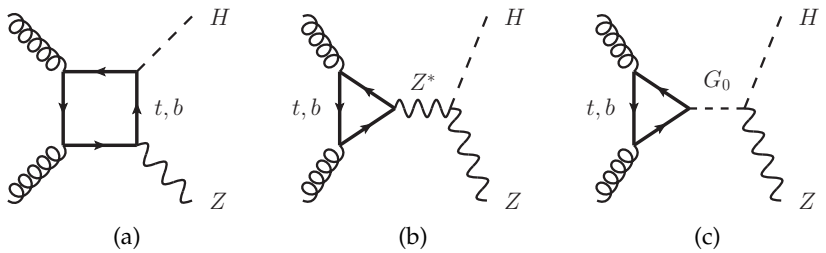

Figure 8: Leading-order Feynman diagrams for $gg \to HZ$.

[3] Compare the Feynman diagrams depicted in Figs. 1a and 7c.

In a general R_ξ gauge, one encounters three types of diagrams contributing to the amplitude for $gg \to HZ$ at LO as shown in Fig. 8. The first type are box diagrams (Fig. 8a). Since they involve the quark Yukawa coupling, only heavy quarks (t,b) have to be considered. The same is true for the triangle diagrams with an attached G_0 propagator (Fig. 8c), where G_0 denotes the neutral Goldstone boson that corresponds to the longitudinal degree of freedom of the Z boson, because the coupling of quarks and Goldstone bosons is proportional to the respective Yukawa coupling as well. Also in case of an intermediate off-shell vector boson (Fig. 8b) the light quarks (u,d,s,c) may be neglected in the triangle loops, but for different reasons. Due to Furry's theorem [65] the vector part of the $q\bar{q}Z$ coupling cancels in the sum of diagrams with opposite fermion number flow. The axial-vector part is proportional to the third component of the weak isospin and vanishes when summing over mass-degenerate isospin doublets.

One might think that the diagrams involving an intermediate vector boson should already be included in the Drell-Yan-like contributions given by Eq. (3.1). However, according to the Landau-Yang theorem [66, 67], the decay of a massive vector into two massless vector particles is forbidden, which applies to the reverse process as well, of course. Thus the amplitude for $gg \to Z^*(q^2)$ must vanish, because it corresponds to the on-shell production of a vector boson with mass $\sqrt{q^2}$.

This fact can be exploited to simplify the calculation of the $gg \to HZ$ amplitude. Note that the projector onto the transverse polarization modes of a vector particle with momentum q^μ is identical to polarization sum over the three (transverse and longitudinal) modes ε_i of an on-shell vector boson with same momentum and mass $\sqrt{q^2}$:

$$-g^{\mu\nu} + \frac{q^\mu q^\nu}{q^2} = \sum_{i=1}^{3} \varepsilon_i^\mu(q)^* \varepsilon_i^\nu(q). \tag{4.2}$$

As a consequence, the transverse modes of the Z propagator cancel when contracted with the sub-amplitude $gg \to Z^*$, and only the longitudinal part contributes. Recall that in a general R_ξ gauge the propagators of the Z and G^0 bosons read

$$D_Z^{\mu\nu}(q) = \frac{-i}{q^2 - M_Z^2}\left[g^{\mu\nu} + (\xi - 1)\frac{q^\mu q^\nu}{q^2 - \xi M_Z^2}\right], \tag{4.3a}$$

$$D_{G^0}(q) = \frac{i}{q^2 - \xi M_Z^2}. \tag{4.3b}$$

One can make the Z propagator purely transverse by going to Landau gauge ($\xi = 0$). Then the Z^* diagrams do not contribute at all and all the remaining diagrams involve the Yukawa coupling of the quark running in the loop.

4.2.2 *Effective Lagrangians*

Now we are ready to employ the limit $M_t \to \infty$ and $M_b \to 0$, which can be regarded as an effective theory where the Yukawa coupling of the bottom quark is set to zero and the top quark is integrated out. To understand what behavior should be expected in the limit of an infinite top-quark mass, let us first recall the situation for the process $gg \to H$. In that case one can use an effective Lagrangian

$$\mathcal{L}_{ggH} \propto G^a_{\mu\nu} G^{a,\mu\nu} H, \tag{4.4}$$

where G denotes the gluonic field strength tensor and the coefficient can be obtained by matching to the full theory in the limit $M_t \to \infty$. Hence it must be proportional to $g_s^2 \lambda_t = g_s^2 \frac{\sqrt{2} M_t}{v}$. Since the operator $G^a_{\mu\nu} G^{a,\mu\nu} H$ has dimension five, the matrix element for $gg \to H$ must involve an additional suppression factor $\frac{1}{M_t}$ in order for the matching to work out. For this reason one expects

$$\mathcal{L}_{ggH} = c_{ggH}(\alpha_S) G^a_{\mu\nu} G^{a,\mu\nu} \frac{H}{v}, \tag{4.5}$$

where $c_{ggH} \propto g_s^2$ is dimensionless and finite in the heavy-top limit.[4]

In view of Fig. 8 an effective theory for $gg \to HZ$ requires several terms, involving effective $ggHZ$, ggZ^*, and ggG_0^* vertices. One can write

$$\begin{aligned} \mathcal{L}_{ggHZ} = G^a_{\mu\nu} \tilde{G}^a_{\rho\sigma} \left\{ \left(c^{(1)}_{ggZ^*} + c^{(1)}_{ggHZ} \frac{H}{v} \right) \partial^\mu Z^\rho g^{\nu\sigma} + \cdots \right\} \\ + c_{ggG_0} G^a_{\mu\nu} \tilde{G}^{a,\mu\nu} \frac{G_0}{v}, \end{aligned} \tag{4.6}$$

where the ellipsis indicates other possible contractions between the vector fields. From parity considerations and the fact that the vector part of the $\bar{q}qZ$ coupling does not contribute, one sees that it is the dual $\tilde{G}^a_{\mu\nu}$ of the gluonic field-strength tensor that appears in the effective vertex. By a similar dimensional analysis as in the $gg \to H$ case we conclude

$$c^{(1)}_{ggZ^*} \propto g_s^2 g_w \frac{1}{M_t^2}, \tag{4.7a}$$

$$c^{(1)}_{ggHZ} \propto g_s^2 g_w \frac{1}{M_t^2}, \tag{4.7b}$$

$$c_{ggG_0} \propto g_s^2, \tag{4.7c}$$

i.e. in the heavy-top limit only the $t\bar{t}G_0$ coupling gives a non-zero contribution to the cross section. In practice, we will not explicitly use these coefficients but expand the diagrams in $\frac{1}{M_t}$ when applicable and then take the limit $M_t \to \infty$.

[4] Indeed one finds $c_{ggH} = \frac{1}{12} \frac{\alpha_S}{\pi} (1 + \mathcal{O}(\alpha_S))$. For the N^{3}LO result (i.e. to $\mathcal{O}(\alpha_S^4)$) see Ref. [68].

The massless-quark limit is easy to understand: If the Yukawa coupling of the bottom quark is set to zero, only the diagrams involving the $b\bar{b}Z$ vertex remain. As explained above, the contribution of the diagrams with a Z propagator vanishes in Landau gauge, so that in the end only top-quark loops have to be evaluated, which can be simplified by asymptotic expansion for the case of large M_t. At higher orders, this will still hold for virtual corrections, which have the same kinematical configuration, but not for real emission contributions, as will be discussed in detail in Section 4.3.

Finally, we give the expression for the LO amplitude in the effective theory, which reads

$$\mathcal{M}^{(0)} = \frac{\alpha_S \alpha}{\sin^2\theta_w \cos^2\theta_w M_Z} \delta^{ab} \epsilon^{\varepsilon_1 \varepsilon_2 p_1 p_2} \frac{p_H \cdot \varepsilon_Z^*}{\hat{s}}, \tag{4.8}$$

where $\alpha = \frac{e^2}{4\pi}$ is the electromagnetic coupling, a and b are the color indices of the gluons, $p_{1,2}$ their momenta, and $\varepsilon_{1,2}$ their polarization vectors, respectively, and we have defined $\epsilon^{vwxz} := \epsilon^{\mu\nu\rho\sigma} v_\mu w_\nu x_\rho y_\sigma$. Furthermore p_H denotes the momentum of the Higgs, ε_Z the polarization vector of the Z boson, and $\hat{s} := (p_1 + p_2)^2$ is the square of the partonic center-of-mass energy.

Performing spin and color sums (indicated by the bar over $|\mathcal{M}|^2$) and expressing α by the Fermi constant G_F via the relation

$$\alpha = \frac{\sqrt{2}\, G_F M_W^2 \sin^2\theta_w}{\pi}, \tag{4.9}$$

one obtains for the LO cross section

$$\begin{aligned} d\sigma^B &= \frac{1}{2\hat{s}} \overline{\left|\mathcal{M}^{(0)}\right|^2} dPS_2 \\ &= \left(\frac{\alpha_S}{\pi}\right)^2 \frac{G_F^2 M_Z^2}{256\,\hat{s}} \lambda(\hat{s}, M_H^2, M_Z^2) dPS_2, \end{aligned} \tag{4.10}$$

where

$$\lambda(x,y,z) = x^2 + y^2 + z^2 - 2xy - 2xz - 2yz \tag{4.11}$$

is the same function that appears in the two-particle phase-space element dPS_2 as given in Eq. (A.14). In the following subsection we will compare this to the full result, which can be calculated using the program `vh@nnlo`, for example.

4.2.3 *Numerical Consequences*

The effective theory with infinite top-quark and vanishing bottom-quark mass can be expected to be a good approximation if

$$M_b \ll \Lambda \ll 2M_t, \tag{4.12}$$

where Λ denotes any relevant scale of the process and $2M_t$ is the threshold for the on-shell production of a top-anti-top-quark pair. Regarding the mass values

$$M_b = 4.75 \text{ GeV}, \tag{4.13a}$$
$$M_Z = 91.1876 \text{ GeV}, \tag{4.13b}$$
$$M_H = 125 \text{ GeV}, \tag{4.13c}$$
$$M_t = 172 \text{ GeV}, \tag{4.13d}$$

this is obviously fulfilled if $\Lambda \in \{M_Z, M_H\}$. A problem arises for the partonic center-of-mass energy, i.e. for $\Lambda = \sqrt{\hat{s}}$, because in principle it is

$$M_H + M_Z \leqslant \sqrt{\hat{s}} \leqslant \sqrt{s}, \tag{4.14}$$

where $\sqrt{s}$ is of order 10 TeV. Whereas the condition $M_b \ll \sqrt{\hat{s}}$ is always met, $\sqrt{\hat{s}}$ can well be greater than $2M_t$. However, since especially the gluon PDFs fall off steeply with increasing momentum fraction, larger values of $\sqrt{\hat{s}}$ are suppressed and contribute less to the hadronic cross section.[5] Therefore one may hope that the region $\sqrt{\hat{s}} < 2M_t$, where the expansion in $\frac{1}{M_t}$ is valid, is dominant in the convolution.

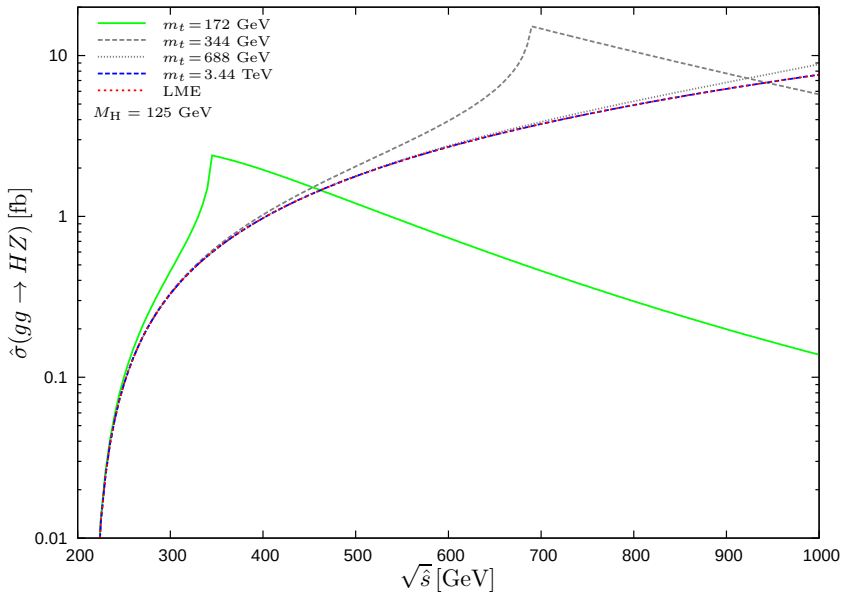

Figure 9: $gg \to HZ$ partonic cross section at LO for different finite values of the top-quark mass and in the heavy-top limit ("LME"); from Ref. [54].

To address this question quantitatively we will compare the LO cross section in the full and the effective theory in the following. As

[5] cf. Eq. (2.25)

numerical input we use the mass values from Eq. (4.13) unless stated otherwise as well as

$$M_W = 80.399 \text{ GeV}, \tag{4.15a}$$

$$G_F = 1.16637 \cdot 10^{-5} \text{ GeV}^{-2}. \tag{4.15b}$$

Hadronic cross sections are evaluated with `MSTW2008LO` PDF sets [69] using the running of α_S provided by the PDF routines. We take the renormalization and factorization scale to be equal to the invariant mass of the HZ system by default:

$$\mu = \mu_R = \mu_F = \sqrt{(p_H + p_Z)^2}. \tag{4.16}$$

Figure 9 compares the partonic cross section as a function of $\sqrt{\hat{s}}$ for different top-quark masses (and $M_b = 0$). First we note that, as expected, the full result approaches the one in the heavy-top limit (red short-dashed line) as the top-quark mass is increased for fixed value of $\sqrt{\hat{s}}$. For the realistic value of $M_t = 172$ GeV (green solid line), the heavy-top limit yields an acceptable result for $\sqrt{\hat{s}} \lesssim 300$ GeV. Around the threshold at $2M_t = 244$ GeV, the enhancement of the full cross section is not reproduced by the heavy-top limit, i.e. it underestimates the cross section in this region. Whereas the full result decreases monotonously above threshold, the heavy-top results still grows, overrating the cross section for $\sqrt{\hat{s}} \gtrsim 500$ GeV.

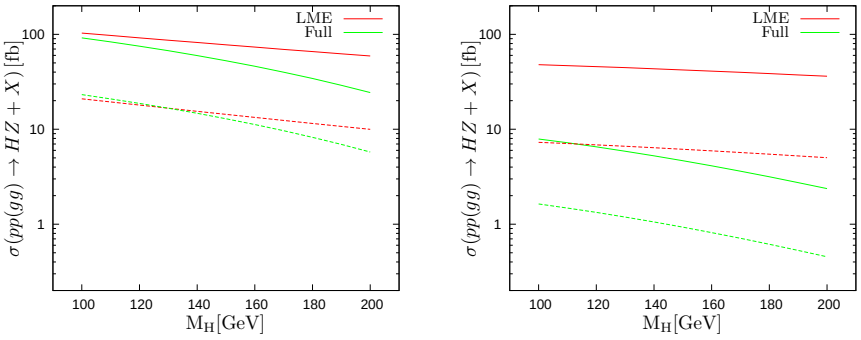

(a) Total cross section

(b) Boosted Higgs ($p_{T,H} > 200$ GeV)

Figure 10: LO hadronic cross section for finite ("Full") and infinite top-quark mass ("LME") at the LHC with $\sqrt{s} = 8$ TeV (dashed) and 14 TeV (solid); from Ref. [54].

In the hadronic cross section these competing effects should tend to average out, which is another reason to hope for the heavy-top limit to work reasonably in addition to the fact that the PDFs suppress higher values of $\sqrt{\hat{s}}$. For the total cross section presented in Fig. 10a as a function of the Higgs mass, this seems to be the case for not too large values of M_H. Not surprisingly, the agreement is better for

$\sqrt{s} = 8$ TeV (dashed lines) than for $\sqrt{s} = 14$ TeV (solid lines) because the probability that $\sqrt{\hat{s}}$ is in the window where the expansion in $\frac{1}{M_t}$ is expected to work, namely

$$M_H + M_Z \leqslant \sqrt{\hat{s}} \leqslant 2M_t, \tag{4.17}$$

decreases with increasing $\sqrt{s}$ as higher center-of-mass energies become less suppressed.

As already mentioned in Section 3.1, to increase the experimental sensitivity to Higgs strahlung at the LHC it is helpful to require the Higgs to be produced at high transverse momentum. For this purpose we consider a boosted scenario where $p_{T,H} \geqslant 200$ GeV. This is problematic for the validity of the heavy-top approximation because now it is

$$\hat{s} \geqslant M_H^2 + M_Z^2 + 2p_{T,H}^2 + 2\sqrt{(M_Z^2 + p_{T,H}^2)(M_H^2 + p_{T,H}^2)}, \tag{4.18}$$

so that the energy window (4.17) is further diminished.[6] Hadronic results for this scenario are shown in Fig. 10b. It appears that the hadronic cross section is already dominated by the region above the $t\bar{t}$ threshold, where the heavy-top limit yields too large results.

To sum up, mass effects are not negligible in the $gg \to HZ$ cross section, but perturbative corrections are potentially large. As long as the NLO calculation including the full mass dependence is out of reach, a compromise is to determine the K factor in the effective theory but to include the LO mass dependence, i.e. to make the approximation

$$\begin{aligned}\sigma^{\text{NLO}}(M_t, M_b) &= \sigma^{\text{LO}}(M_t, M_b)\, K^{\text{NLO}}(M_t, M_b) \\ &\approx \sigma^{\text{LO}}(M_t, M_b)\, K^{\text{NLO}}(M_t \to \infty, M_b = 0).\end{aligned} \tag{4.19}$$

This procedure is known to work well for the $gg \to H$ process as long as one considers the inclusive cross section [70] or not too large values of $p_{T,H}$ in differential distributions [71, 72] and has also been applied to Higgs pair production [73]. However, one cannot expect this strategy to work equally well for $gg \to HZ$ as for $gg \to H$, especially in the boosted scenario, because the convergent region is smaller, and there are regions where $\sqrt{\hat{s}} \geqslant 2M_t$ even if no or only soft extra partons are present in the final state. Unfortunately, it would most likely not be helpful to include higher order terms in the expansion in $\frac{1}{M_t^2}$, at least not if the region where $\hat{s} \ll 4M_t^2$ is dominant, which is why we stick to the strict limit $M_t \to \infty$. In the following section details on the NLO calculation in the effective theory will be discussed.

4.3 NEXT-TO-LEADING ORDER CALCULATION

To regulate the IR divergencies occurring in the calculation of the NLO cross section we use the dipole subtraction method [31] sketched

[6] See also the discussion in Ref. [63].

in Section 2.4.2. There are three different kinds of contributions to the hard partonic cross section $\hat{\sigma}^{\mathrm{NLO}}$:

- regularized virtual corrections,

$$\int_2 \left(\mathrm{d}\sigma^{\mathrm{V}} + \mathrm{d}\sigma^{\mathrm{B}} \otimes \mathrm{I} \right), \tag{4.20}$$

- real corrections minus dipoles,

$$\int_3 \left(\mathrm{d}\sigma^{\mathrm{R}} - \sum_{\text{dipoles}} \mathrm{d}\sigma^{\mathrm{B}} \otimes \mathrm{dV}_{\text{dipoles}} \right), \tag{4.21}$$

- and finite remainder terms from mass factorization,

$$\int_2 \mathrm{d}\sigma^{\mathrm{B}} \otimes (\mathrm{P} + \mathrm{K}), \tag{4.22}$$

  which involve an additional integration over the momentum fraction left after radiation of a collinear parton.

In the next two subsections we will discuss the calculation of the virtual and real corrections in detail. Afterwards numerical results for the hadronic cross section will be presented. To this end for each of the three kinds of integrals the required integrations including the convolution with the PDFs are combined and evaluated using the adaptive Monte-Carlo algorithm `Vegas` [74]. Suitable parametrizations of the two and three-particle phase space are given in Section A.2.1 and Section A.2.2, respectively.

4.3.1 *Virtual Corrections*

Typical diagrams that need to be evaluated for the virtual corrections are shown in Fig. 11. Apart from genuine two-loop diagrams obtained by inserting virtual gluon lines into the LO diagrams (Figs. 11a to 11e), there are diagrams where the H and Z bosons couple to the gluons via separate quark loops (Fig. 11f), and which can hence be reduced to a product of two one-loop diagrams. In both cases it is the interference with the LO amplitude that contributes to $\mathrm{d}\sigma^{\mathrm{V}}$.

As explained in Section 4.2, the diagrams with a Z propagator (Fig. 11c and 11d) vanish when working in Landau gauge. All remaining diagrams are simplified by asymptotic expansions[7] so that only massive one-loop and two-loop vacuum and massless one-loop diagrams need to be evaluated. This can be performed automatically by using the setup described in Section 2.6.[8] Since, however, within this

[7] cf. Section 2.5

[8] In Ref. [54] this setup was used in one of two independent calculations of the virtual corrections.

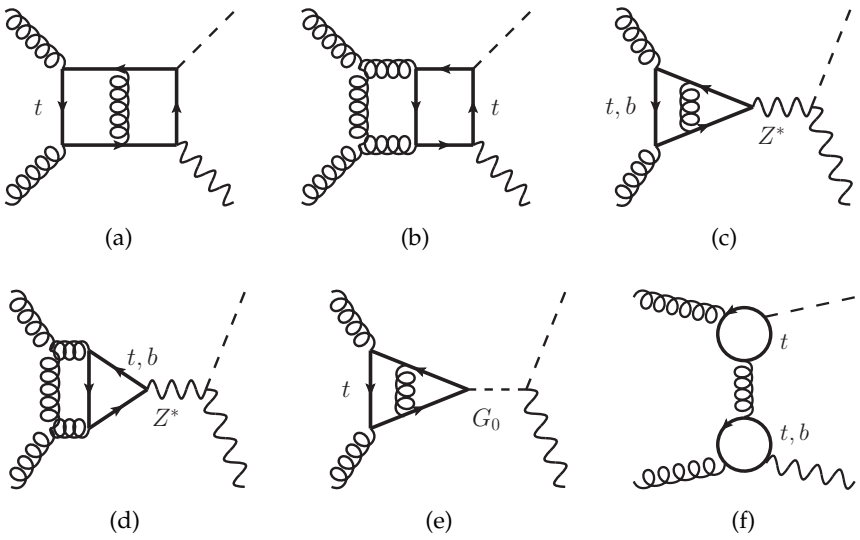

Figure 11: Virtual correction diagrams for $gg \to HZ$.

setup the massless two-loop three-point integrals resulting from the bottom quark loops of Figs. 11c and 11d can be evaluated automatically with the program `mint` [40], we perform the calculation in the unitarity gauge[9] as well. Then the Goldstone bosons disappear and the virtual contributions are completely given by the bottom-quark loops in the effective theory. This provides an excellent check of the calculation.

There are two ingredients to Eq. (4.20). The first one is the UV-renormalized virtual correction given by

$$d\sigma^V = 2\,\mathrm{Re}\left\{\mathcal{M}^{(1)}\left(\mathcal{M}^{(0)}\right)^*\right\}, \tag{4.23}$$

where $\mathcal{M}^{(0)}$ and $\mathcal{M}^{(1)}$ are the LO and NLO terms of the renormalized matrix element expanded in terms of $\frac{\alpha_S}{\pi}$ with the renormalized coupling α_S, which is related to the bare coupling by Eq. (2.17). We will comment on the renormalization procedure below. The second one is the part of the integrated dipoles that has the same kinematics as the Born term. Using the formulas of appendix C of Ref. [31] one obtains for the case of two initial state gluons and a colorless final state

$$\begin{aligned} d\sigma^B \otimes I = d\sigma^B \cdot \frac{\alpha_S}{\pi}\left(\frac{\mu^2}{\hat{s}}\right)^{\epsilon}\left(1-\frac{\pi^2}{12}\epsilon^2\right) \\ \cdot\left[C_A\left(\frac{1}{\epsilon^2}-\frac{\pi^2}{3}\right)+\left(\frac{1}{\epsilon}+1\right)\left(\frac{11}{6}C_A-\frac{2}{3}T_R n_l\right)\right. \\ \left.+\left(\frac{67}{18}-\frac{\pi^2}{6}\right)C_A-\frac{10}{9}T_R n_l\right], \end{aligned} \tag{4.24}$$

[9] The unitarity gauge is obtained from the general R_ξ gauge by letting $\xi \to \infty$ so that the Z propagator contains all three polarization modes (cf. Eq. (4.3)).

where $n_l = 5$ is the number of light quarks and we have set $\mu = \mu_F = \mu_R$. The sum of these two terms is finite in four dimensions and given by

$$d\sigma^V + d\sigma^B \otimes I = \left[1 + \frac{\alpha_S^{(5)}(\mu)}{\pi}\left(\frac{164}{9} + \frac{23}{6}\ln\left(\frac{\mu^2}{\hat{s}}\right)\right)\right] d\sigma^B + d\sigma^{red}, \tag{4.25}$$

where we have inserted the $SU(3)$ color factors $C_A = 3$, $C_F = \frac{4}{3}$, and $T_R = \frac{1}{2}$. The contribution $d\sigma^{red}$ from reducible diagrams of the type of Fig. 11f reads

$$\begin{aligned} d\sigma^{red} = {} & dPS_2 \left(\frac{\alpha_S}{\pi}\right)^3 \frac{G_F^2}{768\,\hat{s}} \frac{1}{\hat{s} - M_Z^2} \\ & \cdot \Big\{ \left(\hat{s} M_Z^2 M_H^2 + \hat{s} M_Z^4 - \hat{s}^2 M_H^2 - 2\hat{s}^2 M_Z^2 + \hat{s}^3\right) \\ & \quad \cdot \left(-2 + \ln\left(\frac{-\hat{u}}{M_Z^2}\right)\frac{M_Z^2}{\hat{u} - M_Z^2} + \ln\left(\frac{-\hat{t}}{M_Z^2}\right)\frac{M_Z^2}{\hat{t} - M_Z^2}\right) \\ & + \left(-\hat{s} M_Z^2 M_H^2 + \hat{s} M_Z^4 + \hat{s}^2 M_H^2 - 2\hat{s}^2 M_Z^2 + \hat{s}^3\right) \\ & \quad \times \left(\frac{-M_Z^2}{\hat{t} - M_Z^2} + \frac{-M_Z^2}{\hat{u} - M_Z^2} + \ln\left(\frac{-\hat{u}}{M_Z^2}\right)\frac{M_Z^4}{(\hat{u} - M_Z^2)^2} \right. \\ & \qquad \left. + \ln\left(\frac{-\hat{t}}{M_Z^2}\right)\frac{M_Z^4}{(\hat{t} - M_Z^2)^2}\right) \Big\}, \end{aligned} \tag{4.26}$$

where $\hat{t} = (p_1 - p_Z)^2$ and $\hat{u} = (p_1 - p_H)^2$.

We conclude the discussion of the virtual corrections by a few remarks about the renormalization procedure:

- Since chiral symmetry is not broken correctly in DR at higher orders in perturbation theory as discussed in Section 2.3, we have to renormalize the pseudoscalar or axial-vector current appearing in Fig. 8c and Fig. 8b by relation (2.23a) or (2.23b), respectively, depending on whether we work in Landau or unitarity gauge.

- In Landau gauge, the LO amplitude contains a factor of $M_t^{-2\epsilon}$, which yields a finite correction independent of the renormalization scheme chosen for M_t, i.e. Eqs. (2.19) and (2.20) give the same result.

- The on-shell renormalization of the external gluons given by Eq. (2.21) introduces a logarithmic dependence on the top-quark mass, which can be eliminated by expressing the results through the coupling $\alpha_S^{(5)}$ defined for five active flavors, where the top-quark is completely decoupled and the limit $M_t \to \infty$ can be

performed. It is connected to $\alpha_S^{(6)}$ with six flavors by the matching relation [75]

$$\alpha_S^{(5)}(\mu) = \alpha_S^{(6)}(\mu)\left[1 - \frac{\alpha_S^{(6)}(\mu)}{6\pi}\ln\left(\frac{\mu^2}{M_t^2}\right) + \mathcal{O}\left(\alpha_S^2\right)\right]. \tag{4.27}$$

In addition this is necessary to be consistent with current PDF sets, which use five active flavors.

4.3.2 *Real Corrections*

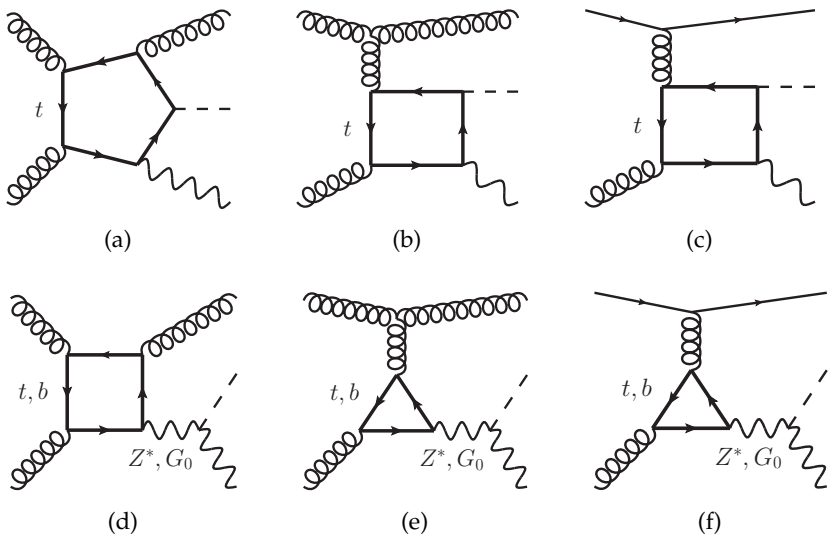

Figure 12: Real emission diagrams for $gg \to HZ$.

The real emission corrections to $gg \to HZ$ are obtained by attaching external gluon lines to the LO diagrams and calculating the absolute square of the sum for each partonic subchannel. Figure 12 shows exemplary diagrams, where it is understood that crossed diagrams have to be considered as well.

Again we find that the diagrams where the Higgs is coupled directly to the quark loop (Figs. 12a to 12c) vanish in the limit $M_t \to \infty$, $M_b \to 0$. In contrast to the virtual corrections, the transverse polarization modes of the Z propagator do not vanish, so that bottom-quark loops, which cannot be simplified by asymptotic expansion, have to be evaluated in the diagrams of types 12d to 12f. The most complicated ones are the box diagrams 12d. Furry's theorem does not simplify matters much because the color structure is not symmetric when the orientation of the loop is changed. If a, b, and c denote the color indices of the three gluons and t^a representation matrices of $SU(3)$,

summation of loops with opposite fermion number flow yields a contribution proportional to

$$\mathrm{Tr}[t^a t^b t^c] \pm \mathrm{Tr}[t^c t^b t^a] = T_R \cdot \begin{cases} d^{abc} \\ i f^{abc} \end{cases}, \tag{4.28}$$

where $+$ applies to the vector and $-$ to the axial-vector part of the $\bar{q}qZ$ coupling. Thus the vector part contributes as well, proportional to the symmetric factor d^{abc}. The axial-vector part receives an antisymmetric factor of f^{abc}. However, it is at least obvious that the vector-axial-vector interference is identical to zero. The four vector particles make the tensor reduction of the loop integrals algebraically quite complex. Within our default setup this task is performed by the routine `tribox`.[10,11]

Upon squaring the amplitude we project on physical gluon polarizations by using a general axial gauge for the external gluons defined with respect to arbitrary light-like vectors n_j ($j = 1, 2, 3$):

$$\sum_{i=1}^{2} \varepsilon_i^{\mu,a}(p_j)^* \varepsilon_i^{\nu,b}(p_j) = \delta^{ab} \left(-g^{\mu\nu} + \frac{p_j^\mu n_j^\nu + p_j^\nu n_j^\mu}{p_j \cdot n_j} \right). \tag{4.29}$$

As expected we find that the result is independent of all n_j, which provides a good check on the calculation. The results for the real emission amplitude are too lengthy to be printed here.

The integration over the three-particle phase space leads to IR divergencies that are canceled by the corresponding dipole terms. Note that the diagrams contributing to the $gg \to HZg$ channel (Fig. 12e) can be subdivided into s, t, and u channel diagrams.[12] Whereas the s channel contribution is finite, we need one dipole each for the t and u channels, which we calculate using the formulas for the case of two initial-state hadrons given in Section 5.5 of Ref. [31]. Similarly, the qg and gq channels (Fig. 12f and crossed diagrams) require one dipole each, while the $q\bar{q}$ channel does not.

4.3.3 *Numerical Results*

Finally we present numerical results for the $gg \to HZ$ cross section at NLO evaluated according to Eq. (4.19). For this purpose we take the same numerical input as in Section 4.2.3 except that `MSTW2008NLO` PDFs are used for NLO quantities.

Figure 13a illustrates the absolute results for the total cross section at LO and NLO for $\sqrt{s} = 8$ TeV and $\sqrt{s} = 14$ TeV as well as the NLO correction factor as a function of the Higgs mass. The same quantities are

[10] Details are given in Section A.1 of the appendix.

[11] This method was used in one of three independent calculations of the real corrections in Ref. [54].

[12] More precisely the corresponding gluon propagators are $\frac{1}{s}$, $\frac{1}{t_3}$ and $\frac{1}{u_3}$ as defined in Eq. (A.31).

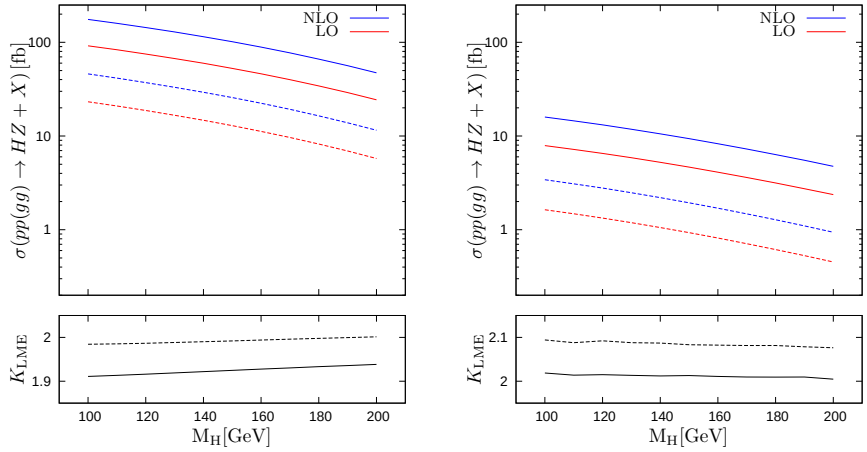

(a) Total cross section (b) Boosted Higgs ($p_{T,H} > 200$ GeV)

Figure 13: LO (lower, red lines) and NLO (upper, blue lines) hadronic cross section (top) and K factor (bottom) at the LHC with $\sqrt{s} = 8$ TeV (dashed) and 14 TeV (solid); from Ref. [54].

shown for the boosted scenario defined by requiring $p_{T,H} > 200$ GeV in Fig. 13b. As expected from the analogy to $gg \to H$, we find huge K factors of around two, where the correction is a bit larger for 8 TeV than for 14 TeV.

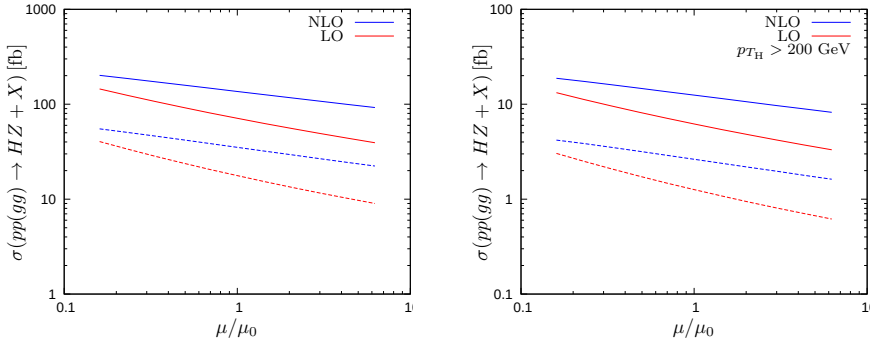

(a) Total cross section (b) Boosted Higgs ($p_{T,H} > 200$ GeV)

Figure 14: Scale dependence of the LO and NLO hadronic cross section for $M_h = 125$ GeV at the LHC with $\sqrt{s} = 8$ TeV (dashed) and 14 TeV (solid), where $\mu_R = \mu_F = \mu$ and $\mu_0 = \sqrt{(p_H + p_Z)^2}$; from Ref. [54].

The dependence of the $gg \to HZ$ cross section on the factorization and renormalization scale as they are varied simultaneously around the central scale $\mu_0 = \sqrt{(p_H + p_Z)^2}$ is depicted in Fig. 14 for $M_H = 125$ GeV, again for the total cross section (Fig. 14a) and for the boosted scenario (Fig. 14b). Both at LO and NLO level the cross section de-

creases monotonously as the scale is increased where the slope is visibly reduced at NLO. When $\frac{\mu}{\mu_0}$ is altered between $\frac{1}{6}$ and 6, σ^{LO} varies by about 100% and σ^{NLO} by about 60% with respect to the central value. As anticipated from the analogy to $gg \to H$, the error band obtained from varying the scale in the LO cross section in an interval $[\frac{1}{2}\mu_0, 2\mu_0]$ or even $[\frac{1}{3}\mu_0, 3\mu_0]$ does not cover the true size of the NLO corrections. However, the variation of the NLO prediction — in an interval $\mu \in [\frac{1}{3}\mu_0, 3\mu_0]$ to be on the safe side — should be a more reliable estimated of missing higher order corrections.

4.4 CONCLUSION

We have considered NLO contributions to gluon-induced HZ production. The correction factor was evaluated in the limit of infinite top-quark and vanishing bottom-quark mass and found to be about two, similarly as in gluon-induced Higgs production.

Since the $gg \to HZ$ channel previously contributed about 5% to the total HZ cross section, the latter is roughly increased by another 5% if the newly evaluated corrections are included. The absolute uncertainty on the total cross section from the scale variation of the $gg \to HZ$ contribution is not reduced but even slightly increased, however, indicating that it was grossly underestimated before. For updated numbers the reader is referred to Refs. [54] and [6]. The new corrections have also been implemented in an updated version of the program `vh@nnlo`.

5

HIGGS STRAHLUNG: FROM SM TO 2HDM

In this chapter a study of Higgs strahlung in the 2HDM will be presented.[1] We start by summarizing basic properties of the 2HDM in the first section before discussing the behavior of the different contributing to Higgs strahlung in the transition from the SM to the 2HDM in Section 5.2. Section 5.3 presents numerical results for exemplary scenarios before we conclude in Section 5.4.

5.1 THE TWO-HIGGS-DOUBLET MODEL

As already mentioned in Section 1.3.2, the Higgs mechanism of the SM could in principle involve several Higgs multiplets, where the simplest extension contains two doublets and is known as the 2HDM.[2]

The vector-boson masses are generated in the 2HDM analogously to the SM but they now receive contributions from the vacuum expectation values (VEVs) of the neutral components of both doublets. The well-known value of $v = \frac{1}{\sqrt{\sqrt{2}G_F}} \approx 246$ GeV for the VEV is shared between the two,

$$v^2 = v_1^2 + v_2^2, \tag{5.1}$$

and one defines

$$\tan\beta = \frac{v_2}{v_1}. \tag{5.2}$$

Since the two Higgs doublets contain eight degrees of freedom but only three of these are absorbed as longitudinal degrees of freedom of the weak vector bosons, the 2HDM predicts five physical particles in the scalar sector. Two of these fields are electrically charged, which we denote by $H^\pm$. If CP conservation is assumed as we do throughout this study, two of the three electrically neutral Higgs bosons will be CP-even and one CP-odd. The CP-even states mix with a mixing angle α and form the two physical states h and H^0, where $M_h < M_{H^0}$, which are referred to as the light and heavy Higgs boson, respectively. Finally, the CP-odd or pseudoscalar state is named A.

We assume not only CP conservation but also no flavor-changing neutral currents at tree level. Then 2HDMs can be split into four different classes according the fermion Yukawa couplings. Since in this study exclusively the quark Yukawa couplings are used, only two

[1] The ideas and results of this chapter have been published previously in Ref. [63].
[2] For reviews see Refs. [76] or [77], for example.

types yield different results. Whereas in the 2HDM of type I both up-type and down-type quarks couple to the same Higgs doublet similarly as in the SM, the masses of the down-type quarks are generated by the other doublet in case of type II. Note that in the MSSM, the structure of the Yukawa sector (without the SUSY partners) is identical to the type II 2HDM, except that SUSY puts additional constraints of the couplings and masses.

The Higgs boson discovered at the LHC with a mass of about 125 GeV is usually interpreted as the light boson h in the context of the 2HDM. The other bosons are then assumed to have escaped detection so far, for example because they have higher masses. Under this assumption, the properties of the observed boson allow to employ constraints on a possibly realized 2HDM.[3]

5.2 THEORY OF HIGGS STRAHLUNG IN THE 2HDM

In the 2HDM there are more varieties of Higgs strahlung than in the SM, which we summarize as ϕV production, where $\phi \in \{h, H^0, A\}$ and $V \in \{W^\pm, Z\}$, i.e. we restrict the discussion to neutral Higgs bosons.[4]

We express the required couplings of ϕ relative to the corresponding ones of the SM Higgs. For the vector bosons it is

$$\langle \phi VV \rangle : \quad i g^{\mu\nu} g_{\phi VV} \frac{e M_V^2}{\sin\theta_w M_W}, \tag{5.3}$$

where $g_{HVV} = 1$ in the SM. The relative couplings are functions of α and β, for example $g_{hVV} = \sin(\beta - \alpha)$. Note that in the limit $\sin(\beta - \alpha) \to 1$ the coupling of the h boson to the vector bosons becomes SM-like.

Similarly we write for the Yukawa couplings

$$\langle \phi f\bar{f} \rangle : \quad -\frac{M_f}{v} g_{\phi,f} \begin{cases} \gamma_5, & \phi = A \\ i, & \phi \in \{h, H^0\}. \end{cases} \tag{5.4}$$

The type II 2HDM offers the possibility of an enhancement of the bottom with respect to the top Yukawa coupling. Since it is

$$\begin{aligned} g_{h,u}^{\text{Type I}} &= g_{h,d}^{\text{Type I}} = g_{h,u}^{\text{Type II}} \\ &= \frac{\cos\alpha}{\sin\beta} = \sin(\beta-\alpha) + \cos(\beta-\alpha)\frac{1}{\tan\beta}, \end{aligned} \tag{5.5a}$$

$$g_{h,d}^{\text{Type II}} = -\frac{\sin\alpha}{\cos\beta} = \sin(\beta-\alpha) - \cos(\beta-\alpha)\tan\beta, \tag{5.5b}$$

[3] Many studies have analyzed experimental data by scanning the parameter space for allowed or excluded regions, see Refs. [78, 79, 80], for example.

[4] For older studies of associated production of scalar neutral Higgs and Z bosons in the context of the MSSM see Refs. [81] and [82], and for the pseudoscalar case Refs. [83, 84, 85, 86, 82].

this is the case for the light Higgs h if $\tan\beta$ is large and $\cos(\alpha-\beta)$ is not too small.

In the following we will discuss the steps required to generalize the SM prediction for the Higgs strahlung cross section as summarized in Eq. (3.2) to the 2HDM. To this end it is not only necessary to rescale the SM couplings but also to take new diagrams into account. We will also comment on the corresponding modifications in our program `vh@nnlo`.

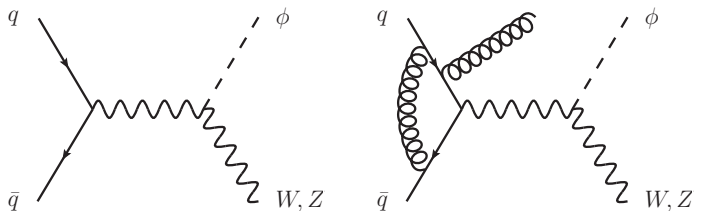

Figure 15: Feynman diagrams for Drell-Yan-like contribution to $qq \to \phi V$.

The Drell-Yan-like contributions, for which example diagrams are shown in Fig. 15, are easily generalized to the 2HDM. Since only the decay $V^* \to \phi V$ is modified, one simply has

$$\sigma_{\phi V,\mathrm{DY}} = g^2_{\phi VV}\,\sigma_{\mathrm{HV,DY}}. \tag{5.6}$$

This holds also to higher orders in α_S, so the result calculated by the corresponding subroutine of `vh@nnlo` can simply be multiplied by $g^2_{\phi VV}$. For the electroweak corrections this is not true, which is why we neglect them in this study.

The top-quark induced terms $\sigma_{\text{top I}}$ and $\sigma_{\text{top II}}$ share this simple scaling behavior neither. In contrast to the SM, the bottom Yukawa coupling is not always negligible as it may be enhanced in certain scenarios. However, these terms are known only in the heavy-top limit and the result including the full mass dependence seems out of reach with current calculational tools because massive two-loop four-point integrals (see Figs. 7e and 7f) are involved. As the heavy-quark limit is unacceptable for the bottom quark, we discard these terms in view of the fact that they only contribute a few percent to the total cross section in the SM.

The most profound and interesting changes take place in the gluon-induced channel depicted in Fig. 16. Not only do the different diagrams that are present in the SM scale differently because they involve either a Yukawa (see Fig. 16a) or the ϕZZ coupling (Fig. 16b), but also new diagrams come into play where the intermediate Z^* boson is replaced by one of the other neutral Higgs bosons ϕ' (Fig. 16c). A combination (ϕ, ϕ') is allowed if one of the bosons is CP-even and the other CP-odd. Depending on the choice of the 2HDM parameters,

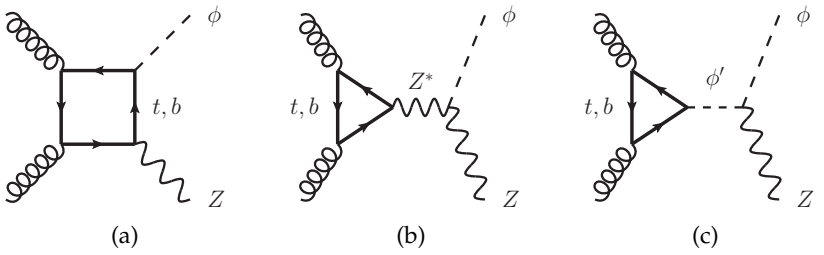

Figure 16: Feynman diagrams contributing to $gg \to \phi Z$ channel.

it is possible that $M_{\phi'} > M_\phi + M_Z$ so that the ϕ' propagator is on the mass shell if $\sqrt{\hat{s}} = M_{\phi'}$. This resonance is regulated by the total width $\Gamma_{\phi'}$ of the intermediate boson ϕ', which we introduce by the replacement

$$\frac{1}{\hat{s} - M^2_{\phi'}} \to \frac{1}{\hat{s} - M^2_{\phi'} + iM_{\phi'}\Gamma_{\phi'}}. \tag{5.7}$$

The implementation of the $gg \to HZ$ contribution in `vh@nnlo` has not only been extended to include these s channel contributions but completely renewed on the basis of `FeynArts/FormCalc` [87, 88] and designed in such a way that physical parameters can be more easily varied. Note that we include $gg \to \phi Z$ at LO only because the influence of the bottom Yukawa coupling on the NLO correction factor for $gg \to HZ$ is unknown.

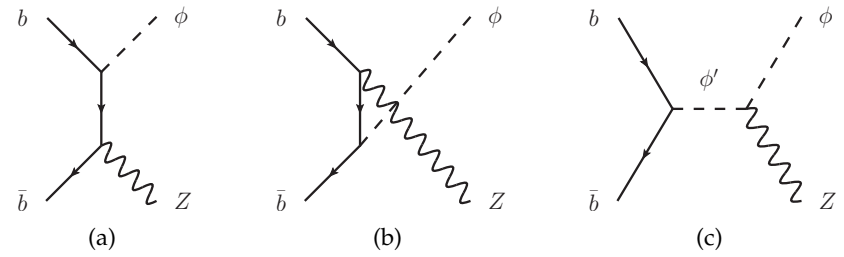

Figure 17: Feynman diagrams contributing to $b\bar{b} \to \phi Z$ channel.

Contributions where both the Z boson and the Higgs couple to an annihilating bottom-quark pair (see Figs. 17a and 17b) are in principle present also in the SM but completely negligible. As already mentioned the bottom Yukawa coupling can be enhanced, so that this channel may become relevant in the 2HDM. Similarly as for $gg \to \phi Z$ resonant s channel contributions (Figs. 17c) appear, which we treat in the same way, i.e. by employing the replacement (5.7). In the present study the $b\bar{b} \to \phi Z$ channel is taken into account at LO. Note that there is no interference with the Drell-Yan-like $b\bar{b} \to Z^* \to \phi Z$ dia-

grams included in $\sigma_{\phi Z,DY}$ for vanishing M_b so that the new contributions can be calculated separately.

An interesting observable related to Higgs strahlung in the context of NP searches was already introduced in Section 3.3, namely the ratio of the HW and HZ cross sections, which we extend to the 2HDM by writing

$$R_{WZ\phi} = \frac{\sigma_{\phi W}}{\sigma_{\phi Z}}. \tag{5.8}$$

In the SM this quantity can be predicted with a precision of about 3%.[5] If the cross section for Higgs strahlung was determined completely by the Drell-Yan term, the ratio would simply be identical to the SM value in the 2HDM because $g_{\phi ZZ} = g_{\phi WW}$. However, the $gg \to \phi Z$ and potentially also the $b\bar{b} \to \phi Z$ channel induce a sensitivity to the 2HDM parameters, which could make the ratio an exciting indicator of NP effects. In the next section it will be studied quantitatively in different 2HDM scenarios.

5.3 NUMERICAL RESULTS

In this section numerical results for the ϕZ production cross section and the ratio $R_{WZ\phi}$ will be presented. After stating the numerical input parameters, we treat the case $\phi = h$ in detail for the 2HDM of Type I and Type II. Then we move on to H^0Z and AZ production in Type II scenarios before discussing the qualitative effect of a lower cut on the Higgs transverse momentum.

5.3.1 *Setup and Choice of Input Parameters*

To produce the numerical results the appropriately modified version of the program `vh@nnlo` is applied, using `LoopTools` [88] for the evaluation of one-loop functions and `CUBA` [89] for the numerical integration.

[5] For numerical values and details on the determination of the uncertainties we refer the reader to Ref. [63].

Our choice of the required SM parameters reads:

$$M_t^{\text{pole}} = 172.3 \text{ GeV}, \tag{5.9a}$$
$$M_b^{\text{pole}} = 4.75 \text{ GeV}, \tag{5.9b}$$
$$M_b^{\overline{\text{MS}}}(M_b) = 4.16 \text{ GeV}, \tag{5.9c}$$
$$M_W = 80.398 \text{ GeV}, \tag{5.9d}$$
$$M_Z = 91.1876 \text{ GeV}, \tag{5.9e}$$
$$\Gamma_W = 2.141 \text{ GeV}, \tag{5.9f}$$
$$\Gamma_Z = 2.4952 \text{ GeV}, \tag{5.9g}$$
$$G_F = 1.16637 \cdot 10^{-5} \text{ GeV}, \tag{5.9h}$$
$$\sin^2\theta_C = 0.0508. \tag{5.9i}$$

Whereas we use the pole masses M_t^{pole} and M_b^{pole} in the Yukawa couplings for $gg \to \phi Z$, the bottom Yukawa is calculated with the running mass $M_b^{\overline{\text{MS}}}$ for the $b\bar{b} \to \phi Z$ channel. Quark mixing is taken into account only for the first two generations described by the Cabbibo angle θ_C. The hadronic cross section is obtained with the `MSTW2008-NNLO` PDF set [69] and α_S from this set with a default scale choice of $\mu_R = \mu_F = \sqrt{(p_\phi + p_Z)^2}$.

Furthermore the new version of `vh@nnlo` can be linked to the program `2HDMC` [90, 91]. In case of a resonance this is mandatory to calculate the required total width Γ_ϕ, but it is also useful for the user to fix the desired 2HDM in various parametrizations. As input for `2HDMC` we specify a value of $\alpha_S(M_Z) = 0.119$.

In the following we will analyze observables as a function of $\sin(\beta - \alpha)$ for fixed values of $\tan\beta$, M_h, M_A, and M_{H^0}. Note, however, that identifying the observed boson at 125 GeV with the light Higgs h requires $|\sin(\beta - \alpha)|$ to be close to one in order to be consistent with experimental data. In this limit, all couplings approach their SM values. The total width Γ_ϕ depends on the parameters $M_{H^\pm}$ and M_{12} (the off-diagonal element of the scalar mass matrix before SSB) as well, for which our default choices are $M_{H^\pm} = M_A$ and $M_{12} = 0$.

5.3.2 *Light Higgs*

5.3.2.1 *2HDM Type I*

Let us start the discussion of hV production with a Type I scenario, where the masses are chosen to be $M_h = 125$ GeV and $M_A = M_{H^0} = 200$ GeV, i.e. the s channel diagrams cannot become resonant yet, and $\tan\beta = 1$. Results for the different contributions to the hZ cross section in this case are illustrated in Fig. 18a, where the black solid line shows their sum. The behavior of the Drell-Yan terms $\sigma_{hZ,DY}$ (green, dotted line) is easy to understand as it is simply proportional to $\sin^2(\beta - \alpha)$. The same applies to the hW cross section because

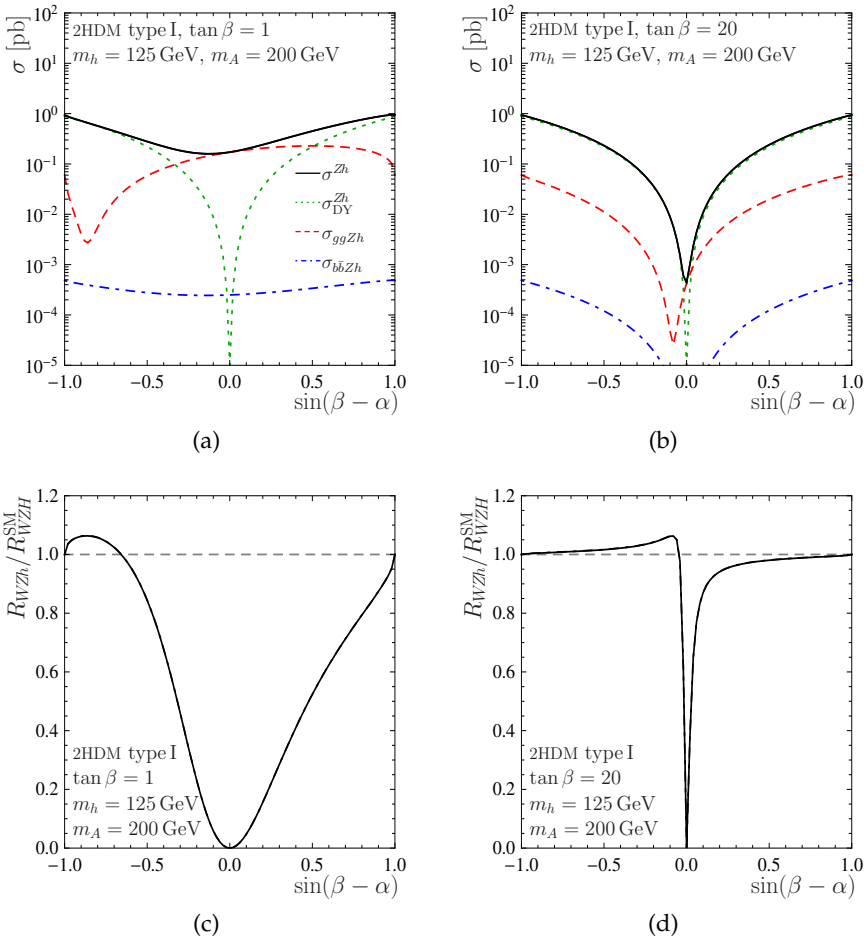

Figure 18: Cross section (top) and ratio R_{WZh} (bottom) for hV production at $\sqrt{s} = 14$ TeV in the 2HDM Type I for $M_h = 125$ GeV, $M_A = M_{H^0} = M_{H^\pm} = 200$ GeV and $\tan\beta = 1$ (left) or $\tan\beta = 20$ (right); from Ref. [63].

we neglect $\sigma_{\text{top I,II}}$ in (the generalization of) Eq. (3.2). In contrast, the gluon-induced contribution $\sigma_{gg\to hZ}$ (red, dashed line) depends both on the quark Yukawa couplings and the ϕZZ coupling, and in addition is influenced by s channel A bosons, leading to non-trivial interference effects. For $|\sin(\beta-\alpha)| \lesssim 0.5$ it is of the same order as or even larger than $\sigma_{hZ,DY}$. The bottom-quark-induced terms $\sigma_{b\bar{b}\to hZ}$ (blue, dash-dotted line) are completely negligible in this scenario just as in the SM.

Next we modify this scenario by choosing $\tan\beta = 20$. The effect of this can be seen in Fig. 18b, which is otherwise analogous to Fig. 18a. Because of this large value for $\tan\beta$, the Yukawa couplings to the light Higgs scale roughly as $\sin(\beta-\alpha)$,[6] and the coupling to the pseudoscalar is suppressed by $g^{\text{Type I}}_{A,u/d} = \pm\cot\beta$. Thus the whole cross

[6] cf. Eq. (5.5a)

section behaves approximately like the Drell-Yan part. These differences are also reflected in the ratio R_{WZh}, which is presented for the two scenarios in Figs. 18c and 18d, respectively, normalized to the SM value obtained at the same level of approximation.[7] Whereas for $\tan\beta = 1$ R_{WZh} depends strongly on $\sin(\beta-\alpha)$ as one leaves the SM values at the edges, the ratio is clearly flatter and drops to zero at $\sin(\beta-\alpha) = 0$ only because the hW cross section becomes zero in our approximation.

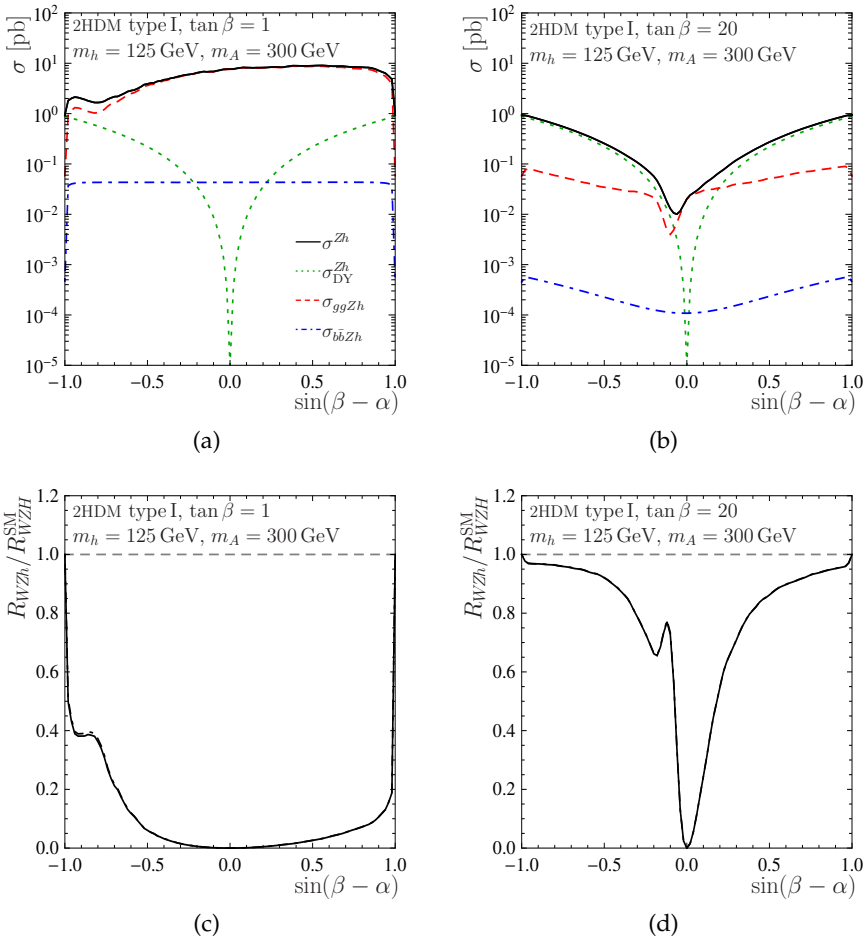

Figure 19: Cross section (top) and ratio R_{WZh} (bottom) for hV production at $\sqrt{s} = 14$ TeV in the 2HDM Type I for $M_h = 125$ GeV, $M_A = M_{H^0} = M_{H^\pm} = 300$ GeV and $\tan\beta = 1$ (left) or $\tan\beta = 20$ (right); from Ref. [63].

Now we consider the case $M_A = 300$ GeV, so that $M_A > M_h + M_Z$ and the processes $gg, b\bar{b} \to A \to hZ$ with A on shell become possible. Results are shown in Fig. 19, which is analogous to Fig. 18 except for the increase in M_A, i.e. again we give results for $\tan\beta = 1$

[7] This means that for consistency the $\sigma_{\text{top I,II}}$ terms as well as the NLO corrections to $\sigma_{gg\to HZ}$ and the electroweak corrections are omitted also for the SM values here.

and $\tan\beta = 20$. The altered behavior of the various contributions can be seen from Figs. 19a and 19b. Note that the Drell-Yan terms are unchanged as they are independent of M_A. The $gg \to hZ$ and $b\bar{b} \to hZ$ contributions, however, are drastically enhanced for $\tan\beta = 1$ and exceed the Drell-Yan part already for small deviations from $|\sin(\beta - \alpha)| = 1$. Accordingly the ratio R_{WZh} (Fig. 19c) drops sharply close to the edges. Increasing $\tan\beta$ to 20 again foils this enhancement for the reasons explained above and it is the Drell-Yan part that dominates most of the $\sin(\beta - \alpha)$ range. The ratio (see Fig. 19d) decreases only slightly, yet visibly, as one leaves the SM values at the edges before finally dropping to zero at $\sin(\beta - \alpha) = 0$.

5.3.2.2 *2HDM Type II*

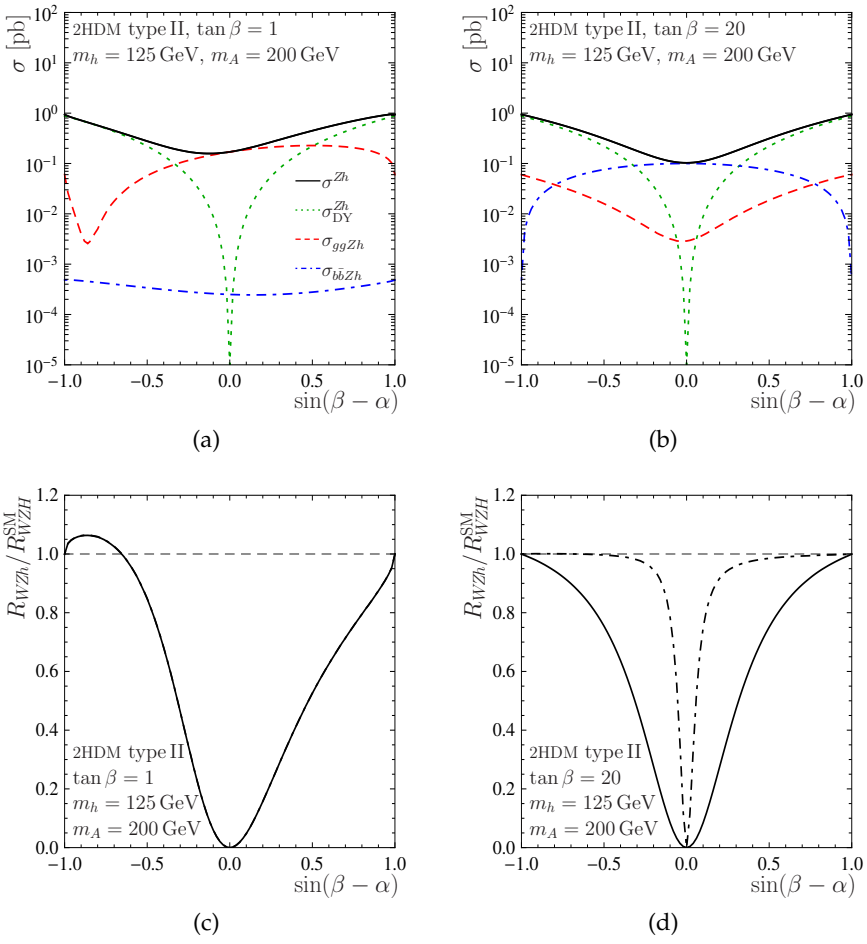

Figure 20: Cross section (top) and ratio R_{WZh} (bottom) for hV production at $\sqrt{s} = 14$ TeV in the 2HDM Type II for $M_h = 125$ GeV, $M_A = M_{H^0} = M_{H^\pm} = 200$ GeV and $\tan\beta = 1$ (left) or $\tan\beta = 20$ (right); from Ref. [63].

Next we turn to the 2HDM Type II. Figure Fig. 20 has the same structure as Fig. 18 and shows results for the non-resonant case $M_A = 200$ GeV. Whereas the Drell-Yan terms are identical to the case of the Type I 2HDM, the other contributions can change significantly due to the fact that, above all, the behavior of the bottom Yukawa is altered.

For $\tan\beta = 1$, however, the results for hZ cross section (see Fig. 20a) and for the ratio (Fig. 20c) still resemble those for Type I, especially the $b\bar{b} \to hZ$ contribution is still small. As can be seen from Fig. 20b, this changes for $\tan\beta = 20$. Now the $b\bar{b} \to hZ$ terms are competitive to the $gg \to hZ$ terms, which suffer from destructive interference effects, and even dominant for small values of $|\sin(\beta - \alpha)|$. The dash-dotted curve in Fig. 20d shows ratio R_{WZh} without the $b\bar{b} \to hZ$ terms, which might be useful if b jets are suppressed in experimental analyses. As this curve is much flatter than the full curve for R_{WZh}, this underlines the importance of the $b\bar{b} \to hZ$ contribution for large $\tan\beta$.

To complete the discussion of hV production we give results for $M_A = 300$ GeV in the 2HDM Type II in Fig. 21. Again we find that the results for $\tan\beta = 1$ (see Figs. 21a and 21c) are similar to those in the 2HDM Type I and that the resonant A propagator leads to an enormous enhancement of especially the $gg \to hZ$ contribution. In contrast to the Type I results, also for large $\tan\beta$ the ratio (see Fig. 21d) drops very fast for $|\sin(\beta - \alpha)| \neq 1$, which is due to the largely enhanced $b\bar{b} \to hZ$ terms that are clearly dominant in the bulk of the $\sin(\beta - \alpha)$ range (see Fig. 21b).

5.3.3 *Heavy and Pseudoscalar Higgs*

So far we have discussed hV production from the perspective that the h boson has already been discovered and we are interested in deviations from the SM cross section. In case of H^0V and AZ production the observation of such a channel would itself constitute the discovery of a NP effect.

We begin the discussion with heavy Higgs associated production. In this case the coupling to the vector bosons is complementary to the one of the light Higgs, i.e. proportional to $g_{H^0VV} = \cos(\beta - \alpha)$. This is why the Drell-Yan part is suppressed for $\sin(\beta - \alpha) \to \pm 1$ when the light Higgs becomes SM-like. However, the Yukawa couplings need not vanish in this limit. Thus larger cross sections are to be expected in Type II scenarios, to which we restrict the discussion in the following. In Fig. 22 the different contributions to the H^0Z cross section are shown (labeled like before) for $M_{H^0} = 200$ GeV and $\tan\beta = 20$, without ($M_A = 200$ GeV, see Fig. 22a) and with a resonance ($M_A = 300$ GeV, Fig. 22b). For $M_A = 200$ GeV the Drell-Yan terms give the largest contribution except very close to the edges where it vanishes and the $b\bar{b} \to H^0Z$ contribution is dominant. The

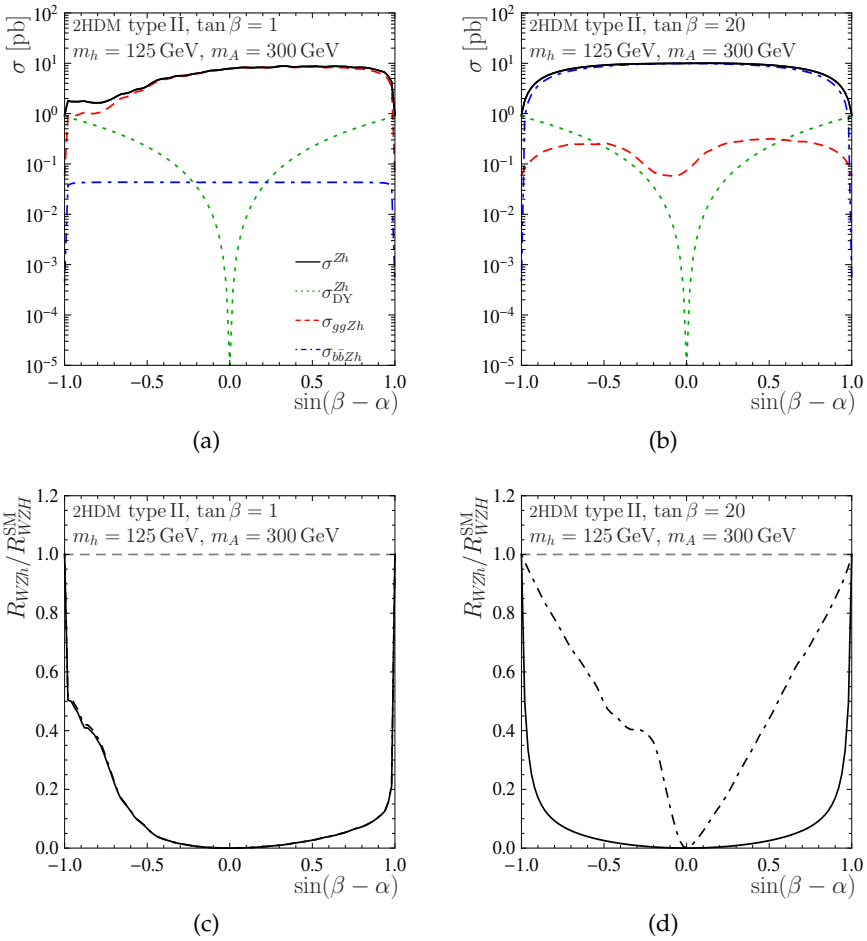

Figure 21: Cross section (top) and ratio R_{WZh} (bottom) for hV production at $\sqrt{s} = 14$ TeV in the 2HDM Type II for $M_h = 125$ GeV, $M_A = M_{H^0} = M_{H^\pm} = 300$ GeV and $\tan\beta = 1$ (left) or $\tan\beta = 20$ (right); from Ref. [63].

resonance present for $M_A = 300$ GeV enlarges the region where the latter is the case. However, this effect is not as large as with hZ production, which can be understood as follows. Since other decays of A are possible, for example $A \to hZ$, there is (assuming the narrow width approximation) a suppression factor $\frac{\Gamma_{A\to H^0 Z}}{\Gamma_A}$, which would cancel if the decay $A \to H^0 Z$ was dominant and lead to a similarly large effect as observed in the previous subsection.[8]

Finally we consider AZ production, for which results in a similar scenario as for the H^0V case are shown in Fig. 23, the only difference being that the values for M_A and M_{H^0} are swapped. If $M_{H^0} = 300$ GeV, it is the intermediate H^0 boson that can become resonant. As the coupling of the pseudoscalar to the gauge bosons is identi-

[8] In principle, if the H^0 and $H^\pm$ bosons were light enough, this suppression would also appear in hZ production.

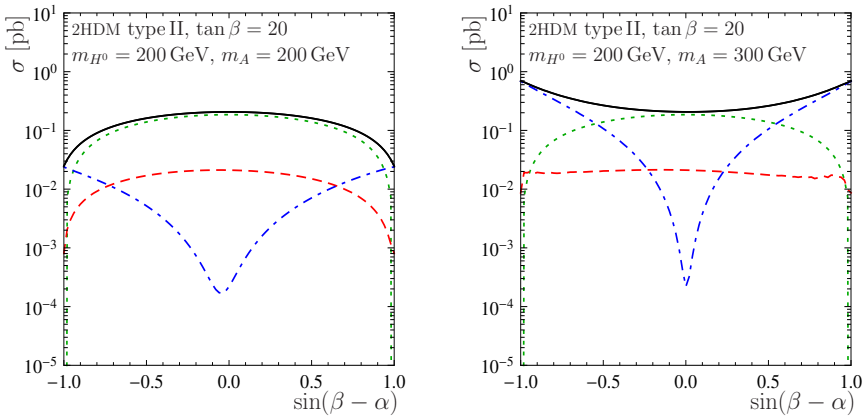

(a) (b)

Figure 22: Cross section for H^0Z production at $\sqrt{s} = 14$ TeV in the 2HDM Type II for $M_h = 125$ GeV, $M_{H^0} = M_{H^\pm} = 200$ GeV, $\tan\beta = 20$, and $M_A = 200$ GeV (left) or $M_A = 300$ GeV (right); from Ref. [63].

cally zero, there is no Drell-Yan part as thus no AW production at all because the Yukawa effects for ϕW are neglected in our approximation. In the non-resonant case shown in Fig. 23a the cross section is hardly dependent on α for this angle enters the calculation only indirectly via the total width Γ_{H^0}. In presence of the resonance (see Fig. 23b) this dependence is more pronounced.

5.3.4 *Boosted Scenario*

In Section 3.1 it was already mentioned that the experimental sensitivity to Higgs strahlung can be improved by requiring the Higgs transverse momentum to be large. As pointed out also in Ref. [92], the fraction of the $gg \to \phi Z$ channel, which is particularly sensitive to NP effect as we have seen, can be enhanced by such a lower $p_{T,\phi}$ cut. According to Ref. [61], this fraction can be doubled compared to the total cross section for $p_{T,H} > 150$ GeV in the SM.

In the following we will estimate the effect of this requirement on the results presented in this chapter, restricting ourselves to hV production, however. We will argue as follows: The Drell-Yan terms have the same form of the p_T spectrum as in the SM, as they are simply rescaled by an overall factor. This will not be true for the $gg \to hZ$ and $b\bar{b} \to hZ$ channels. To estimate how their sensitivity to NP effects is altered when the cut is applied, we evaluate σ_{ggHZ} over the SM value σ_{ggHZ} (and the corresponding fraction for $b\bar{b} \to hZ$) with and without p_T cut.

In general, from the statements made above, one would expect the influence of modification of the couplings with respect to SM to be enhanced. However, the sensitivity to possible resonances can

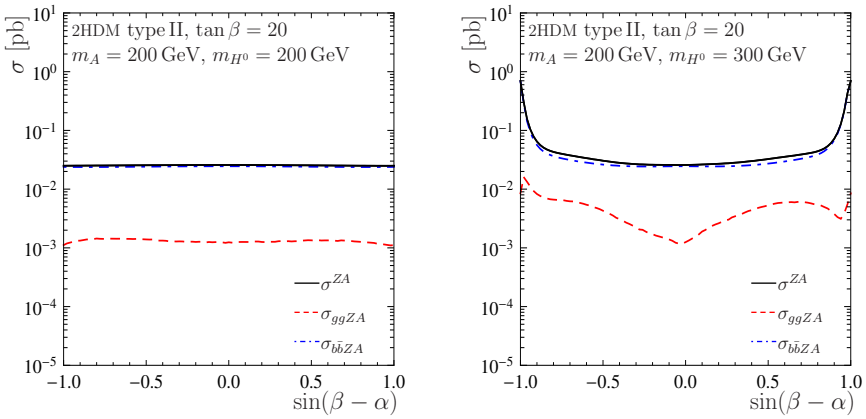

(a) (b)

Figure 23: Cross section for AZ production at $\sqrt{s} = 14$ TeV in the 2HDM Type II for $M_h = 125$ GeV, $M_A = M_{H^\pm} = 200$ GeV, $\tan\beta = 20$, and $M_{H^0} = 200$ GeV (left) or $M_{H^0} = 300$ GeV (right); from Ref. [63].

be significantly lowered. Application of Eq. (4.18) shows that the cut $p_{T,\phi} > 150$ GeV implies a minimal partonic center-of-mass energy of $\sqrt{\hat{s}} > 370$ GeV (for $M_\phi = 125$ GeV), i.e. a resonance at 300 GeV would be cut away.

For hZ production, this negative effect is even visible for $M_A = 200$ GeV when the A propagator is only close to resonant. In Fig. 24 the influence of requiring $p_{T,\phi} > 150$ GeV on the $gg \to hZ$ and $b\bar{b} \to hZ$ contributions normalized to the SM cross section in each case is shown, where the parameters are chosen like in Fig. 20. For small $\tan\beta$ (see Fig. 24a) the p_T cut reduces the relative size of the $gg \to hZ$ channel visibly. This effect is even stronger for the $b\bar{b} \to hZ$ channel, which is negligible in this case, however. In the case of large $\tan\beta$ (see Fig. 24b) the $gg \to hZ$ channel is reduced significantly only for small $|\sin(\beta - \alpha)|$. The contribution from the $b\bar{b} \to hZ$ channel, however, which is dominant in this scenario, is lowered by an order of magnitude almost over the complete range in $\sin(\beta - \alpha)$.

In case of a real resonance, like for $M_A = 300$ GeV, as shown in Fig. 25 with the same parameters as used for Fig. 21, this becomes even more drastic. The 2HDM effects in both the $gg \to hZ$ and the $b\bar{b} \to hZ$ channel are reduced by up to about two orders of magnitude.

5.4 CONCLUSIONS

In this study the possible influence of an extended Higgs sector in the form of the 2HDM on associated production of Higgs and heavy vector boson was considered.

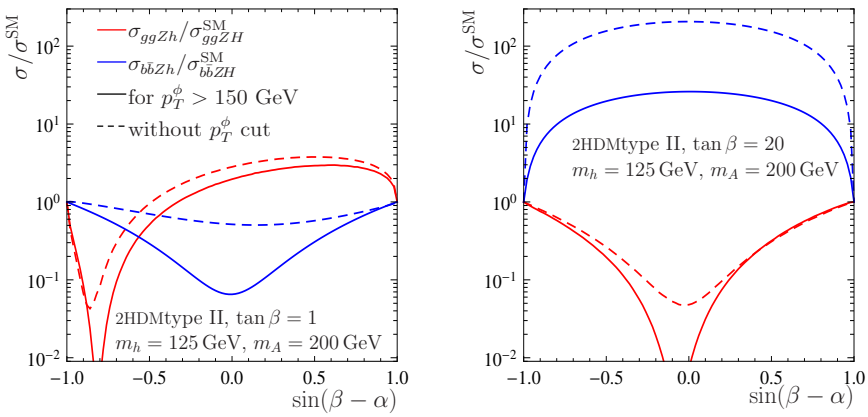

(a) (b)

Figure 24: Cross section for $gg \to hZ$ (red) and $b\bar{b} \to hZ$ (blue) normalized to corresponding SM prediction with (solid) and without $p_{T,\phi}$ cut (dashed) at $\sqrt{s} = 14$ TeV in Type II 2HDM with $M_h = 125$ GeV and $M_A = 200$ GeV for $\tan\beta = 1$ (left) and $\tan\beta = 20$ (right); from Ref. [63].

As a potentially useful observable the ratio of the HW and HZ production cross section was proposed, which is theoretically well under control and sensitive to deviations from the SM because such effects are expected to have a significantly larger impact on HZ than on HW production.

Concretely it was demonstrated that even if the light Higgs of the 2HDM is SM-like, the ratio drops in various exemplary scenarios because of an enhancement in hZ production, especially if s channel resonances due to additional bosons are present. However, such resonant enhancements may be lost if only events with boosted Higgs bosons are analyzed. It would be desirable not to restrict the searches for Higgs strahlung exclusively to the boosted regime. If such a resonance was realized, it would most likely improve the signal-to-background ratio anyway and allow for a measurement of the total cross section.

From the theoretical point of view it would be desirable to examine the effects in the boosted regime more precisely. Especially interesting would be to better understand the influence of the NLO QCD effects on the $gg \to \phi Z$ contribution, which have been shown to be large (see Chapter 4) in the SM case but are known only in the limit $M_t \to \infty$ and $M_b \to 0$. The former limit is problematic for large $p_{T,\phi}$ and the latter if the bottom Yukawa is enhanced. Hence these results cannot be generalized to extended scenarios, but the full calculation would be highly complex. For the $b\bar{b} \to \phi Z$ channel NLO effects are far more easily obtained and already available [86].

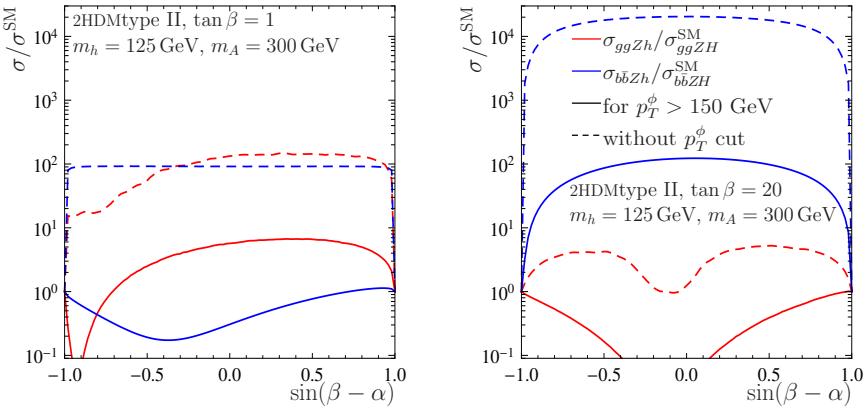

(a) (b)

Figure 25: Cross section for $gg \to hZ$ (red) and $b\bar{b} \to hZ$ (blue) normalized to corresponding SM prediction with (solid) and without $p_{T,\phi}$ cut (dashed) at $\sqrt{s} = 14$ TeV in Type II 2HDM with $M_h = 125$ GeV and $M_A = 300$ GeV for $\tan\beta = 1$ (left) and $\tan\beta = 20$ (right); from Ref. [63].

Phenomenologically, it would be interesting to study the experimental sensitivity to the ratio in more detail including the relevant decay rates, for example, but also to extend this study to other models like the MSSM.

Part III

NUMERICAL INTEGRATION OF LOOP INTEGRALS IN FOUR-DIMENSIONAL REGULARIZATION

In this part we will explore the alternative regularization method FDR with emphasis on the numerical evaluation of IR-finite two-loop diagrams using suitable counterterms. A method to contruct such counterterms is presented and implemented for the case of vanishing external momenta. Finally, for selected physical applications agreement to known results is shown.

6 INTRODUCTION TO FDR

Four-Dimensional Regularization was proposed by Roberto Pittau in 2012 [93] as an alternative approach to regularization and renormalization of quantum field theories. It is based on the idea to absorb infinities by a redefinition of the vacuum rather than adding counterterms to the Lagrangian. This is achieved by a reinterpretation of loop integrals in such a way that they can be integrated in four dimensions while gauge symmetry is maintained.

In this work we will rather think of FDR as a calculational tool and focus on practical aspects,[1] with special emphasis on the numerical integration of loop integrals with the help of local counter terms presented in Chapter 7. In the following the basic ideas of FDR including in particular the definition of the FDR integral will be summarized.

6.1 ISOLATION OF UV DIVERGENCIES

Consider a generic one-loop integral with internal masses $\{m_i\}$ and external momenta $\{p_i\}$ in DR,

$$I^{DR} = I(\{p_i, m_i\}, \mu_R, \epsilon) = \mu_R^{2\epsilon} \int d^d l \, J(l, \{p_i, m_i\}, \epsilon), \tag{6.1}$$

where $d = 4 - 2\epsilon$ and μ_R denotes the renormalization scale. Assume that there is a splitting of J into a UV-finite part J_F and a part J_V that is independent of any masses and external momenta:

$$J(l, \{p_i, m_i\}, \epsilon) = \lim_{\mu \to 0} \left[J_V(l, \mu, \epsilon) + J_F(l, \{m_i, p_i\}, \mu) \right]. \tag{6.2}$$

In other words, J_V contains all the UV divergencies and does not depend on details of the underlying process. The reason for the new arbitrary scale μ will become clear soon. Inserting Eq. (6.2) into (6.1) yields a corresponding splitting of I^{DR}:

$$I^{DR} = \lim_{\mu \to 0} \left[I_V(\mu, \mu_R, \epsilon) + I_F(\{m_i, p_i\}, \mu) \right], \tag{6.3a}$$

$$I_V(\mu, \mu_R, \epsilon) = \mu_R^{2\epsilon} \int d^d l \, J_V(l, \mu, \epsilon), \tag{6.3b}$$

$$I_F(\{m_i, p_i\}, \mu) = \int d^4 l \, J_F(l, \{m_i, p_i\}, \mu). \tag{6.3c}$$

The limit $\mu \to 0$ is to be understood as the asymptotic behavior for small μ. Now it is evident why an additional scale is needed. Otherwise Eq. (6.3b) would be zero since scaleless integrals vanish in DR.

[1] The idea that FDR may help facilitate NNLO calculations was pointed out in Ref. [94].

Realizing that μ is the only scale in the integrand J_V, the structure of I_V can be anticipated easily. In case of a polynomial UV divergency of degree k, the result must be proportional to μ^k by power counting. Thus it will vanish when the limit $\mu \to 0$ is taken and not contribute to I^{DR}. A logarithmic divergency on the other hand leads to a factor of $\mu^{-2\epsilon}$ and a pole in ϵ. In this case one can write

$$\begin{aligned} I_V &= \left(\frac{\mu_R^2}{\mu^2}\right)^{\epsilon} \left[\sum_{k=-1}^{\infty} a_k \epsilon^k\right] \\ &= a_{-1}\left[\frac{1}{\epsilon} + \ln\left(\frac{\mu_R^2}{\mu^2}\right)\right] + a_0 + \mathcal{O}(\epsilon). \end{aligned} \tag{6.4}$$

Note that if J_V contained convergent vacuum integrals, these would behave like powers of $\frac{1}{\mu}$ and make the splitting (6.2) more complicated than necessary. Thus this situation should be avoided.

Let us now assume that there is a logarithmic divergency that we remove by $\overline{\text{MS}}$ renormalization, i.e. by subtraction of the pole:

$$\begin{aligned} I^{\overline{\text{MS}}} &= I - a_{-1}\frac{1}{\epsilon} \\ &= \ln\left(\frac{\mu_R^2}{\mu^2}\right) + a_0 + \lim_{\mu\to 0} I_F(\{m_i, p_i\}, \mu). \end{aligned} \tag{6.5}$$

Note that since I and $I^{\overline{\text{MS}}}$ cannot depend on μ but only on μ_R, the dependence of $I^{\overline{\text{MS}}}$ on μ_R must be the same as the dependence of $\lim_{\mu\to 0} J_F$ on μ. Thus it makes sense to identify μ with μ_R and to write

$$I^{\overline{\text{MS}}} = a_0 + \lim_{\mu\to 0} I_F(\{m_i, p_i\}, \mu)\Big|_{\mu=\mu_R}. \tag{6.6}$$

Suppose there is a method to obtain a splitting as in Eq. (6.2) and reasoning to believe that a_0 is completely universal. Then Eq. (6.6) discloses a strategy to perform the renormalization of UV divergencies *before* the integration so that there is no need to evaluate any dimensionally regulated integrals. This is exactly what FDR claims to do. The quantity defined by

$$I^{\text{FDR}} := \lim_{\mu\to 0} I_F(\{m_i, p_i\}, \mu)\Big|_{\mu=\mu_R} \tag{6.7}$$

is finite in four dimensions and related to $I^{\overline{\text{MS}}}$ by a finite renormalization like the usual translation between two different renormalization schemes. In the following section, details on the separation of UV divergencies in the FDR framework will be discussed.

6.2 DEFINITION OF THE FDR INTEGRAL

As indicated in the previous section, within FDR loop integrals are defined by separating and dropping divergent vacuum contributions

on the integrand level. The method to arrive at the separation $J = J_V + J_F$ is best illustrated with a simple example. Consider the one-loop two-point function,

$$\begin{aligned} B_0(p^2) &= \mu_R^{2\epsilon} \int d^d l \, \frac{1}{(l^2 - M^2)((l+p)^2 - M^2)} \\ &= \frac{i}{16\pi^2} \left(\frac{\mu_R^2}{M^2}\right)^{\epsilon} \left[\frac{1}{\epsilon} + 2 - \beta \ln\left(\frac{\beta+1}{\beta-1}\right)\right] + \mathcal{O}(\epsilon), \\ \beta &= \sqrt{1 - \frac{4m^2}{s}}. \end{aligned} \tag{6.8}$$

This dimensionally-regulated integral has a logarithmic UV divergence resulting in a pole in ϵ. The new scale μ is introduced as an additional mass, yielding for the integral from Eq. (6.8)

$$B_0(p^2) = \lim_{\mu \to 0} \mu_R^{2\epsilon} \int d^d l \, \underbrace{\frac{1}{(l^2 - \mu^2 - M^2)((l+p)^2 - \mu^2 - M^2)}}_{\equiv J}. \tag{6.9}$$

Using the *partial-fraction relations*

$$\frac{1}{\bar{l}^2 - M^2} = \frac{1}{\bar{l}^2}\left(1 + \frac{M^2}{\bar{l}^2 - M^2}\right), \tag{6.10a}$$

$$\frac{1}{\overline{(l+p)}^2 - M^2} = \frac{1}{\bar{l}^2}\left(1 + \frac{M^2 - p^2 - 2l\cdot p}{\overline{(l+p)}^2 - M^2}\right), \tag{6.10b}$$

where $\bar{l}^2 := l^2 - \mu^2$, we may now rewrite the integrand in the following way:

$$\begin{aligned} J &= \frac{1}{(\bar{l}^2 - M^2)(\overline{(l+p)}^2 - M^2)} \\ &= \frac{1}{\bar{l}^2(\overline{(l+p)}^2 - M^2)} + \frac{M^2}{\bar{l}^2(\bar{l}^2 - M^2)(\overline{(l+p)}^2 - M^2)} \\ &= \underbrace{\frac{1}{\bar{l}^4}}_{\equiv J_V} + \underbrace{\frac{M^2 - p^2 - 2l\cdot p}{\bar{l}^4(\overline{(l+p)}^2 - M^2)} + \frac{M^2}{\bar{l}^2(\bar{l}^2 - M^2)(\overline{(l+p)}^2 - M^2)}}_{\equiv J_F}. \end{aligned} \tag{6.11}$$

Note that the UV divergency has been isolated in the first term J_V, as can be checked by power counting, and that this term is independent of M and p. By dropping this term, the UV divergencies are traded in for IR divergencies regulated by μ.

The question remains how to fix the difference between the $\overline{\text{MS}}$ and the FDR results.[2] For our example, it is

$$\mu_R^{2\epsilon} \int d^d l \, J_V = \frac{i}{16\pi^2}\left[\frac{1}{\epsilon} + \ln\left(\frac{\mu_R^2}{\mu^2}\right) + \mathcal{O}(\epsilon)\right]. \tag{6.12}$$

[2] cf. Eq. (6.6)

Thus the subtraction of J_V before the integration has the same effect as the $\overline{\text{MS}}$ subtraction when identifying $\mu = \mu_R$. In this case one expects $I^{\overline{\text{MS}}} = I^{\text{FDR}}$, which will be verified in Section 7.4.

The procedure shown for B_0 can easily be generalized to any scalar integral:

- replace all propagators according to

$$\frac{1}{(l+p)^2 - m^2} \to \frac{1}{(l+p)^2 - m^2 - \mu^2}, \tag{6.13}$$

- use the relations (6.10) to separate J_V and J_F,
- calculate $\int d^4l\, J_F$ in four dimensions,
- take the asymptotic behavior for $\mu^2 \to 0$,
- evaluate the result at $\mu = \mu_R$.

In Ref. [93] it was argued that for ϕ^3 and ϕ^4 theory the dropping of J_V can be understood as a simple redefinition of the vacuum which replaces the usual renormalization procedure and thus the results obtained in FDR should be consistent.

Let us now extend the discussion to theories involving gauge bosons and fermions. A key feature of FDR is that it respects gauge symmetry. At first sight, an additional mass μ introduced in the gauge boson propagators is in conflict with this claim. To compensate for this, the replacement $l^2 \to \bar{l}^2 = l^2 - \mu^2$ must be performed in the numerator as well, and the μ^2 part has to be treated in the same way as the l^2 part during the separation of J_V and J_F.[3] This construction is meant to ensure that all the cancellations between numerators and propagators that occur in DR also take place in FDR, so that the consequences of gauge symmetry, such as Ward identities, are automatically fulfilled. According to Ref. [93], this fixes the constant in Eq. (6.6), because it could be corrected by demanding that the Ward identities be fulfilled, which they are by construction, however.

Concerning integrals involving fermions, in the original paper [93] it was required to replace

$$\frac{1}{\not{l} + \not{p} - m} \to \frac{1}{\not{l} + \not{p} - m - \mu}. \tag{6.14}$$

Later in Ref. [95], it was clarified that one may as well take the trace over fermion lines first and consistently replace $l^2 \to l^2 - \mu^2$ afterwards. This is the understanding we will apply in this thesis.

[3] As a consequence, a factor of μ^2 in the numerator must be counted as l^2 when the UV behavior of an integral is examined. This point will be discussed in more detail in Section 8.1.2.1.

6.3 PROPERTIES OF THE FDR INTEGRAL

Adopting the notation from Ref. [93], we write the FDR interpretation of a dimensionally regulated L-loop integral

$$I^{\mathrm{DR}} = \prod_{i=1}^{L} \int d^d l_i \, J(\{l_i, l_i^2, p_i, m_i\}, \epsilon) \tag{6.15}$$

as

$$\begin{aligned} I^{\mathrm{FDR}} &= \prod_{i=1}^{L} \int [d^4 l_i \,] J(\{l_i, \overline{l_i}^2, p_i, m_i\}, 0) \\ &:= \lim_{\mu \to 0} \prod_{i=1}^{L} \int d^4 l_i \, J_F(\{l_i, \overline{l_i}^2, p_i, m_i\}, 0) \Big|_{\mu=\mu_R} \\ &= I^{\mathrm{DR}} - \lim_{\mu \to 0} \prod_{i=1}^{L} \int d^4 l_i \, J_V(\{l_i, \overline{l_i}^2, p_i, m_i\}, 0) \Big|_{\mu=\mu_R}, \end{aligned} \tag{6.16}$$

where the squared brackets indicate that the integral is to be treated according to the rules presented in the last section. The rules (6.10) generalize easily to the multi-loop case. A difference is that possibly sub-divergencies come up, which have to be isolated using the partial-fraction relations with respect to a part of the integral only, treating the other loop momenta as external ones as explained already in Ref. [93] for the two-loop case. As a consequence, one cannot expect the FDR integral to be simply the finite piece of the DR result anymore. From the second line in Eq. (6.16), where the FDR integral is represented as the difference of two DR integrals, it is clear that it fulfills basic properties of integrals, such as shift invariance.

In Ref. [94] differences between FDR and DR are discussed. One feature of FDR mentioned there is that at most a finite renormalization is needed to express the result of the calculation in terms of experimental observables.[4] Another advantage of FDR for multi-loop calculations is the fact that no $\frac{\epsilon}{\epsilon}$ terms occur. Thus there is for example no need to determine higher terms in the expansion in ϵ when an L-loop result is included in the $(L+1)$-loop calculation. However, a different kind of spurious terms shows up, namely those with μ^2 in the numerator. It appears that they balance the missing $\frac{\epsilon}{\epsilon}$ terms, at least in the context of tensor reduction. Consider for example the integral

$$\begin{aligned} \int [d^4 l] \frac{l^\mu l^\nu}{\bar{l}^2 (\bar{l}^2 - m^2)^2} &= \frac{g^{\mu\nu}}{4} \int [d^4 l] \frac{l^2}{\bar{l}^2 (\bar{l}^2 - m^2)^2} \\ &= \frac{g^{\mu\nu}}{4} \int [d^4 l] \left(\frac{1}{(\bar{l}^2 - m^2)^2} + \frac{\mu^2}{\bar{l}^2 (\bar{l}^2 - m^2)^2} \right), \end{aligned} \tag{6.17}$$

[4] We will have to do this for the top-quark mass in Section 8.3.

where we are allowed to replace $l^\mu l^\nu \to \frac{l^2}{4} g^{\mu\nu}$ because of the four-dimensionality, but l^2 can be canceled against $\bar{l}^2$ only for the price of an extra term. In DR on the other hand, one would replace $l^\mu l^\nu \to \frac{l^2}{d} g^{\mu\nu}$, which produces an $\frac{\epsilon}{\epsilon}$ term if the integral is divergent. Similarly, the extra μ^2 term gives a finite contribution if the original integral was divergent, as shown in Ref. [93].

IR divergencies in the loop integrals, both soft and collinear, are regulated by the introduction of the small mass μ^2 as well. These will produce terms of the form $\ln^k(\mu^2)$, $k \leqslant 2L$, which are compensated by the real emission. To achieve this cancellation, one has to perform the phase-space integration with photons and gluons having a small mass μ^2. This has been shown to work at one loop in Ref. [96] for $H \to gg$ at NLO QCD.

7 LOCAL COUNTERTERMS FOR FDR INTEGRALS

In summary the technical challenge that follows from the previous chapter is as follows. After the removal of the UV divergencies by making use of the partial-fraction identities and dropping divergent vacuum integrals, which can be automatized easily, the task is to calculate integrals that are finite in four dimensions but depend on the additional small mass parameter μ. In fact, we need the asymptotic behavior of these integrals for vanishing μ, but evaluated at $\mu = \mu_R$. In this chapter we will demonstrate how this can be performed with the help of local counterterms that have the same asymptotic behavior but can be integrated more easily. The difference can then be evaluated numerically with $\mu = 0$.

7.1 MOTIVATION

In principle the four-dimensionality welcomes numerical evaluation of the integrals. Nevertheless it is challenging to determine the behavior for $\mu \to 0$ numerically. To be able to discuss this in more detail, let us recall that we expect the integrals to behave like

$$I = \sum_i A_i \ln^i \left(\frac{\mu^2}{M^2}\right) + \sum_j B_j \left(\frac{\mu^2}{M^2}\right)^j + C, \tag{7.1}$$

where M denotes a scale at the order of the physical scales in the integrand. Following the FDR prescription, we have to set $B_j = 0$ for all j and evaluate the result at $\mu = \mu_R$, which should be chosen at the order of M to achieve a reasonable convergence of the perturbation series. That is, if we simply tried to suppress the B_j terms by choosing $\mu^2 \ll M^2$, the result would not be sensible. In addition, this might cause the convergence of the numerical integration to slow down to unacceptable extent.

One possible solution would be to determine the coefficients A_i in some other way, e.g. by calculating the behavior of the subtracted vacuum integrands or by making use of lower order results and renormalization group arguments. Then one could subtract the logarithmic terms from the result evaluated at some value $\mu = \mu_0$, where $\mu_0^2 \ll M^2$, to determine C. However, the problem of possibly bad convergence would remain. In practice, one would even have to perform the integration several times varying μ_0 to ensure that the B_j terms are sufficiently suppressed.

Therefore we pursue a different approach, namely to aim at finding auxiliary integrands with the same local behavior as the original in-

tegrands in the regions where the divergencies for small μ originates from. In the following sections we will analyze typical FDR integrals on the level of Feynman parameters and propose counterterms for one-loop integrals and a large class of two-loop integrals.

7.2 GENERAL CONSIDERATIONS

To identify the region in the integration space where the logarithmic dependence on μ^2 has its origin, let us examine the Feynman parametrization of a typical FDR L-loop integral. In Section B.1 it is argued that this parametrization has the form

$$\mathcal{I} = \prod_{i=1}^{N_x} \int_0^1 dx_i \prod_{j=1}^{N_y} \int_0^1 dy_j \; \delta\left(1 - \sum_{k=1}^{N_x} x_k - \sum_{l=1}^{N_y} y_l\right) \cdot \frac{p(x_1, \cdots, x_{N_x}, y_1, \cdots, y_{N_y})}{(b^T \operatorname{adj}(A) b + \det(A) c)^{N_1} \det(A)^{N_2}}, \tag{7.2}$$

where

$$c = \sum_{i=1}^{N_x} x_i (m_i^2 - q_i^2) + \mu^2 - i\varepsilon. \tag{7.3}$$

We distinguish between parameters for propagators with non-zero mass m_i and/or momentum q_i and the ones for propagators that depend on μ^2 (and the loop momenta) only, and label them x_i and y_i, respectively. Furthermore p is a polynomial determined by the structure of the numerator and the powers of the propagators, the $L \times L$-dimensional matrix A has components given by the structure of the corresponding graph, and b is an L-dimensional vector containing linear combinations of the external momenta.

The logarithmic dependence on μ^2 must originate from a region where the denominator would vanish if μ^2 was zero. Since μ^2 enters the denominator at the right-hand side of Eq. (7.2) only via c, Eq. (7.3) should be the key to single out this region. Let us first demand that $q_i^2 \ll m_i^2$ for all i so that $c > 0$, and also that all other momentum invariants appearing in $b^T \operatorname{adj}(A) b$ are such that the denominator is positive-definite. We will discuss a possible generalization below. Under this assumption, since μ^2 is assumed to be smaller than any other scale appearing in the integrand, it follows that all x_i must be small in order for c to become small in the limit $\mu^2 \to 0$. Note that this also implies $b \to 0$, so that indeed the denominator of (7.2) is of order μ^2 for $x \to 0$.

If we release the constraints on the momenta, additional singularities will occur. In case they originate from an IR divergency that is regulated by μ^2 playing the role of a small mass of otherwise massless particles, they would have to be canceled by logarithms from

the phase-space integration of the real emission amplitude or even by mass factorization. This would have to be done consistently in FDR, which is beyond the scope of this work, where we restrict ourselves to IR-finite quantities. Otherwise they simply signal that we have crossed a threshold for the on-shell production of intermediate particles and are merely a practical complication. In an analytic calculation, one would perform the integration assuming the denominator is positive-definite, and afterwards analytically continue the result to the region above the threshold, taking into account the $+i\varepsilon$ prescription. For the numerical evaluation this problem is more severe. Setting ε to a small positive value would in principle suffice but lead to sharply peaked integrands that are difficult to integrate. In practice, one has to deform the integration contour in the complex plane to achieve a well-behaved numerical integration [97]:

$$\prod_{i=1}^{n} \int_0^1 dx_i \; \theta\left(1 - \sum_{j=1}^{n} x_i\right) f(x_1, \cdots, x_n) \to \int_C d^n z \, f(z_1, \cdots, z_n), \tag{7.4}$$

where a possible parametrization is given by

$$\begin{aligned} \int_C d^n z \, f(z) &= \prod_{i=1}^{n} \int_0^1 d\xi_i \; \theta\left(1 - \sum_{j=1}^{n} \xi_i\right) f(z_1(\xi), \cdots, z_n(\xi)), \\ z_i(\xi) &= \frac{\xi_i + i\eta_i(\xi)}{1 + i\sum_j \eta_j(\xi)}. \end{aligned} \tag{7.5}$$

One can verify easily that this deformation vanishes at the integration boundaries, provided that $\eta_i(\xi) \to 0$ for $\xi_i \to 0$. If, in addition, the deformation can be performed continuously from the start without crossing any singularities, the result must be the same due to Cauchy's integral theorem. This idea is used in the second version of `SecDec` [98], for example, a program for the numerical evaluation of dimensionally regulated integrals. We will demonstrate later how this could work for our approach at least in the one-loop case.

Another complication arises when $\det(A)$ becomes small. At first glance one might think that these singularities are not regulated by μ^2, since the coefficient of μ^2 disappears and hence it does not seem to be able to prevent the denominator from vanishing in this situation. The conclusion would be that such singularities must be integrable independently of μ^2 and thus do not contribute to the $\ln(\mu^2)$ terms. However, it turns out that the integral over the y_i parameters can become divergent for vanishing x_i, meaning that indirectly μ^2 does regulate these singularities as well. In the one-loop case, which will be studied in the next section, it is always $A = 1$, so this problem cannot occur. For more than one loop, this overlapping of divergencies appears to be the most serious technical difficulty in the construction

the counterterms. This will be discussed in detail for the two-loop case later on.

7.3 THE ONE-LOOP INFRARED-FINITE CASE

At the one-loop level, a typical scalar FDR-regulated integral has the form

$$\mathcal{J}^{(1l)} = \int d^4 l \left\{ \prod_{j=1}^{N_x} \frac{1}{\left((l+q_j)^2 - m_j^2 - \mu^2\right)^{\alpha_j}} \right\} \frac{1}{\left(l^2-\mu^2\right)^{\beta}}. \quad (7.6)$$

Following the notation from Section B.1, the coefficients of the loop momenta in the quadratic form obtained by Feynman or Schwinger parametrization are

$$A = \sum_{i=1}^{N_x} x_i + y, \quad (7.7)$$

$$b = \sum_{i=1}^{N_x} x_i q_i, \quad (7.8)$$

simply because there is only one loop momentum l. Thus Eq. (B.19) reduces to

$$\frac{\mathcal{J}^{(1l)}}{i\pi^2} = (-1)^N \Gamma(N-2) \prod_{i=1}^{N_x} \int_0^1 \frac{dx_i}{\Gamma(\alpha_i)} \int_0^1 \frac{dy}{\Gamma(\beta)}\, \delta\left(1 - y - \sum_{k=1}^{N_x} x_k\right) \cdot \frac{x_i^{\alpha_i - 1} y^{\beta-1}}{\left(\mu^2 + \sum_{j=1}^{N_x} x_j (m_j^2 - q_j^2) + b^T b\right)^{N-2}}, \quad (7.9)$$

where $N = \sum_{i=1}^{N_x} \alpha_i + \beta$, and we have used the delta function to simplify $\det(A) = 1$. The next step is to integrate out y by means of the delta function, which yields

$$\frac{\mathcal{J}^{(1l)}}{i\pi^2} = (-1)^N \frac{\Gamma(N-2)}{\Gamma(\beta)} \prod_{i=1}^{N_x} \int_0^1 \frac{dx_i}{\Gamma(\alpha_i)}\, \theta\left(1 - \sum_{k=1}^{N_x} x_k\right) \cdot \frac{x_i^{\alpha_i - 1} \left(1 - \sum_{k=1}^{N_x} x_k\right)^{\beta-1}}{\left(\mu^2 + \sum_{j=1}^{N_x} x_j (m_j^2 - q_j^2) + b^T b\right)^{N-2}}. \quad (7.10)$$

Next we introduce a reference mass scale M to write the integral in terms of dimensionless parameters:

$$\frac{\mathcal{J}^{(1l)}}{i\pi^2} = \frac{(-1)^N}{(M^2)^{N-2}} \frac{\Gamma(N-2)}{\Gamma(\beta)} \prod_{i=1}^{N_x} \int_0^1 \frac{dx_i}{\Gamma(\alpha_i)}\, \theta\left(1 - \sum_{k=1}^{N_x} x_k\right) \cdot \frac{x_i^{\alpha_i - 1} \left(1 - \sum_{k=1}^{N_x} x_k\right)^{\beta-1}}{\left(a + \sum_{j=1}^{N_x} x_j c_j + \sum_{j,k=1}^{N_x} c_{jk} x_j x_k\right)^{N-2}}. \quad (7.11)$$

The new parameters are defined as $a := \frac{\mu^2}{M^2}$, $c_j := \frac{m_j^2 - q_j^2}{M^2}$, and $\frac{b^T b}{M^2}$ has been written in a form, where c_{jk} are momentum invariants divided by M^2.

Let us now apply the general idea sketched in the previous section to this integral. Assuming the external momenta are such that one can integrate Eq. (7.11) without the need to change the integration contour in the complex plane, singularities can occur only when all x_i are small. To single out the behavior of the integrand in this region, the relation shown in Eq. (B.44) turns out to be very useful:

$$\begin{aligned}&\prod_{i=1}^{n} \int_0^1 dx_i \; \theta\left(1 - \sum_{k=1}^{n} x_k\right) f(x_1, \cdots, x_n) \\ =&\prod_{i=1}^{n} \int_0^1 dx_i \; \delta\left(1 - \sum_{k=1}^{n} x_k\right) \int_0^1 dr \, r^{n-1} f(rx_1, \cdots, rx_n). \end{aligned} \tag{7.12}$$

Making use of it we can write

$$\begin{aligned}\frac{J^{(1l)}}{i\pi^2} = \frac{(-1)^N}{(M^2)^{N-2}} \frac{\Gamma(N-2)}{\Gamma(\beta)} \prod_{i=1}^{N_x} \int_0^1 \frac{dx_i \, x_i^{\alpha_i - 1}}{\Gamma(\alpha_i)} \, \delta\left(1 - \sum_{k=1}^{N_x} x_k\right) \\ \cdot \int_0^1 dr \, \frac{r^{N-\beta-1}(1-r)^{\beta-1}}{\left(a + r\sum_{j=1}^{N_x} x_j c_j + r^2 \sum_{j,k=1}^{N_x} c_{jk} x_j x_k\right)^{N-2}},\end{aligned} \tag{7.13}$$

where we have inserted $\sum_{i=1}^{N_x} \alpha_i = N - \beta$ when counting powers of r. What we have achieved by this transformation is that the divergency for $a \to 0$ is now associated with the region of small r, assuming sufficiently many c_i are non-zero, rather than the region where all x_i are small. The degree of divergence can now be determined easily by power counting. If $\beta = 1$, the integrand is finite at $r = 0$ even for $a = 0$, while in the case $\beta = 2$, the integrand would behave like $\frac{1}{r}$ for vanishing a and produce a logarithmic divergency. For even larger β, the integral would diverge like $\frac{1}{(\mu^2)^{\beta-2}}$, which one should avoid as pointed out in Section 6.1. Looking back to Eq. (7.6), this is exactly what one would expect from counting the powers of μ^2 in the limit $l \to 0$.

The advantage of the representation (7.13) is that after performing a single integration over r we may already take the limit $\mu \to 0$. The coefficients of $\ln^k(\mu^2)$, $k = 0, 1$, are then given by integrals over the x_i that are expected to converge if there are no additional IR singularities, and do no longer depend on μ. Since we aim at numerical evaluation of these integrals anyway, we can make our life even simpler by approximating Eq. (7.13) by a simpler integral with the same structure in the divergent region, and taking the difference afterwards.

The basic idea for the simplification is to linearize the denominator. To illustrate this, let us first consider a simple, logarithmically divergent example:

$$\begin{aligned}
&\int_0^1 \mathrm{d}r\, \frac{1}{a+br+cr^2} \\
&= \frac{2}{\sqrt{4ac-b^2}} \left[\arctan\left(\frac{b+2c}{\sqrt{4ac-b^2}}\right) - \arctan\left(\frac{b}{\sqrt{4ac-b^2}}\right)\right] \\
&= \frac{-1}{b}\left[\ln\left(\frac{a}{b}\right) + \ln\left(\frac{b+c}{b}\right) + \mathcal{O}(a)\right]. \qquad (7.14)
\end{aligned}$$

Instead of calculating the exact dependence on a and expanding in small a, we can evaluate a simpler integral producing the same $\ln(a)$ term, and add back the difference integrated with $a \to 0$:

$$\begin{aligned}
&\lim_{a\to 0}\int_0^1 \mathrm{d}r\, \frac{1}{a+br+cr^2} \\
&= \int_0^1 \mathrm{d}r\, \frac{1}{a+br} + \int_0^1 \mathrm{d}r\, \lim_{a\to 0}\left[\frac{1}{a+br+cr^2} - \frac{1}{a+br}\right] + \mathcal{O}(a) \\
&= \frac{-1}{b}\ln\left(\frac{a}{b}\right) + \int_0^1 \mathrm{d}r\, \frac{-c}{b(b+cr)} + \mathcal{O}(a) \\
&= \frac{-1}{b}\ln\left(\frac{a}{b}\right) + \frac{-1}{b}\ln\left(\frac{b+c}{b}\right) + \mathcal{O}(a). \qquad (7.15)
\end{aligned}$$

Similarly, additional powers of r in the numerator can be neglected when determining the dependence on $\ln(a)$.

Before applying this idea to Eq. (7.13), we rewrite it as

$$\begin{aligned}
\frac{\mathcal{J}^{(1L)}}{i\pi^2} = \frac{(-1)^N}{(M^2)^{N-2}}\frac{\Gamma(N-2)}{\Gamma(\beta)}\prod_{i=1}^{N_x}\int_0^1 \frac{\mathrm{d}x_i\, x_i^{\alpha_i-1}}{\Gamma(\alpha_i)}\,\delta\left(1-\sum_{k=1}^{N_x} x_k\right) \\
\cdot \int_0^1 \mathrm{d}r\, I_1^{(N-2,2-\beta,\beta-1)}\left(a, \sum_{j=1}^{N_x} x_j c_j, \sum_{j,k=1}^{N_x} c_{jk} x_j x_k, r\right), \qquad (7.16)
\end{aligned}$$

where we have introduced a generic notation for the integrand:[1]

$$I_1^{(N_1,n_1,n_2)}(a,c_1,c_2,r) := \frac{r^{N_1-1+n_1}(1-r)^{n_2}}{(a+c_1 r+c_2 r^2)^{N_1}}. \qquad (7.17)$$

The definition of n_1 is such that the integral is logarithmically divergent if $n_1 = 0$. The corresponding *auxiliary integrand*, which serves as a local counterterm, can be chosen as

$$\begin{aligned}
A_1^{(N_1,n_1)}(a,c_1,r) &:= I_1^{(N_1,n_1,0)}(a,c_1,0,r) \\
&= \frac{r^{N_1-1+n_1}}{(a+c_1 r)^{N_1}}. \qquad (7.18)
\end{aligned}$$

[1] In the appendix, Section B.3, this integrand is slightly more generalized.

In the logarithmically divergent case, $n_1 = 0$, its integral is given by

$$\int_0^1 dr\, A_1^{(N_1,n_1)}(a,c_1,r) = -\frac{1}{c_1^{N_1}}\left(\ln\left(\frac{a}{c_1}\right) + H_{N_1-1}\right), \tag{7.19}$$

where $H_n = \sum_{i=1}^{n} \frac{1}{n}$ denotes the n^{th} harmonic number.

Defining the difference between integrand and counterterm as

$$R_1^{(N_1,n_1,n_2)}(c_1,c_2,r) := \lim_{a\to 0}\left\{ I_1^{(N_1,n_1,n_2)}(a,c_1,c_2,r) - A_1^{(N_1,n_1)}(a,c_1,r)\right\}, \tag{7.20}$$

we arrive at our final expression for $\mathcal{I}^{(1l)}$ in the case of a logarithmic divergency:

$$\begin{aligned}\frac{\mathcal{I}^{(1l)}}{i\pi^2} = \frac{(-1)^N\Gamma(N-2)}{(M^2)^{N-2}}\prod_{i=1}^{N_x}\int_0^1 \frac{dx_i\, x_i^{\alpha_i-1}}{\Gamma(\alpha_i)}\,\delta\left(1-\sum_{k=1}^{N_x} x_k\right) \\ \cdot\left\{\frac{1}{\left(\sum_{j=1}^{N_x} c_j x_j\right)^{N-2}}\left(-\ln(a)+\ln\left(\sum_{j=1}^{N_x} c_j x_j\right) - H_{N-3}\right)\right. \\ \left. + \int_0^1 dr\, R_1^{(N-2,0,1)}\left(\sum_{j=1}^{N_x} x_j c_j, \sum_{j,k=1}^{N_x} c_{jk} x_j x_k, r\right) + \mathcal{O}(a)\right\}.\end{aligned} \tag{7.21}$$

The formal limit $\mu^2 \to 0$ can now be performed by omitting terms of order a, and Eq. (7.21) can be evaluated numerically with arbitrary $\mu = \mu_R$.

The result shown in Eq. (7.21) reflects the general remarks on possible additional singularities due to different configurations of the external momenta given in Section 7.2. Either we have to require $\left(\sum_{j=1}^{N_x} c_j x_j\right) \neq 0$ here, or, for momentum configurations above threshold, deform the integration contour in a way consistent with the $+i\varepsilon$ prescription. In case of an IR divergency, this does not suffice, and one has to perform more integrations analytically before it is legitimate to take $a \to 0$, which will in general lead to a $\ln^2(a)$ term.

7.4 ANALYTIC CONTINUATION: A ONE-LOOP EXAMPLE

To illustrate the method described in the previous section, especially the aspect of analytic continuation, let us return to the simple, but instructive example we have already considered in Section 6.2, namely the one-loop two-point function:

$$B_0(q^2) = \int \frac{[d^4l]}{(2\pi)^4}\frac{1}{\left(\bar{l}^2 - m^2\right)\left(\overline{(l+q)}^2 - m^2\right)}. \tag{7.22}$$

Using the partial-fraction identities (6.10) we write the integrand as

$$\int d^4l \left[\frac{1}{\bar{l}^4}\right] + \underbrace{\int d^4l \frac{m^2 - 2l\cdot q - q^2}{\bar{l}^4\left(\overline{(l+q)}^2 - m^2\right)}}_{=:I_1}$$
$$+ \underbrace{\int d^4l \frac{m^2}{\bar{l}^2\left(\bar{l}^2 - m^2\right)\left(\overline{(l+q)}^2 - m^2\right)}}_{=:I_2}. \tag{7.23}$$

The first term forms the divergent vacuum integral that will be dropped as indicated by the square brackets, and thus it is

$$(2\pi)^4 B_0(q^2) = \lim_{\mu^2\to 0}\{I_1 + I_2\}\big|_{\mu=\mu_R}. \tag{7.24}$$

For I_1 and I_2 we introduce Feynman parameters as described in Section B.1, yielding

$$\frac{I_1}{i\pi^2} = -\int_0^1 dx \frac{(1-x)\,[(1+(2x-1)s)]}{a + x(1-s) + x^2 s - i\varepsilon},$$
$$\frac{I_2}{i\pi^2} = -\int_0^1 dx_1 \int_0^1 dx_2 \frac{\theta\,(1-x_1-x_2)}{a + x_1 + x_2 - s x_2(1-x_2) - i\varepsilon}, \tag{7.25}$$

where $a = \frac{\mu^2}{m^2}$ and $s = \frac{q^2}{m^2}$.

I_2 is already finite for $\mu = 0$, so we can simply integrate it with a suitable contour deformation. For I_1 we put Eq. (7.21) to use. The integrated auxiliary integral can be analytically continued by writing

$$\ln(1 - s - i\varepsilon) = \ln|1-s| - i\pi\,\theta(s-1). \tag{7.26}$$

The difference function R_1 is integrated numerically after applying the contour deformation using the `NIntegrate` routine of `Mathematica`.

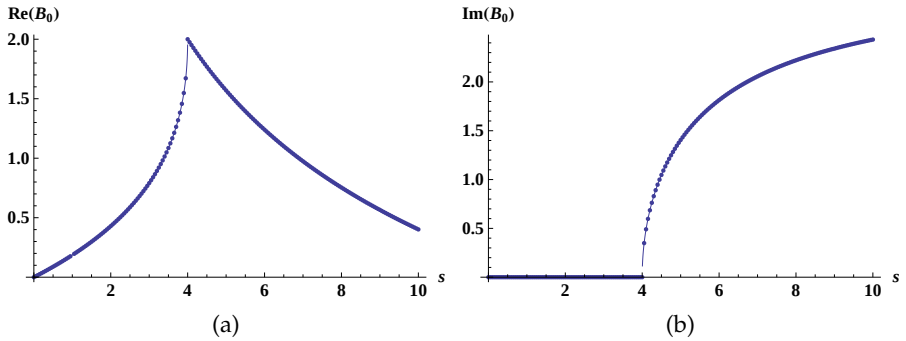

(a) (b)

Figure 26: Real and imaginary part of B_0 as a function of $\frac{q^2}{m^2}$

The results for the real and imaginary part of B_0 are shown as dots in Fig. 26, where the solid line is the finite part of Eq. (6.8), corresponding to the $\overline{\text{MS}}$-renormalized result. As anticipated in Section 6.2, we

find agreement between the two because the divergent vacuum integral that is discarded in FDR has a vanishing finite part. Note that I_1 and I_2 separately develop an imaginary part already for $s > m^2$, i.e. below the threshold for the on-shell production of a pair of particles with mass m. This is due to the additional propagators with vanishing mass μ and corresponds to the production of a massive and a massless particle. As required, this effect cancels in the sum, leaving an imaginary part only above the expected threshold at $s > 4m^2$. These additional thresholds in intermediate steps seem to be a general feature of the FDR approach.

7.5 THE TWO-LOOP CASE

To make the notation from Section B.1 more specific to the case $L = 2$, we define $l_{12} := l_1 + l_2$ and note that then each propagator contains either l_1, l_2, or l_{12}. If we use this to subdivide the massive propagators into three groups and collect their indices in three sets $\mathcal{X}_i$, $i = 1, 2, 3$, we can write the argument of the exponential as[2]

$$\begin{aligned} D = &\sum_{k\in\mathcal{X}_1} x_k \left(l_1^2 + 2q_k \cdot l_1 + q_k^2 - m_k^2\right) \\ &+ \sum_{k\in\mathcal{X}_2} x_k \left(l_2^2 + 2q_k \cdot l_2 + q_k^2 - m_k^2\right) \\ &+ \sum_{k\in\mathcal{X}_3} x_k (l_{12}^2 + 2q_k \cdot l_{12} + q_k^2 - m_k^2) \\ &+ y_1 l_1^2 + y_2 l_2^2 + y_3 l_{12}^2 - \mu^2, \end{aligned} \tag{7.27}$$

where $\mathcal{X}_1 \cup \mathcal{X}_2 \cup \mathcal{X}_3 = \{1, \cdots, N_x\}$ and $\mathcal{X}_1 \cap \mathcal{X}_2 \cap \mathcal{X}_3 = \{\,\}$. Without loss of generality we can assume the x_i to be ordered in a way such that

$$\begin{aligned} \mathcal{X}_1 &= \{1, \cdots, N_1\}, \\ \mathcal{X}_2 &= \{N_1 + 1, \cdots, N_1 + N_2\}, \\ \mathcal{X}_3 &= \{N_1 + N_2 + 1, \cdots, N_1 + N_2 + N_3\}, \end{aligned} \tag{7.28}$$

where $N_1 + N_2 + N_3 = N_x$. In general, the y_i terms need not all be present and also the sets X_i could partly be empty. Some of these special cases have to be distinguished and are discussed in Section B.2 of the appendix. For now, we simply assume N_1, N_2, N_3, and N_y to be always sufficiently large.

[2] cf. Eq. (B.6)

To obtain the connection to equation (B.19) we write

$$\begin{aligned}
D = &\underbrace{(y_1 + \sum_{k=1}^{N_1} x_k)}_{=:a_1} l_1^2 + 2 \underbrace{\sum_{k=1}^{N_1} x_k q_k}_{=:b_1} \cdot l_1 \\
&+ \underbrace{(y_2 + \sum_{k=N_1+1}^{N_1+N_2} x_k)}_{=:a_2} l_2^2 + 2 \underbrace{\sum_{k=N_1+1}^{N_1+N_2} x_k q_k}_{=:b_2} \cdot l_2 \\
&+ \underbrace{(y_3 + \sum_{k=N_1+N_2+1}^{N_x} x_k)}_{=:a_3} l_{12}^2 + 2 \underbrace{\sum_{k=N_1+N_2+1}^{N_x} x_k q_k}_{=:b_3} \cdot l_{12} \\
&- \underbrace{\left\{ \left(\sum_{k=1}^{N_k} x_k + \sum_{l=1}^{N_y} y_l \right) \mu^2 + \sum_{k=1}^{N_x} x_k (m_k^2 - q_k^2) \right\}}_{=:c} \\
= &\, (a_1 + a_3) l_1^2 + (a_2 + a_3) l_2^2 + 2 a_3 l_1 \cdot l_2 \\
&+ 2(b_1 + b_3) \cdot l_1 + 2(b_2 + b_3) \cdot l_2 - c,
\end{aligned} \tag{7.29}$$

Comparing to equation (B.6) one can read off the coefficient matrix A and the vector b:[3]

$$A = \begin{pmatrix} a_1 + a_3 & a_3 \\ a_3 & a_2 + a_3 \end{pmatrix}, \tag{7.30a}$$

$$b = \begin{pmatrix} b_1 + b_3 \\ b_2 + b_3 \end{pmatrix}. \tag{7.30b}$$

Equation (B.19) now takes the form

$$\begin{aligned}
\frac{\mathcal{J}^{(2l)}}{(i\pi^2)^2} = (-1)^N \Gamma(N-4) \prod_{i=1}^{N_x} \int_0^1 dx_i \, \frac{x_i^{\alpha_i - 1}}{\Gamma(\alpha_i)} \prod_{j=1}^{N_y} \int_0^1 dy_j \, \frac{y_j^{\beta_j - 1}}{\Gamma(\beta_j)} \\
\cdot \delta \left(1 - \sum_{k=1}^{N_x} x_k - \sum_{l=1}^{N_y} y_l \right) \frac{\det(A)^{N-6}}{\left(b^T \operatorname{adj}(A) b + \det(A) c \right)^{N-4}},
\end{aligned} \tag{7.31}$$

where

$$N = \sum_{i=1}^{N_x} \alpha_i + \sum_{j=1}^{N_y} \beta_j \tag{7.32a}$$

$$\det(A) = a_1 a_2 + a_1 a_3 + a_2 a_3, \tag{7.32b}$$

$$b^T \operatorname{adj}(A) b = a_3 (b_1 - b_2)^2 + a_2 (b_1 + b_3)^2 + a_1 (b_2 + b_3)^2, \tag{7.32c}$$

[3] Note that the meaning of the b_i has changed slightly.

and $N_y \in \{1,2,3\}$. Note that in any case the delta function induces

$$a_1 + a_2 + a_3 = \sum_{i=1}^{N_y} y_i + \sum_{i=1}^{N_x} x_i = 1. \tag{7.33}$$

If there are non-trivial numerators, we take them into account by taking the derivative of the corresponding Schwinger parameters as explained in Section B.1.2. The evaluation of the derivatives will not change the structure of the denominator significantly but only influence its power. Accordingly, most of the following analysis, which is focused on scalar integrals, can be carried over for the case of non-trivial numerators.

The next step is to find a parametrization suited to tailor the auxiliary integrals. As pointed out earlier, it is essential to understand when a zero of $\det(A)$ overlaps with the region of interest, namely where all x_i are small. To disentangle this situation, we will make use of Eq. (7.12) several times. Afterwards it can be judged which terms in the denominator can be neglected without changing the logarithmic dependence on μ^2 and thus need not be included in the auxiliary integral. To illustrate how this will work, let us consider an example:

$$\mathcal{J} = \int_0^1 dx \int_0^1 dy \, \frac{\theta(1-x-y)}{(x+y)(a+bx)+cx^2}. \tag{7.34}$$

This integral has a logarithmic divergency for small a. Suppose we want to find out whether the cx^2 term has any influence on the $\ln(a)$ terms of the result without performing the analytic integration. Recalling the situation in the one-loop case,[4] one might expect that it only enters the finite piece of the result. However, as x approaches zero, the integral over y becomes logarithmically divergent, i.e. x serves as a regulator here. In fact, both divergencies are in the end regulated by μ. To make this apparent, let us apply Eq. (7.12) to Eq. (7.34), which yields

$$\begin{aligned}\mathcal{J} &= \int_0^1 dx \int_0^1 dy \int_0^1 dr \, \frac{r\,\delta(1-x-y)}{r(x+y)(a+brx)+cr^2x^2} \\ &= \int_0^1 dx \int_0^1 dr \, \frac{1}{a+brx+crx^2}.\end{aligned} \tag{7.35}$$

Now the divergent region is symmetric in the two integration variables: r or x must be small. The leading term b will certainly contribute to the logarithm. In the region of small x, the c term is suppressed compared to the b term, but if, conversely, r is small and x is

[4] cf. Eq. (7.15)

not, the two terms will be of the same order. So c is indeed expected to influence the logarithmic term. In fact, the integrated result is

$$\begin{aligned}\mathcal{J} = &\frac{1}{2b}\ln^2(a) + \frac{1}{b}\left[-2\ln(b) + \ln(b+c)\right]\ln(a) \\ &+ \frac{1}{b}\left[\frac{\pi^2}{6} + \ln^2(b) - \frac{1}{2}\ln^2(b+c) - 2\,\mathrm{Li}_2\left(-\frac{c}{b}\right)\right] + \mathcal{O}(a)\,,\end{aligned} \tag{7.36}$$

i.e. c contributes not to the leading but to the sub-leading logarithm. As a consequence, only terms that are suppressed with respect to the leading term in all regions, where the denominator is of order a, can safely be neglected.

Now we apply this idea to the two-loop integral (7.31). Since $a_i \geqslant 0$ for $i = 1,2,3$ and $a_1 + a_2 + a_3 = 1$, $\det(A)$ has a zero if and only if two of the three a_i vanish. The question is which of these zeros can increase the logarithmic divergency as described above. A typical structure that produces a logarithmic dependence on μ^2 at the two-loop level has the form

$$\frac{1}{\overline{l_1}^4\overline{l_2}^2\overline{l_{12}}^2}. \tag{7.37}$$

It turns out to be convenient to always eliminate the parameter of the divergent propagator with the highest power by means of the overall delta function. The most severe divergency occurs when the parameter for this propagator goes to one (and all other parameters go to zero), because it has the highest power in the numerator and thus decreases the ability of the numerator to compensate for a zero of the denominator. Let us assume in the following that y_1 has the highest power and is chosen to be eliminated. Then it is

$$\det(A) = (1 - a_2 - a_3)(a_2 + a_3) + a_2 a_3. \tag{7.38}$$

Now we would like to factorize the simultaneous vanishing of a_2 and a_3. For this purpose, we apply Eq. (7.12) to all variables contributing to a_2 and a_3, i.e. to y_i, $i \in \{2, \cdots, N_y\}$, and x_i, $i \in \{N_1 + 1, \cdots, N_x\}$,[5] so that

$$\begin{aligned} a_{2,3} &\to r a_{2,3}, \\ a_2 + a_3 &\to r, \\ b_{2,3} &\to r b_{2,3}, \\ \det(A) &\to r\left[1 - r + r a_2 a_3\right] \\ b^T \operatorname{adj}(A) b &\to r\left[a_3(b_1 - r b_2)^2 + a_2(b_1 + r b_3)^2 \right. \\ &\qquad \left. + r a_1 (b_2 + b_3)^2\right]. \end{aligned} \tag{7.39}$$

[5] Note that introducing an additional theta function of the form $\theta(1 - \sum \text{any subset of parameters})$ is legitimate here.

The differentials and integration boundaries transform as

$$\begin{aligned}
&\prod_{i=1}^{N_x}\int_0^1 dx_i \prod_{j=1}^{N_y}\int_0^1 dy_j\ \delta\left(1-\sum_{k=1}^{N_x} x_k-\sum_{l=1}^{N_y} y_l\right)\\
&=\prod_{i=1}^{N_x}\int_0^1 dx_i \prod_{j=2}^{N_y}\int_0^1 dy_j\ \theta\left(1-\sum_{k=1}^{N_x} x_k-\sum_{l=2}^{N_y} y_l\right)\\
&\to\int_0^1 dr\, r^{N_2+N_3+N_y-2}\prod_{i=1}^{N_x}\int_0^1 dx_i \prod_{j=2}^{N_y}\int_0^1 dy_j\\
&\quad\theta\left(1-\sum_{k=1}^{N_1} x_k-r\right)\ \delta\left(1-\sum_{l=N_1+1}^{N_x} x_l-\sum_{m=2}^{N_y} y_m\right). \qquad (7.40)
\end{aligned}$$

What we have achieved is that factors of r can be split off from the denominator and be canceled against corresponding factors from the transformed differential.

Before writing the integrand explicitly, we perform another transformation. Recall that we are still interested in the region where all x_i are small. To parametrize this region in the one-loop case, we applied Eq. (7.12) to all the x_i. Here, we do this separately for $i \in \{1,\cdots,N_1\}$ and for $i \in \{N_1+1,\cdots,N_x\}$, naming the scaling variable s and t, respectively. In addition, we rescale the remaining y_i by u. This yields

$$\begin{aligned}
&\int_0^1 dr\int_0^1 ds\int_0^1 dt\int_0^1 du\, r^{N_2+N_3+N_y-2}s^{N_2+N_3-1}t^{N_1-1}u^{N_y-2}\\
&\quad\cdot\theta(1-t-r)\ \delta(1-s-u)\quad\prod_{i=1}^{N_x}\int_0^1 dx_i\prod_{j=2}^{N_y}\int_0^1 dy_j\\
&\quad\cdot\delta\left(1-\sum_{l=N_1+1}^{N_x} x_l\right)\ \delta\left(1-\sum_{m=1}^{N_1} x_m\right)\ \delta\left(1-\sum_{n=2}^{N_y} y_n\right).
\end{aligned} \qquad (7.41)$$

The integration over u can be performed immediately:

$$\begin{aligned}
&\int_0^1 dr\int_0^1 ds\int_0^1 dt\, r^{N_2+N_3+N_y-2}s^{N_2+N_3-1}t^{N_1-1}(1-s)^{N_y-2}\\
&\quad\cdot\theta(1-t-r)\quad\prod_{i=1}^{N_x}\int_0^1 dx_i\prod_{j=2}^{N_y}\int_0^1 dy_j\\
&\quad\cdot\delta\left(1-\sum_{l=N_1+1}^{N_x} x_l\right)\ \delta\left(1-\sum_{m=1}^{N_1} x_m\right)\ \delta\left(1-\sum_{n=2}^{N_y} y_n\right).
\end{aligned} \qquad (7.42)$$

For the sake of symmetry the other delta functions are kept as they are for now. To get rid of the remaining theta function, we substitute

$t \to (1-r)t$. The complete transformation can be summarized as follows:

$$x_i \to (1-r)t x_i \qquad i \in \{1, \cdots, N_1\}, \tag{7.43a}$$

$$x_i \to r s x_i \qquad i \in \{N_1+1, \cdots, N_x\}, \tag{7.43b}$$

$$y_1 \to (1-r)(1-t), \tag{7.43c}$$

$$y_i \to r(1-s) y_i \qquad i \in \{2, \cdots, N_y\}, \tag{7.43d}$$

and

$$\begin{aligned}
&\prod_{i=1}^{N_x} \int_0^1 dx_i \prod_{j=1}^{N_y} \int_0^1 dy_j \; \delta\left(1 - \sum_{k=1}^{N_x} x_k - \sum_{l=1}^{N_y} y_l\right) \\
&= \prod_{i=1}^{N_x} \int_0^1 dx_i \prod_{j=2}^{N_y} \int_0^1 dy_j \int_0^1 dr \int_0^1 ds \int_0^1 dt \\
&\quad \cdot \delta\left(1 - \sum_{l=N_1+1}^{N_x} x_l\right) \delta\left(1 - \sum_{m=1}^{N_1} x_m\right) \delta\left(1 - \sum_{n=2}^{N_y} y_n\right) \\
&\quad \cdot r^{N_2+N_3+N_y-2} s^{N_2+N_3-1} t^{N_1-1} (1-r)^{N_1} (1-s)^{N_y-2}.
\end{aligned} \tag{7.44}$$

Application of this transformation to Eq. (7.31) yields the final parametrization of the two-loop FDR integral:

$$\begin{aligned}
&\frac{\mathcal{J}^{(2l)}}{(i\pi^2)^2} \\
&= \frac{(-1)^N \Gamma(N-4)}{\Gamma(\beta_1)} \left(\prod_{i=1}^{N_x} \int_0^1 dx_i \, \frac{x_i^{\alpha_i - 1}}{\Gamma(\alpha_i)}\right) \left(\prod_{j=2}^{N_y} \int_0^1 dy_j \, \frac{y_j^{\beta_j - 1}}{\Gamma(\beta_j)}\right) \\
&\quad \cdot \delta\left(1 - \sum_{l=N_1+1}^{N_x} x_l\right) \delta\left(1 - \sum_{m=1}^{N_1} x_m\right) \delta\left(1 - \sum_{n=2}^{N_y} y_n\right) \\
&\quad \cdot \int_0^1 dr \int_0^1 ds \int_0^1 dt \, I^{(2l)}(r,s,t),
\end{aligned} \tag{7.45}$$

where

$$\begin{aligned}
&I^{(2l)}(r,s,t) \\
&= r^{-2+\sum_{j=2}^{N_y} \beta_j} (rs)^{-1+\sum_{i=N_1+1}^{N_x} \alpha_i} [(1-r)t]^{-1+\sum_{i=1}^{N_1} \alpha_i} \\
&\quad \cdot \frac{(1-r+r\,d(s))^{N-6} (1-r)^{\beta_1} (1-s)^{-1+\sum_{j=2}^{N_y} \beta_j} (1-t)^{\beta_1 - 1}}{[(1-r+r\,d(s))\,(\mu^2 + c_1 rs + c_2(1-r)t) + e(r,s,t)]^{N-4}}.
\end{aligned} \tag{7.46}$$

The coefficients

$$c_1 = \sum_{l=N_1+1}^{N_x} x_l (m_l^2 - q_l^2), \tag{7.47a}$$

$$c_2 = \sum_{k=1}^{N_1} x_k (m_k^2 - q_k^2), \tag{7.47b}$$

are constants with respect to r, s, and t, whereas d and e are polynomials in these variables:

$$d(s) = a_2(s)a_3(s), \tag{7.48a}$$

$$\begin{aligned} e(r,s,t) = {} & (1-r)^2t^2b_1^2 + 2rs(1-r)t\,[a_2(s)b_3 - a_3(s)b_2]\cdot b_1 \\ & + r^2s^2\left[a_2(s)b_3^2 + a_3(s)b_2^2\right] + rs^2(1-r)(b_2+b_3)^2. \end{aligned} \tag{7.48b}$$

Whereas for the combinations of the external momenta b_i the old definitions before the transformations still apply, for the terms a_i the s dependence does not factorize in general and we define[6]

$$a_2(s) = (1-s)y_2 + s\sum_{k=N_1+1}^{N_2} x_k, \tag{7.49a}$$

$$a_3(s) = (1-s)y_3 + s\sum_{k=N_2+1}^{N_x} x_k. \tag{7.49b}$$

The purpose of the transformation was to disentangle the divergencies of the integrations over the x_i and y_i parameters, as it was done earlier in this section for a simpler example (going from Eq. (7.34) to (7.35)), in order to understand how to construct possible counterterms. The parametrization given in Eqs. (7.45) and (7.46) still looks complicated, but after studying it in detail, we will be able to write down the counterterms. The core is the term

$$(1-r+r\,d(s))\left(\mu^2 + c_1rs + c_2(1-r)t\right) \tag{7.50}$$

in the denominator, which is the only place where μ^2 enters the integrand. In order for this to be of order μ^2 and produce a logarithmic dependence on μ^2, rs *and* $(1-r)t$ have to be small. This would be a suitable criterion to find suppressed terms that can be omitted in the auxiliary integral. However, there are two conditions that must be fulfilled. First of all, c_1 and c_2 as given in Eq. (7.47) may not vanish. If we require $q_i^2 < m_i^2$ for all i, this will be the case because of the delta functions in Eq. (7.45). They ensure that the sum of the x_i appearing in c_1 and c_2 is one in each case. Secondly, the factor in front of μ^2 must not approach zero too fast in the region of interest, otherwise the disentangling of the divergencies would not have been successful. We note that this factor is independent of t and is close to one when r is small for all s. Thus only the region where r is close to one (and s close to zero) could be problematic. The factor then behaves like $d(s)$. Looking at Eqs. (7.48a) and (7.49), we see that $d(0) = y_2y_3$, which obviously has two zeros at $y_2 = 0$ and $y_3 = 0$. In view of Eq. (7.43), these zeros in the limit $(r,s) \to (1,0)$ correspond to $a_1 = a_2 = 0$ and

[6] In case $N_y < 3$, when y_2 and/or y_3 are not present in $a_{2,3}$, they are omitted here as well, of course.

$a_1 = a_3 = 0$, respectively. Here we have recovered the two other zeros of $\det(A)$, that, however, we expect to be less severe than the one at $a_2 = a_3 = 0$, since we required the power of y_1 to be the highest of all y_i. Thus there is an additional suppression factor in the numerator, which in Eq. (7.46) shows up as $(1-r)^{\beta_1}$, and we conclude that the integral should be convergent in this region.[7] Accepting this, the criterion proposed above (rs and $(1-r)t$ small) to find the origin of the logarithmic μ^2 dependence should be valid.

To eventually construct the auxiliary integral, we have to consider the complete denominator

$$D := (1 - r + r\,d(s))\left(\mu^2 + c_1 rs + c_2(1-r)t\right) + e(r,s,t). \tag{7.51}$$

In the region where this is of order μ^2, the terms with c_1 and c_2 are dominant. As stated before, the idea is to neglect terms that are suppressed relative to the leading ones. To begin with, we approximate $d(s)$ by $d(0)$, which means neglecting terms of order $rs\mu^2$, r^2s^2, or $rs(1-r)t$. Taking a close look at Eq. (7.48b), one sees that only the term proportional to $(b_2+b_3)^2$ is not sufficiently suppressed to be neglected. Thus one may write

$$D = \tilde{D} + \mathcal{O}\left(rs\mu^2, r^2s^2, rs(1-r)t, (1-r)^2t^2\right), \quad \text{where} \tag{7.52a}$$

$$\tilde{D} = (1 - r + r\,d(0))\left(\mu^2 + c_1 rs + c_2(1-r)t + rs^2(b_2+b_3)^2\right). \tag{7.52b}$$

In the auxiliary integral, we can replace D by $\tilde{D}$, which is an enormous simplification for the analytical integration, because $\tilde{D}$ is factorized. The factors of $(1 - r + r\,d(0))$ can then be combined with those in the numerator.

In Chapter 8 these ideas will be put to use for the special case of vacuum integrals, where the $(b_2+b_3)^2$ term does not appear. The presence of this term would make the integration and expansion in small a slightly more demanding, but certainly not impossible.

[7] If this were not the case, one could separate the integration volume in such a way that the three zeros of $\det(A)$ are well separated, and control each zero in the way we did for $a_2 = a_3 = 0$. However, the number of integrals would increase and the boundaries of the cut integration volumes would be disadvantageous. This is why we refrain from doing this unless it should turn out to be indispensable.

8

APPLICATION TO TWO-LOOP VACUUM INTEGRALS

For a first test of how the method presented in Chapter 7 works out in practice for the two-loop case, we assume all momentum invariants to be so small that no thresholds are ever crossed, neither physical thresholds nor thresholds at lower energies in intermediate results induced by the propagators with a mass of μ[1]. Then a contour deformation will never be required. If we accept this, it makes sense to apply another simplification, namely to perform asymptotic expansions in small external momenta before the Feynman parametrization, so that only vacuum integrals have to be considered. In most cases the physical range of validity would not be much larger if finite momenta were allowed but always required to be below any threshold.

In the first section of this chapter an implementation for two-loop vacuum integrals will be described. Afterwards some physical applications of this program will be shown.

8.1 IMPLEMENTATION

The software setup presented in this section will be referred to as `FDRcalc` in the following. Making use of `FORM` [38] and `Mathematica`, it creates `c++` code to finally obtain an executable file for the numerical evaluation of the regularized integrals.

8.1.1 *Overview and Input*

The setup within and around `FDRcalc` is illustrated schematically in Fig. 27. At the beginning, `FDRcalc` uses `FORM` to perform three important steps:

- partial fractioning of the integrand to separate the divergent vacuum integrals from the physical, finite part (`partfrac2l.prc`),
- introduction of a suitable parametrization for each integrand (`feynpar2l.prc`), and
- matching of the integrands to standard ones that can be easily integrated with `Mathematica` (`match2l.prc`).

The input file, here generically denoted as <problem>, must contain four sections, so-called folds. The first three folds are read by `FORM` before the corresponding procedure is called, and the fourth one before

[1] cf. Section 7.4

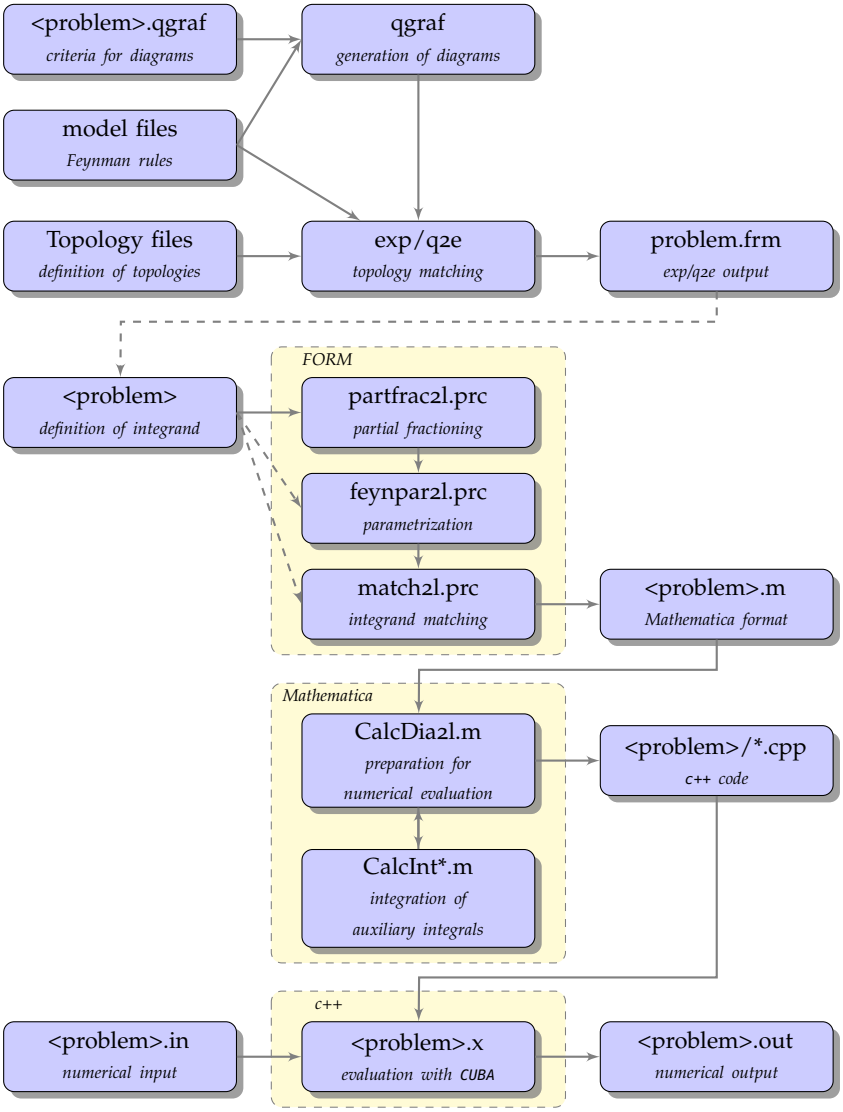

Figure 27: Schematic overview of the `FDRcalc` setup, optionally used in combination with `qgraf` and `q2e/exp`

the output is written in `Mathematica` format. A minimal input file is shown in Listing 1. The integrand must be defined in the first fold as an expression, whose name should be given in the preprocessor variable `EXPR`. The notation for the propagators reads

$$\begin{aligned} \texttt{Di(M,q)} &= \frac{1}{(l_i+q)^2-M^2}, \\ \texttt{D0i} &= \frac{1}{l_i^2}, \end{aligned} \tag{8.1}$$

where $i \in \{1,2,12\}$ and $l_{12} = l_1 + l_2$. The numerators can simply be given as scalar products using the dot operator.

Listing 1: Minimal input file for FDRcalc

```
*--#[ partfrac :
*
#define EXPR "dia"
#define MAXENUMPOW "4"
l dia = D1(M1,vec0)^2*D2(M2,vec0)^2*l2.l2*D012;
*
*--#] partfrac :

*--#[ feynpar :
*
*--#] feynpar :

*--#[ match :
*
*--#] match :

*--#[ write :
*
*--#] write :
```

Since the purpose of the program is the automatic evaluation of many integrals to calculate complete amplitudes rather than just a single one, it is useful to link it to other programs, e.g. the setup of `qgraf` and `q2e/exp`, which was described in Section 2.6. In the topology selection (topsel) file, one should provide all the topologies needed in the specific problem. The corresponding integration procedures then only have to express the integrand in terms of l_1, l_2, l_{12}, and the external momenta in the format given above, readily setting $\epsilon = 0$. Subsequently, the output can be included in the first fold of the input file for `FDRcalc`.

Next the result, expressed in terms of the standard integrals, is processed by the `Mathematica` package `CalcDia2l`, which plugs in the integrated auxiliary integrals and creates `c++` code for the numerical evaluation of the remaining integrations. The integration of the auxiliary integrals is performed by individual modules `CalcInt*.m` for the various types of integrals listed in Section B.3.

In the following subsections, the key ideas for the implementation of each step will be presented in brief.

8.1.2 *Part I: FORM*

Since the first steps of the calculation involve repeated insertion of identities and potentially a large number of terms at least in subexpressions, they are performed in `FORM`.

8.1.2.1 *Partial Fractioning*

As explained in Section 6.2, the first task is to separate the divergent vacuum integrals from the physical pieces and to remove the former in order to obtain integrals that are finite in four dimensions. At the two-loop level, this is done in two steps: overall divergencies should be removed first and possible sub-divergencies afterwards.

In order to eliminate the overall divergencies, we make repeated use of relations like those in Eq. (6.10b), namely

$$\frac{1}{\overline{(l_i+p)}^2-M^2}=\frac{1}{\overline{l_i}^2}\left(1+\frac{M^2-p^2-2l_i\cdot p}{\overline{(l_i+p)}^2-M^2}\right),\qquad i\in\{1,2,12\}, \tag{8.2}$$

as often as necessary. To begin with, we analyze for each term the behavior at large loop momenta by simple power counting. In terms of an effective number of propagators[2]

$$\begin{aligned}P :=\ &\text{number of propagators}\\ &-\lfloor\frac{1}{2}\text{powers of } l_i \text{ in the numerator}\rfloor,\end{aligned} \tag{8.3}$$

a necessary condition for the integral to be finite is $P > 4$. If an integrand with $P = N \leqslant 4$ is found, Eq. (8.2) is applied (at most once for each i) and the power counting is performed once again. This is repeated in a while loop until no terms with $P = N$ containing other than pure μ^2 propagators are left. Thus all terms for which $P = N$ still holds are divergent vacuum integrals and can be dropped. With the remaining terms, it is $P \geqslant N + 1$ and the procedure is repeated for $N + 1$ unless this is already larger than four. In this way, overall divergencies are successively removed, starting from the highest degree of divergency one expects to occur in intermediate results, e.g. $P = 0$, up to logarithmical divergencies with $P = 4$.

The integrands are now convergent in the region where both integration momenta are large, but can still contain divergencies if only one momentum is large, as e.g. in

$$\frac{1}{\left(\overline{l_1}^2-M^2\right)^3\left(\overline{l_2}^2-M^2\right)\overline{l_{12}}^2}, \tag{8.4}$$

when l_2 is large but l_1 is not. The proper way to proceed is to consider only the integration over one loop momentum, treating the other one as an external momentum.[3] If we regard l_1 as external momentum with respect to the integral over l_2, we can make use of the relation

$$\frac{1}{\overline{l_{12}}^2}=\frac{1}{\overline{l_2}^2}-\frac{l_1^2+2l_1\cdot l_2}{\overline{l_2}^2\overline{l_{12}}^2} \tag{8.5}$$

[2]Note that a single factor of l does not impair the UV behavior and can be neglected by rounding down the powers in the numerator to an even number.

[3]cf. Section 5 of Ref. [93]

in combination with Eq. (8.2) for $i = 2$, in order to decouple the divergency of the l_2 integration from l_1. In this case, the term that has to be classified as divergent vacuum integral and consequently be dropped is the integral over l_2 of

$$\frac{1}{\left(\overline{l_1}^2 - M^2\right)^3} \cdot \frac{1}{\overline{l_2}^4}. \tag{8.6}$$

To be completely general, relation (8.5) is needed for non-zero mass and momentum as well:

$$\frac{1}{\overline{(l_{12}+p)}^2 - M^2} = \frac{1}{\overline{l_2}^2} + \frac{M^2 - p^2 - l_1^2 - 2l_1 \cdot l_2 - 2l_{12} \cdot p}{\overline{l_2}^2 \overline{l_{12}}^2}. \tag{8.7}$$

In the implementation we proceed in a similar way as with overall divergencies. Sub-divergencies are searched for by power counting, but only with respect to two of the three momenta l_1, l_2, and l_{12}. Since we deal with one-loop sub-integrals, the condition for a finite integral is that the effective number of propagators belonging to the sub-integral is larger than two. To apply the proper partial-fraction relations, analogous while loops are used to successively eliminate sub-divergencies of decreasing degree of divergence. In fact, there are three constellations in which sub-divergencies can occur. Either one of l_1, l_2, and l_{12} may be the one to be treated as external momentum with respect to the divergent sub-integral. To find the required partial-fraction identities for the cases not discussed so far, one can for example interchange $l_1 \leftrightarrow l_2$ or $l_2 \leftrightarrow l_{12}$ in Eq. (8.7).

Two remarks about the partial fractioning are in order. Firstly, integrals that can be factorized into two one-loop integrals are treated separately as two independent one-loop integrals to avoid unnecessary complication. The final remark concerns the appearance of μ^2 in the numerator. As pointed out in Section 6.2, it is important to treat the μ^2 part of a $\overline{l_i}^2$ in the numerator in the same way as the l_i^2 part. In the current implementation this is achieved by writing them as inverse propagators, i.e.

$$\overline{l_i}^2 = \texttt{1/D0i} \ , \qquad i \in \{1, 2, 12\}. \tag{8.8}$$

Alternatively, one could distinguish μ_1^2, μ_2^2, and μ_{12}^2 depending on their origin, and give these factors the same weight as l_i^2 during the power counting.

8.1.2.2 *Parametrization*

The next step is to introduce the parametrization presented in Section 7.5. First it is determined which one of the variables will be eliminated using the overall delta function. Recall that in the motivation

of the parametrization it was assumed that the parameter of the μ^2 propagator with the highest power should be eliminated. Since in general we do not only have to deal with scalar integrals, we should take into account powers of the loop momenta in the numerator as well in this reckoning. In other words, we perform a power counting for small loop momenta and select the variable of the propagator associated with the most severe IR divergency. The result is stored for each term by multiplication of a tag.

Afterwards Schwinger parameters are introduced for each propagator and also for scalar products of momenta in the numerator. In the latter case, a derivative with respect to the corresponding parameter will be performed later instead of an integration, and these parameters will be named z_i in order to be distinguishable. In doing so, the values of the coefficients a_i, b_i, $i = \{1, 2, 12\}$, and c as defined in Eq. (7.29) are stored as function arguments for each term.

Now the loop momenta are integrated out after completing the square in the exponential. The result is given by Eq. (B.22), which for vanishing external momenta reads

$$\mathcal{I} = (-1)^N (i\pi^2)^L \prod_{i=1}^{N_x} \int_0^\infty dx_i \, \frac{x_i^{\alpha_i - 1}}{\Gamma(\alpha_j)} \prod_{j=1}^{N_y} \int_0^\infty dy_j \, \frac{y_j^{\beta_j - 1}}{\Gamma(\beta_k)} \cdot \exp(-c) \prod_{k=1}^{N_z} \frac{\partial^{\gamma_k}}{\partial z_k^{\gamma_k}} \frac{1}{\det(A)^2} \bigg|_{z_k = 0}. \tag{8.9}$$

Note that this formula is valid only if $b_i = 0$ for all i, i.e. scalar products of loop and external momenta stemming from an asymptotic expansion, for example, have to be removed in advance. This can be achieved in a straight-forward way using reduction identities based on Lorentz invariance.

Next the derivatives with respect to z_i are evaluated. In FORM this is done algebraically by writing all factors that depend on z_i as non-commuting objects, multiplying $\frac{\partial}{\partial z_i}$ from the left, and commuting it all the way to the right using relations of the form

$$\left[\frac{\partial}{\partial z}, f(z)\right] = f'(z). \tag{8.10}$$

At the very right, $\frac{\partial}{\partial z_i}$ is set to zero. For the case of vanishing external momenta we only need to implement two types of relations:

$$\left[\frac{\partial}{\partial z_i}, \frac{1}{\det(A)^n}\right] = -\frac{n}{\det(A)^{n+1}} \left\{ \frac{\partial a_1}{\partial z_i}(a_2 + a_3) + \frac{\partial a_2}{\partial z_i}(a_1 + a_3) + \frac{\partial a_3}{\partial z_i}(a_1 + a_2) \right\}, \tag{8.11a}$$

$$\left[\frac{\partial}{\partial z_i}, a_j\right] = \frac{\partial a_j}{\partial z_i}. \tag{8.11b}$$

The derivatives $\frac{\partial a_j}{\partial z_i}$ are either one or zero. This fact is used as soon as possible in order not to generate unnecessarily many terms.

Then the transformation from Schwinger to Feynman parameters is performed by inserting the relations (B.15), (B.16), and (B.18) explicitly. This is necessary for we do not have a closed formula at hand because of the derivatives. For factorizable integrals this is done separately in order to obtain a product of two independent Feynman parameter integrals.

The next step is the one which requires most careful distinction of cases, namely to decide which parameters will be scaled by new variables r, s, t, and u. In doing so, the choice which parameter to eliminate made at the beginning, the number of μ^2 propagators N_y, and the information which parameters contribute to a_1, a_2, and a_3 are taken into account. The special cases described in Section B.2, where not all new variables are needed, are handled automatically in this way, because in the case where an empty set of parameters is supposed to be transformed, simply nothing will be done. The result of this decision is once again stored as function arguments for each term. Needless to say that factorizable integrals are processed separately in this step as well.

Subsequently, the scaling of the chosen variables by r, s, t, u, and $1-r$ is executed by explicit replacement of the parameters and multiplication of corresponding factors for the differentials. The information which variables have to be integrated later on, as well as possible theta and delta functions, are kept track of all the time. Parts of the arisen delta functions are used for simplifications, where again the distinction of different cases is at order.

In the end, integrals that share the same denominator are collected in order to decrease the number of integrals and to avoid possible cancellations. Now the integrals are ready to be matched to standard integrals.

8.1.2.3 *Matching to Generic Integrals*

The last step performed in `FORM` is the matching of the integrals to the generic ones listed in Section B.3, which involve the integration over r, r and s, or r,s, and t.[4]

In principle, all that needs to be done is to select the suitable generic integral and read off the coefficients of the different powers of r, s, t, and combinations of these. In addition, factors of r, $1-r$, s, $1-s$, and t, as well as μ^2 in the numerator are counted. The preprocessor `MAXENUMPOW` defined in the input file[5] determines the highest power r and s expected in the remaining polynomial of the numerator. During the matching of the coefficients, a reference scale M is introduced in

[4] It turns out that integrals involving r and t can be avoided by a clever choice of the parametrization for the physical applications considered in this thesis.

[5] cf. Listing 1

order to obtain integrals that depend only on the ratios of the physical scales appearing in the problem over M, i.e. on dimensionless quantities. The dimension of the integral itself can then be factorized in terms of powers of M^2.

The coefficients and parameters determined in this way are stored in long chains of function arguments. In this way, the next step consisting in pattern matching with `Mathematica` will be sufficiently efficient. Finally, the result is printed in `<problem>.m` formatted for `Mathematica`.

8.1.3 *Part II: Mathematica*

Now that the integrals are expressed in terms of the generic ones defined in Section B.3, we need to integrate the corresponding auxiliary integrals analytically. Since they depend on many parameters, a closed form appears difficult to obtain. Instead, we keep only the dependence on those parameters that depend on the remaining integration variables or masses and momenta. The other parameters, mostly integer powers, are inserted before the integration. The auxiliary integrals are then calculated as necessary by `Mathematica` routines.

As a first step, `Mathematica` reads the content of `<problem>.m` and searches for generic integrals and their coefficients and other parameters via pattern matching. This matching is done by the function `CalcDia2l`. Whenever such an integral is found, the appropriate integration routine `CalcInt*` is called with the matched values of the parameters. The asterisk stands for the type of generic integral that has been matched, e.g. `CalcIntrst` calculates integrals that depend on all three variables `r`,`s`, and `t`. The return values of the `CalcInt*` functions are of the form

$$\ln^2\left(\frac{\mu^2}{M^2}\right)\texttt{Int[i]} + \ln\left(\frac{\mu^2}{M^2}\right)\texttt{Int[i+1]} + \texttt{Int[i+2]} + \texttt{Int[i+3]}, \tag{8.12}$$

where `Int[i]` stands for the result of the i^{th} numerical integration which will be performed by the `c++` code later. There are two integrals contributing to the finite term, because the finite piece of the auxiliary integral and the regularized integral, i.e. the difference between primary and auxiliary integral, have to be integrated over different variables.

Let us briefly discuss how the `CalcInt*` routines work. At first it calls the definitions of the original, the auxiliary, and the integrated auxiliary integral and plugs in the parameters it has been given as arguments. The definition of the integrated auxiliary integrals is such that a corresponding routine is called unless the result is already known. In the former case the auxiliary integral is integrated over `r`, `s`, and `t`, or parts of these, and expanded in small a afterwards,

while in the latter case the known result is returned. Additionally, these results are saved at the very end of the `Mathematica` part of `FDRcalc` and loaded at the beginning of the next run to make them reusable. Details about the choice of the auxiliary integrals are given in Section B.3 of the appendix. Next `CalcInt*` calls a subroutine that writes standardized `c++` code passing all information needed for the numerical integration: the integrand definition, the integration variables, constraints of the form $\sum_i x_i = 1$, and the number of the integral. In case of such a constraint, a suitable parametrization is automatically inserted. As indicated in Eq. (8.12), there are up to four numerical integrations to be done per matched integral.

Finally, after all the matched integrals have been treated, the expression for the final result given in terms of $\ln\left(\frac{\mu^2}{M^2}\right)$ and `Int[i]` is written as `c++` code to another source file.

8.1.4 *Part III: c++*

The output written by the `Mathematica` routine `CalcDia2l` together with some generic `c++` code can be compiled and linked immediately to create an executable. In the following the structure of the program will be briefly discussed.

The task is to perform several numerical integrations that differ in dimension and required precision. To be able to store the information about these integrations in a convenient way, we introduce the class `FDRint`. It contains all relevant parameters for the numerical evaluation, in particular a pointer to the integrand function. The actual numerical integration is then initiated by calling a member function of this class. For this purpose we use the `CUBA` library [89], which implements different Monte Carlo and deterministic integration algorithms. It appears that the deterministic Cuhre algorithm is best suited for our current purposes, because it allows for high precision with a reasonable number of function calls in moderate dimensions, as long as the integrand does not have any sharp peaks. In the case of (integrable) singularities, which could appear above thresholds where a contour deformation is required, one might have to switch to Monte Carlo methods such as `Vegas` [74].

After reading numerical input parameters, such as masses and momentum invariants, the generic main file calls the problem specific function `setintegrands`. This function returns a vector of `FDRint` objects with integrands and number of dimensions set accordingly. The main function then iterates through this vector calling the integration member function for each element. Afterwards another problem specific function named `finalresult` calculates the final result from the outcome of the single integrations, returning three numbers for the coefficients of $\ln^i(\mu^2)$, where $i = 1, 2, 3$.

A practical question is how to choose the precision goal for the various numerical integrations. Let ϵ be the desired precision for the complete result. The impact of a single integral I_k on the final result J depends not only on its value but also on the derivative $\frac{\partial J}{\partial I_k}$. According to Gaussian propagation of uncertainties the estimate for the uncertainty of J reads

$$(\Delta J)^2 = \sum_{k=1}^{n} \left(\frac{\partial}{\partial I_k} J(I_1, \cdots, I_k, \cdots, I_n) \Delta I_k \right)^2 . \tag{8.13}$$

To estimate the derivatives, we perform a quick run for all integrals with only moderate relative precision $\gtrsim 10^{-3}$ and calculate

$$\begin{aligned} w_k &:= |J(I_1, \cdots, (1+\delta)I_k, \cdots, I_n) \\ &\quad + J(I_1, \cdots, (1-\delta)I_k, \cdots, I_n)| / (2\delta) \\ &\approx \frac{\partial J}{\partial I_k} \end{aligned} \tag{8.14}$$

with $\delta = \mathcal{O}(0.1)$. Then in a second run we require

$$\Delta I_k < \frac{\epsilon}{\sqrt{n} w_k} \tag{8.15}$$

so that

$$\Delta J \approx \sqrt{\sum_{k=1}^{n} (w_k \Delta I_k)^2} < \epsilon. \tag{8.16}$$

Apart from computation time the possible accuracy is limited by instabilities of the integrands on the borders of the integration area. As simple remedies we use longer floating point numbers than usual in the critical part of the calculation (`long double` instead of `double` in c++) and extrapolate the integrand if one (or more) of the variables is closer to the border than a certain limit. The extrapolation which is currently implemented has the form

$$\tilde{f}(x) = \begin{cases} f(\kappa), & \text{if } x < \kappa, \\ f(x), & \text{if } \kappa \leqslant x \leqslant 1-\kappa, \\ f(1-\kappa), & \text{if } x > 1-\kappa, \end{cases} \tag{8.17}$$

i.e. the integrand is simply set to a constant value close to the borders. For typically choices $\kappa = \mathcal{O}\left(10^{-8}\right)$, the impact of replacing f by $\tilde{f}$ should be small compared to the uncertainty of the integration. Otherwise a more elaborate extrapolation might have to be used.

8.2 $\phi \to \gamma\gamma$ AT NLO QCD

The first complete two-loop calculation in FDR was presented in Ref. [94] for the decay of a Higgs boson into two photons at NLO QCD in the

heavy-top limit. Agreement with the well-known DR result [99, 100] was found. As a first check of our program, we reproduce this result in this section. In addition, we also study the case of a pseudoscalar Higgs boson [101]. It will be interesting to see whether a finite renormalization for the pseudoscalar current is needed in FDR as it is the case for DR at higher loop orders.[6]

8.2.1 *Notation for the Amplitude*

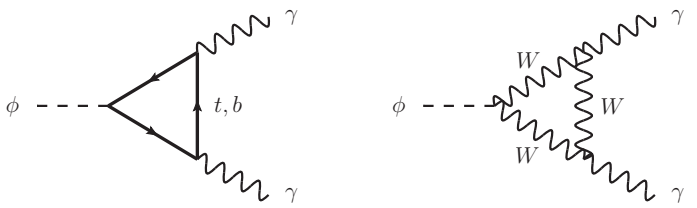

(a) Leading order

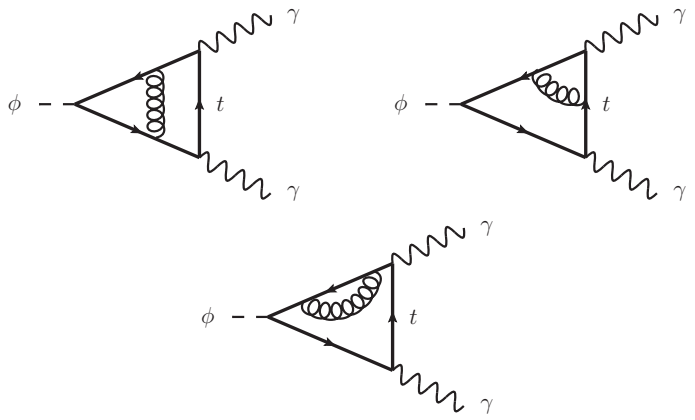

(b) QCD corrections

Figure 28: Feynman diagrams for $\phi \to \gamma\gamma$, $\phi \in \{h, H, A\}$

The decay of the scalar or pseudoscalar Higgs boson ϕ is induced by heavy charged particles, i.e. heavy quarks or W bosons, as shown in Fig. 28a. In any case, the amplitude can be written as

$$\mathcal{M}_{\phi\to\gamma\gamma} = \mathcal{M}_{\phi}^{\mu_1\mu_2}\varepsilon_1^{\mu_1}(q_1)^*\varepsilon_2^{\mu_2}(q_2)^*, \tag{8.18}$$

where $q_{1,2}$ denote the momenta of the photons and $\varepsilon_{1,2}$ their polarization vectors. For the decay of a scalar Higgs boson h we use the fact that the photons must be longitudinally polarized. Since $\varepsilon_i \cdot q_i = 0$ $(i = 1, 2)$, only terms proportional to $g^{\mu_1\mu_2}$ and $q_1^{\mu_2}q_2^{\mu_1}$ in

[6] cf. Section 2.3

$\mathcal{M}_h^{\mu_1\mu_2}$ can contribute. Their ratio is fixed by gauge invariance, which implies $\mathcal{M}_\phi^{\mu_1\mu_2} \cdot q_{i,\mu_i} = 0$ $(i = 1, 2)$, so one can write

$$\mathcal{M}_h^{\mu_1\mu_2} = (\mathcal{M}_{h,t} + \mathcal{M}_{h,b} + \mathcal{M}_{h,W}) \left(g^{\mu_1\mu_2} - \frac{q_1^{\mu_2} q_2^{\mu_1}}{q_1 \cdot q_2} \right). \tag{8.19}$$

In case of the pseudoscalar boson A, the only available structure for the amplitude is $\epsilon^{\varepsilon_1\varepsilon_2 q_1 q_2}$. Thus we write

$$\mathcal{M}_A^{\mu_1\mu_2} = (\mathcal{M}_{A,t} + \mathcal{M}_{A,b})\, \epsilon^{\mu_1\mu_2 q_1 q_2}, \tag{8.20}$$

where we assume that the pseudoscalar does not couple to the heavy vector bosons as it is the case in the 2HDM.

Here we are only interested in QCD corrections to the top quark contribution, i.e.

$$\mathcal{M}_{\phi,t} = \mathcal{M}_{\phi,t}^{(0)} + \frac{\alpha_S}{\pi} \mathcal{M}_{\phi,t}^{(1)} + \mathcal{O}\left(\alpha_S^2\right). \tag{8.21}$$

Since the bottom-quark contribution is suppressed at least in SM-like scenarios when the bottom Yukawa is not enhanced and $\mathcal{M}_{h,W}$ does not receive QCD corrections at this order in the electroweak couplings, we assume these to be the dominant QCD corrections. Because of color conservation there is no real emission at NLO QCD, and the corrections to $\mathcal{M}_{\phi,t}$ are given by the diagrams in Fig. 28b plus additional ones obtained by inverting the fermion flow or crossing the two photons. For the $t\bar{t}$-Higgs vertices we insert[7]

$$\langle t_i \bar{t}_j h \rangle : \quad i g_t M_{t,0} \delta_{ij}, \tag{8.22a}$$

$$\langle t_i \bar{t}_j A \rangle : \quad i \tilde{g}_t M_{t,0} \gamma_5 \delta_{ij}, \tag{8.22b}$$

where i and j denote color indices, and we have factorized the bare top-quark mass $M_{t,0}$ from the Yukawa couplings leaving the generic factors g_t and $\tilde{g}_t$, respectively.

8.2.2 *Results in Dimensional Regularization*

For comparison we need results in DR, which we obtain with the `qgraf/q2e/exp/MATAD` setup described in Section 2.6. Since all external legs are connected to massive lines only, the asymptotic expansion[8] in $\frac{1}{M_t^2}$ simply amounts to expanding the massive propagators in terms of small external momenta. In case of the pseudoscalar decay, we proceed with γ_5 as described in Section 2.2, i.e. replacing

$$\gamma_5 = \frac{i}{4!} \epsilon^{\mu\nu\rho\sigma} \gamma_\mu \gamma_\nu \gamma_\rho \gamma_\sigma \tag{8.23}$$

and keeping the epsilon tensor outside the d-dimensional calculation until the renormalization has been performed. Then we renormalize

[7] cf. Eq. (5.4)

[8] cf. Section 2.5

the pseudoscalar current by Z_5^P as given in Eq. (2.23a). Furthermore, only the top-quark mass requires renormalization at this order in α and α_S. However, this has no effect on the first non-vanishing term in the expansion in $\frac{1}{M_t^2}$ because it does not depend on M_t. Finally, one obtains

$$\mathcal{M}_{h,t} = \frac{i\alpha}{4\pi} g_t \left(Q_t\right)^2 s \left\{ \frac{4}{3} n_c - n_c C_F \frac{\alpha_S}{\pi} + \mathcal{O}\left(\alpha_S^2, \frac{s}{M_t^2}\right) \right\}, \tag{8.24a}$$

$$\mathcal{M}_{A,t} = \frac{-\alpha}{4\pi} \tilde{g}_t \left(Q_t\right)^2 \left\{ 4 n_c + \mathcal{O}\left(\alpha_S^2, \frac{s}{M_t^2}\right) \right\}, \tag{8.24b}$$

where $Q_t = \frac{2}{3}$ is the top-quark charge, $n_c = 3$ the number of colors, $C_F = \frac{4}{3}$, and $s = (p_1 + p_2)^2 = M_h^2$. In both cases the leading term proportional to M_t^2 vanishes so that the limit $M_t \to \infty$ exists. For the pseudoscalar decay, the $\mathcal{O}(\alpha_S)$ corrections are zero in this limit after multiplying the finite renormalization to restore the correct chiral anomaly.

8.2.3 *Evaluation with FDRcalc*

Now we put the program `FDRcalc` to use in combination with `qgraf` and `q2e/exp` as explained in Section 8.1. Some additional steps are necessary, which we insert in the appropriate fold of the input file[9] and will be explained in the following. Afterwards, numerical results will be presented.

8.2.3.1 *Details of the Setup*

We start by using `qgraf` and `q2e/exp` as usual except that we take the fermion traces in four dimensions so that `FORM` uses relations for traces involving γ_5. In the end, instead of the `MATAD` files that perform the integration of the vacuum integrals, new routines are called, which interpret the integrand in FDR and print them so that they can be included from the input file for `FDRcalc`.

In order to use the current implementation correctly, we have to make sure that external momenta appear neither in the propagators nor in scalar products with loop momenta. The expansion of the propagators is dealt with by `exp`. For the numerator this can be achieved in a straight-forward way using reduction identities based on Lorentz

[9] cf. Listing 1

invariance, which hold for two-loop vacuum integrals in four dimensions:

$$l_{i_1}^{\mu_1} l_{i_2}^{\mu_2} = \frac{1}{4} l_{i_1} \cdot l_{i_2} g^{\mu_1\mu_2}, \tag{8.25a}$$

$$\begin{aligned} l_{i_1}^{\mu_1} l_{i_2}^{\mu_2} l_{i_3}^{\mu_3} l_{i_4}^{\mu_4} = \frac{1}{72} &\left(g^{\mu_1\mu_2} g^{\mu_3\mu_4} \quad g^{\mu_1\mu_3} g^{\mu_2\mu_4} \quad g^{\mu_1\mu_4} g^{\mu_2\mu_3} \right) \\ &\cdot \begin{pmatrix} 5 & -1 & -1 \\ -1 & 5 & -1 \\ -1 & -1 & 5 \end{pmatrix} \begin{pmatrix} l_{i_1} \cdot l_{i_2} l_{i_3} \cdot l_{i_4} \\ l_{i_1} \cdot l_{i_3} l_{i_2} \cdot l_{i_4} \\ l_{i_1} \cdot l_{i_4} l_{i_2} \cdot l_{i_4} \end{pmatrix}, \end{aligned} \tag{8.25b}$$

$$l_{i_1}^{\mu_1} \cdots l_{i_n}^{\mu_n} = 0 \quad \text{for } n \text{ odd}, \tag{8.25c}$$

where $i_1, i_2 \in \{1, 2\}$. These relations are sufficient for the first non-vanishing terms for $\phi \to \gamma\gamma$. Calculation of higher terms in the $\frac{1}{M_t}$ expansion would require relations for higher-rank tensor integrals. After employing these relations, the tensor structure of the result is disclosed. In case of the scalar Higgs decay, we take the coefficient of $g^{\mu_1\mu_2}$, whereas for the pseudoscalar decay there is only one structure $\epsilon^{\mu_1\mu_2 q_1 q_2}$ at this point, which we simply set to one.

The questions is whether and if yes, when to cancel scalar products of loop momenta against propagators, using for example the relation

$$\frac{l_i^2}{\overline{l_i}^2} = 1 + \frac{\mu^2}{\overline{l_i}^2}, \quad i = 1, 2, \tag{8.26}$$

because the μ^2 terms in the numerator need special treatment. In Ref. [94] this is done right after the tensor reduction but before the partial fractioning, treating the μ^2 terms as separate objects. For a completely analytic calculation this certainly makes sense, but in our approach, which aims for a high degree of automation, this appears to produce unnecessary complication. The partial fractioning leads to additional scalar products in the numerator anyway, which are dealt with by the introduction of derivatives of Schwinger parameters, as discussed in Section B.1.2. However, a lot of powers l_i in the numerator cause several derivatives and thus higher powers of $\det(A)$ in the denominator. Since the region where $\det(A)$ becomes small is slightly problematic anyway,[10] we make repeated use of Eq. (8.26).

$$\frac{l_i^2}{\overline{l_i}^2 - M^2} = 1 + \frac{M^2 + \mu^2}{\overline{l_i}^2 - M^2}, \quad i = 1, 2, \tag{8.27}$$

for the sake of numerical stability right after the partial fractioning. The price to pay is that integrals with powers of μ^2 in the numerator are introduced. Potentially, the term on the very right may cause polynomially divergent integral which gives a finite contribution if multiplied with powers of μ^2. This causes some new types of integrals that have to be treated case by case, which however fit easily in the `CalcInt*` routines.

[10] See Section B.3 for details.

In the problem at hand, it is useful to fix the reference scale M introduced during the matching to standard integrals. The only scale entering the loop integrations is the top-quark mass, so we set $M = M_t$ before the intermediate result for `Mathematica` is written. This enables us to separate different terms in the $\frac{1}{M_t}$ expansion at this point, because the integrals no longer depend on any scale.

8.2.3.2 *Numerical Results*

The structure of the one-loop vacuum integrals is so simple that the auxiliary integrals are identical to the original ones and no numerical integration is required. Because of this, the LO results are reproduced exactly by `FDRcalc`.

Next we determine the NLO correction factors $\frac{\mathcal{M}^{(1)}_{\phi,t}}{\mathcal{M}^{(0)}_{\phi,t}}$ for $\phi = h, A$. Our default choice for the aspired accuracy and the distance from the integration boundaries, up to which the integrand is extrapolated, are $\epsilon = 10^{-6}$ and $\kappa = 10^{-10}$, respectively. Using these parameters we obtain

$$\frac{\mathcal{M}^{(1)}_{h,t}}{\mathcal{M}^{(0)}_{h,t}} = (1.9 \pm 3.3) \cdot 10^{-6} \frac{M_t^2}{s} - 1 - (2.7 \pm 0.7) \cdot 10^{-6} + \mathcal{O}\left(\frac{s}{M_t^2}\right), \tag{8.28a}$$

$$\frac{\mathcal{M}^{(1)}_{A,t}}{\mathcal{M}^{(0)}_{A,t}} = (0.1 \pm 0.8) \cdot 10^{-6} + \mathcal{O}\left(\frac{s}{M_t^2}\right). \tag{8.28b}$$

This agrees well with the DR result given in Eq. (8.24), although for the scalar case the deviation is a bit larger than ϵ.

Note that we did not have to perform any renormalization. It was already shown in Ref. [93] that FDR produces the correct axial anomaly at one-loop. The fact that we did not need to renormalize the pseudoscalar current can be seen as strong indication that FDR respects chiral symmetry also at higher orders in contrast to DR.

8.3 THE ρ PARAMETER TO ORDER $G_F M_t^2 \alpha_S$

As a second physical application at the two-loop level we consider QCD corrections to the ρ parameter. As discussed in Section 1.3.2, the relation

$$\rho = \frac{M_W^2}{\cos\theta_w^2 M_Z^2} = 1 \tag{8.29}$$

imposes an important constraint on a possible extended Higgs sector.

However, this relation is valid only at tree level. Heavy-quark loops, as shown in Fig. 29a, yield small corrections. Writing

$$\rho = 1 + \delta\rho, \tag{8.30}$$

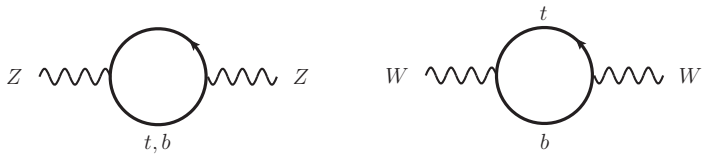

(a) One loop

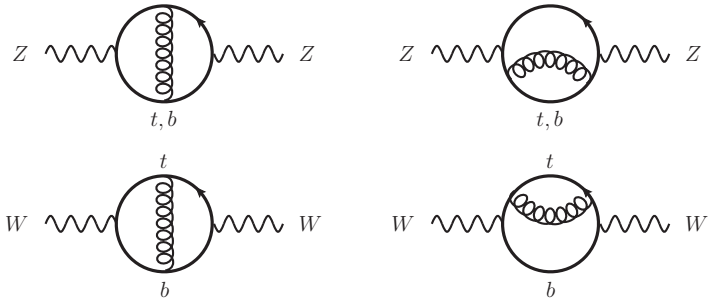

(b) Two loop

Figure 29: Heavy-quark contributions to the W and Z propagator

these can be expressed as

$$\delta\rho = \frac{\Pi_{ZZ}(0)}{M_Z^2} - \frac{\Pi_{WW}(0)}{M_W^2}, \tag{8.31}$$

where $\Pi_{VV}(0)$, $V \in \{W, Z\}$, denotes the transverse part of the weak gauge boson polarization function evaluated at vanishing momentum. Since $g^{\mu\nu}$ is the only available tensor structure at vanishing momentum, we can simply multiply by the projector $\frac{1}{4}g^{\mu\nu}$ to obtain the coefficient. We will recalculate the contribution from the top-bottom doublet in the limit $M_b \to 0$ to order $G_F M_t^2 \alpha_S$ using `FDRcalc` in the same way as described in Section 8.2.3.[11] To this end, diagrams like those in Fig. 29b need to be evaluated.

The DR result, which we quote from Ref. [102] for comparison, depends on the renormalization scheme for the top-quark mass and reads

$$\delta\rho^{\overline{\text{MS}}} = \frac{3G_F\left(M_t^{\overline{\text{MS}}}\right)^2}{8\sqrt{2}\pi^2}\left[1 + \frac{\alpha_S}{\pi}\left(2 - \frac{4}{3}\zeta_2 + 2L\right) + \mathcal{O}\left(\alpha_S^2\right)\right], \tag{8.32a}$$

$$\delta\rho^{\text{pole}} = \frac{3G_F\left(M_t^{\text{pole}}\right)^2}{8\sqrt{2}\pi^2}\left[1 + \frac{\alpha_S}{\pi}\left(-\frac{2}{3} - \frac{4}{3}\zeta_2\right) + \mathcal{O}\left(\alpha_S^2\right)\right], \tag{8.32b}$$

in the terms of the $\overline{\text{MS}}$ and the pole mass, respectively, where $L = \ln\left(\frac{\mu^2}{M_t^2}\right)$.

[11] For DR results in this limit up to $\mathcal{O}\left(G_F M_t^2 \alpha_S^2\right)$ see Ref. [102].

In FDR we obtain at first the following result:

$$\begin{aligned}\delta\rho^{\text{FDR}} &= \frac{3G_F\left(M_t^{\text{FDR}}\right)^2}{8\sqrt{2}\pi^2}\left[1+\frac{\alpha_S}{\pi}\left(2L+0.4734216(3)\right)\right]\\ &= \frac{3G_F\left(M_t^{\text{FDR}}\right)^2}{8\sqrt{2}\pi^2}\left[1+\frac{\alpha_S}{\pi}\left(2L+\frac{8}{3}-\frac{4}{3}\zeta_2\right.\right.\\ &\qquad\left.\left.+(4\pm3)\cdot10^{-7}\right)\right],\end{aligned} \tag{8.33}$$

where M_t^{FDR} is the bare FDR mass. Note that this mass is *not* the $\overline{\text{MS}}$ mass although the result from Section 7.4 might suggest that one-loop corrections evaluated in FDR are always identical to the $\overline{\text{MS}}$ result. Comparing Eq. (8.33) to Eq. (8.32a) we see that the logarithmic term is the same as in the $\overline{\text{MS}}$ scheme but the finite part is not. The relation to the pole mass is given by [94]

$$\frac{M_t^{\text{FDR}}}{M_t^{\text{pole}}} = 1+\frac{\alpha_S}{\pi}\left(-L-\frac{5}{3}\right)+\mathcal{O}\left(\alpha_S^2\right). \tag{8.34}$$

Performing this finite renormalization and discarding the numerical error yields

$$\delta\rho^{\text{FDR}} = \frac{3G_F\left(M_t^{\text{pole}}\right)^2}{8\sqrt{2}\pi^2}\left[1+\frac{\alpha_S}{\pi}\left(-\frac{2}{3}-\frac{4}{3}\zeta_2\right)+\mathcal{O}\left(\alpha_S^2\right)\right] \tag{8.35}$$

for the FDR result, which is identical to the DR result expressed in terms of the pole mass as given in Eq. (8.32b).

8.4 THE PHOTON PROPAGATOR TO ORDER $\alpha\alpha_S$

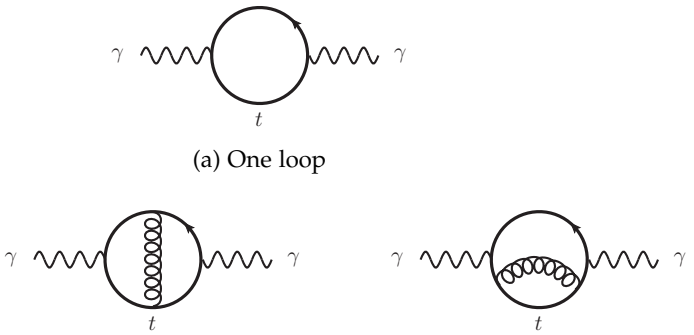

(a) One loop

(b) Two loop

Figure 30: Top-quark contributions to the photon propagator at NLO QCD

Using the same setup as in the previous sections we also calculate QCD corrections to the top-quark contribution to the photon propagator at vanishing momentum. Diagrams contributing at order α and

$\alpha\alpha_S$ are shown in Figs. 30a and 30b, respectively, and are similar to the ones evaluated in Section 8.3, except that only vector couplings are present.

Note that the quantity $\Pi_{\gamma\gamma}$ defined analogously to Π_{VV} vanishes due to the Ward identity, which we also verify numerically with our setup:

$$\begin{aligned}\Pi^{\text{FDR}}_{\gamma\gamma}(0) = \frac{\alpha}{4\pi} n_c \left(M_t^{\text{FDR}}\right)^2 (0L + 0) \\ + \frac{\alpha}{4\pi}\frac{\alpha_S}{4\pi} N_A T_R \left(M_t^{\text{FDR}}\right)^2 \left(0L + (0.5 \pm 4.7)\cdot 10^{-5}\right)\end{aligned} \tag{8.36}$$

As before we have defined $L = \ln\left(\frac{\mu^2}{M_t^2}\right)$ and $n_c = 3$ denotes the number of colors.

More interesting is the quantity $\Pi'_{\gamma\gamma}(0)$, which corresponds to the usual Quantum Electrodynamics (QED) vacuum polarization function at zero momentum. To calculate it, we multiply by the projector

$$\frac{1}{(d-1)q^2}\left(g^{\mu\nu} - \frac{q^\mu q^\nu}{q^2}\right)$$

(with $d = 4$ for FDR) and let $q^2 \to 0$ afterwards. Let us first show the DR result for comparison. In this case the unrenormalized result, which we calculate with `MATAD`, reads for vanishing momentum:

$$\begin{aligned}\Pi'_{\gamma\gamma}(0) = \frac{\alpha}{4\pi} n_c \left(-\frac{4}{3\epsilon} - \frac{2}{3}\zeta_2\epsilon\right)\left(\frac{\mu^2}{M_{t,0}^2}\right)^\epsilon \\ + \frac{\alpha}{4\pi}\frac{\alpha_S}{4\pi} N_A T_R \left(\frac{6}{\epsilon} - \frac{13}{3}\right)\left(\frac{\mu^2}{M_{t,0}^2}\right)^{2\epsilon} + \mathcal{O}\left(\alpha^2, \alpha\alpha_S^2\right),\end{aligned} \tag{8.37}$$

where $M_{t,0}$ is the bare top-quark mass. The result does not depend on the renormalization scheme for M_t at this order. Using either Eq. (2.19) or Eq. (2.20) and expanding in ϵ yields

$$\begin{aligned}\Pi'_{\gamma\gamma}(0) &= \frac{\alpha}{4\pi} n_c \left(-\frac{4}{3\epsilon} - \frac{4}{3}\ln\left(\frac{\mu^2}{M_t^2}\right)\right)\left(1 + 2\frac{\alpha_S}{\pi}C_F\frac{3}{4}\right) \\ &\quad + \frac{\alpha}{4\pi}\frac{\alpha_S}{4\pi} N_A T_R \left(\frac{6}{\epsilon} + 12\ln\left(\frac{\mu^2}{M_t^2}\right) - \frac{13}{3}\right) \\ &= \frac{\alpha}{4\pi} n_c \left(-\frac{4}{3\epsilon} - \frac{4}{3}\ln\left(\frac{\mu^2}{M_t^2}\right)\right) \\ &\quad + \frac{\alpha}{4\pi}\frac{\alpha_S}{4\pi} N_A T_R \left(-\frac{2}{\epsilon} + 4\ln\left(\frac{\mu^2}{M_t^2}\right) - \frac{13}{3}\right).\end{aligned} \tag{8.38}$$

In the last line we have used that $n_c C_F = N_A T_R$.

In the calculation with `FDRcalc` the numerical stability appears to be more difficult for this problem. Setting the integration parameters to $\kappa = 10^{-6}$ and $\epsilon = 10^{-3}$ we obtain

$$\Pi'(0)^{\text{FDR}}_{\gamma\gamma} = \frac{\alpha}{4\pi} n_c \left(-\frac{4}{3}L + 0\right) + \frac{\alpha}{4\pi}\frac{\alpha_S}{4\pi} N_A T_R \left(4.0000L - 1.7917(4)\right). \tag{8.39}$$

Comparing this result to the finite DR terms, we observe a similar behavior as for the ρ parameter. The one-loop result and the logarithmic term of the two-loop contribution are identical but the finite two-loop part is not. Note that this is not problematic at all because $\Pi'(0)$ is not a proper observable. This merely shows once again that unrenormalized FDR results are generally different from the $\overline{\text{MS}}$ scheme.

8.5 CONCLUSION AND OUTLOOK

A method to calculate IR-finite two-loop integrals in FDR numerically was introduced and an implementation for the case of vanishing external momenta was presented. For important physical applications we found satisfying agreement with existing results, reassuring the consistency of the FDR approach.

The logical next step would be to modify the implementation to allow for finite external momenta. To this end, it would be necessary to generalize the calculation of the derivatives based on the algebra (8.10), which is needed to take into account scalar products in the numerator. This task is in principle straight-forward, but as it might generate much more terms than before, it must be organized efficiently. Secondly, the non-linear rs^2 terms[12] must be included in the auxiliary integrals, leading to more complicated expressions during the analytic integration in `Mathematica`. If arbitrary values of the external momenta are to be allowed, the construction of suitable contour deformations for the numerical evaluation like in Section 7.4 must be implemented, which is more involved for two-loop case, however.

Furthermore it would be desirable to extend the class of integrals that are covered by the method. For example one could aim at including IR-divergent two-loop integrals, or at increasing the loop order. In both cases, contributions proportional to $\ln^i(\mu^2)$ with $i > 2$ would have to be incorporated.

In addition, the use of reduction techniques like integration-by-parts identities, as proposed in Ref. [103], would be desirable to reduce the cost of the calculation of complete amplitudes.

Since observables calculated in FDR are finite by construction and require a finite renormalization at most, one might interpret unrenormalized FDR results as physical quantities expressed in a new scheme,

[12] cf. Eq. (7.52b)

which is similar, yet not identical, to the $\overline{\text{MS}}$ scheme. It appears worthwhile to investigate this possibility in more detail.

Part IV

APPENDIX

A

DIMENSIONALLY-REGULATED INTEGRALS

A.1 MASSLESS ONE-LOOP INTEGRALS

A.1.1 *Definitions*

The integrals appearing explicitly in this work have vanishing internal masses. For scalar integrals, i.e. such without loop momenta in the numerator, we use the notation

$$B_0(p^2) := \mu^{4-d} \int \frac{d^d l}{(2\pi)^d} \frac{1}{l^2 (l+p)^2}, \tag{A.1a}$$

$$C_0(p_1^2, p_2^2, p_{12}^2) := \mu^{4-d} \int \frac{d^d l}{(2\pi)^d} \cdot \frac{1}{l^2 (l+p_1)^2 (l+p_1+p_2)^2}, \tag{A.1b}$$

$$\begin{aligned} &D_0(p_1^2, p_2^2, p_3^2, p_{123}^2, p_{12}^2, p_{23}^2) \\ &\quad := \mu^{4-d} \int \frac{d^d l}{(2\pi)^d} \frac{1}{l^2 (l+p_1)^2 (l+p_{12})^2 (l+p_{123})^2}, \end{aligned} \tag{A.1c}$$

where $p_{12} := p_1 + p_2$ etc. The scale μ fixes the mass dimension for $d \neq 4$ and can be identified with the renormalization or factorization scale. Tensor integrals we write as

$$B^{\mu_1 \cdots \mu_k}(p) := \mu^{4-d} \int \frac{d^d l}{(2\pi)^d} \frac{l^{\mu_1} \dots l^{\mu_k}}{l^2 (l+p)^2}, \tag{A.2a}$$

$$C^{\mu_1 \cdots \mu_k}(p_1, p_2) := \mu^{4-d} \int \frac{d^d l}{(2\pi)^d} \frac{l^{\mu_1} \dots l^{\mu_k}}{l^2 (l+p_1)^2 (l+p_1+p_2)^2}, \tag{A.2b}$$

$$\begin{aligned} &D^{\mu_1 \cdots \mu_k}(p_1, p_2, p_3) \\ &\quad := \mu^{4-d} \int \frac{d^d l}{(2\pi)^d} \frac{l^{\mu_1} \dots l^{\mu_k}}{l^2 (l+p_1)^2 (l+p_{12})^2 (l+p_{123})^2}. \end{aligned} \tag{A.2c}$$

A.1.2 *Scalar Integrals*

We use analytic results for the scalar integrals as presented in Ref. [104]. The two-point integral reads

$$B_0(s) = \frac{i r_\Gamma}{(4\pi)^{2-\epsilon}} \left(-\frac{\mu^2}{s}\right)^\epsilon \left[\frac{1}{\epsilon} + 2 + 4\epsilon + 8\epsilon^2 + \mathcal{O}\left(\epsilon^3\right)\right], \tag{A.3}$$

where $d = 4 - 2\epsilon$ has been inserted and

$$r_\Gamma = 1 - \gamma_E \epsilon + \left(\frac{\gamma_E^2}{2} - \frac{\pi^2}{12}\right) \epsilon^2. \tag{A.4}$$

For the three-point function we only need two special cases:

$$C_0(0,0,s_{12}) = \frac{ir_\Gamma}{(4\pi)^{2-\epsilon}} \frac{1}{s_{12}^2} \left(-\frac{\mu^2}{s_{12}^2}\right)^\epsilon \frac{1}{\epsilon^2}, \tag{A.5a}$$

$$C_0(p_1^2,p_2^2,0) = \frac{ir_\Gamma}{(4\pi)^{2-\epsilon}} \frac{1}{p_1^2-p_2^2} \left[\left(-\frac{\mu^2}{p_1^2}\right)^\epsilon - \left(-\frac{\mu^2}{p_2^2}\right)^\epsilon\right] \frac{1}{\epsilon^2}. \tag{A.5b}$$

The four-point function with one massive external leg is given by

$$\begin{aligned} &D_0(0,0,0,p_4^2,s_{12},s_{23}) \\ &= \frac{ir_\Gamma}{(4\pi)^{2-\epsilon}} \frac{1}{s_{12}s_{23}} \left\{ \frac{2}{\epsilon^2} \left[\left(-\frac{\mu^2}{s_{12}}\right)^\epsilon + \left(-\frac{\mu^2}{s_{23}}\right)^\epsilon - \left(-\frac{\mu^2}{p_4^2}\right)^\epsilon\right] \right. \\ &\quad \left. -2\,\mathrm{Li}_2\left(1-\frac{p_4^2}{s_{12}}\right) - 2\,\mathrm{Li}_2\left(1-\frac{p_4^2}{s_{23}}\right) - \ln^2\left(\frac{s_{12}}{s_{23}}\right) - \frac{\pi^2}{3}. \right\} \end{aligned} \tag{A.6}$$

A.1.3 *Passarino-Veltman Reduction*

At the one-loop level, tensor integrals can always be reduced to scalar integrals. To this end we apply the traditional reduction approach by Passarino and Veltman [105]. It is based on the observation that scalar products of loop and external momenta can be written in terms of inverse propagators and thus be canceled, e.g.

$$\frac{p\cdot l}{l^2(l+p)^2} = \frac{1}{2}\left[\frac{1}{l^2} - \frac{1}{(l+p)^2} - \frac{p^2}{l^2(l+p)^2}\right]. \tag{A.7}$$

If the momentum p enters the loop integral, such a relation can always be found. Thus the power of l in the numerator is reduced by one. Successively one arrives at scalar integrals.

General n-point tensor integrals can be written in the form

$$I^{\mu_1\cdots\mu_k}(p_1,\cdots,p_n) = \sum_j T_j^{\mu_1\cdots\mu_k}(p_1,\cdots,p_n) I_j(\{p_a\cdot p_b\}), \tag{A.8}$$

where the sum is over all symmetric tensor structure $T_j^{\mu_1\cdots\mu_k}$ that can be build from the external momenta and $g^{\mu\nu}$. The coefficients, which only depend on invariants of the external momenta, can then be obtained by inverting the matrix equation

$$\sum_j T_{ij} I_j = T_{i,\mu_1\cdots\mu_k} I^{\mu_1\cdots\mu_k}, \tag{A.9a}$$

$$T_{ij} := T_{i,\mu_1\cdots\mu_k} T_j^{\mu_1\cdots\mu_k}. \tag{A.9b}$$

A practical problem may arise from the determinant of T_{ij} appearing in the denominator in phase-space regions where it becomes small. This is why we will try to cancel it as often as possible.

A.1.4 *Integration Routine tribox*

The integration routine `tribox` applies Passarino-Veltman reduction to massless triangle and box diagrams to obtain an analytic result in terms of scalar integrals like Eqs. (A.3) to (A.6). It is written in `FORM`, used in combination with the `exp/q2e` setup described in Section 2.6, and is an advanced version of the code developed in Refs. [106, 55].

For box integrals there are three different topologies, where the first one corresponds to the integral (A.1c) and the two other ones result from swapping either $p_1 \leftrightarrow p_2$ or $p_1 \leftrightarrow p_3$. Depending on the topology the terms are matched to tensor integrals as in Eq. (A.2). Then the corresponding expansions as defined in the next subsection are inserted.

Next the results for tensor coefficients are plugged in. Simplification is achieved mainly by partial fractioning e.g. with respect to t by repeatedly making use of relations like

$$\frac{t}{(t-m_4^2)} = 1 + \frac{m_4^2}{(t-m_4^2)}, \tag{A.10a}$$

$$\frac{1}{t(t-m_4^2)} = -\frac{1}{m_4^2 t} + \frac{1}{m_4^2(t-m_4^2)}. \tag{A.10b}$$

Finally, the ϵ expansions of scalar integrals shown in Section A.1.2 are inserted as well.

A.1.5 *Definition of Coefficients*

In the following we fix the definition of the coefficients implemented in `tribox` used in this work. They have been calculated by solving Eq. (A.9) but are too long to be printed here.

The two-point tensor integrals up to rank four we write as

$$B^{\mu} = B_{11} p^{\mu}, \tag{A.11a}$$

$$B^{\mu\nu} = B_{21} p^{\mu} p^{\nu} + B_{22} g^{\mu\nu}, \tag{A.11b}$$

$$B^{\mu\nu\rho} = B_{31} p^{\mu} p^{\nu} p^{\rho} + B_{32} g^{[\mu\nu} p^{\rho]}, \tag{A.11c}$$

$$B^{\mu\nu\rho\sigma} = B_{41} p^{\mu} p^{\nu} p^{\rho} p^{\sigma} + B_{42} g^{[\mu\nu} p^{\rho} p^{\sigma]} + B_{43} g^{[\mu\nu} g^{\rho\sigma]}, \tag{A.11d}$$

where the coefficients depend on p^2.

The three-point coefficients are functions of p_1^2, p_2^2, and p_{12}^2:

$$C^{\mu} = C_{11} p_1^{\mu} + C_{12} p_2^{\mu}, \tag{A.12a}$$

$$C^{\mu\nu} = C_{21} p_1^{\mu} p_1^{\nu} + C_{22} p_2^{\mu} p_2^{\nu} + C_{23} p_1^{[\mu} p_2^{\nu]} + C_{24} g^{\mu\nu}, \tag{A.12b}$$

$$\begin{aligned} C^{\mu\nu\rho} = {} & C_{31} p_1^{\mu} p_1^{\nu} p_1^{\rho} + C_{32} p_2^{\mu} p_2^{\nu} p_2^{\rho} + C_{33} p_1^{[\mu} p_1^{\nu} p_2^{\rho]} \\ & + C_{34} p_1^{[\mu} p_2^{\nu} p_2^{\rho]} + C_{35} g^{[\mu\nu} p_1^{\rho]} + C_{36} g^{[\mu\nu} p_2^{\rho]}. \end{aligned} \tag{A.12c}$$

In case of four-point integrals, the coefficients are only functions of p_{12}^2, p_{13}^2, p_{23}^2, and p_{123}^2, since we assume $p_1^2 = p_2^2 = p_3^2 = 0$. The following ones are required in this work:

$$D^{\mu} = D_{11} p_1^{\mu} + D_{12} p_2^{\mu} + D_{13} p_3^{\mu}, \tag{A.13a}$$

$$\begin{aligned} D^{\mu\nu} = {} & D_{21} p_1^{\mu} p_1^{\nu} + D_{22} p_2^{\mu} p_2^{\nu} + D_{23} p_3^{\mu} p_3^{\nu} \\ & + D_{24} p_1^{[\mu} p_2^{\nu]} + D_{25} p_1^{[\mu} p_3^{\nu]} + D_{26} p_2^{[\mu} p_3^{\nu]} \\ & + D_{27} g^{\mu\nu}, \end{aligned} \tag{A.13b}$$

$$\begin{aligned} D^{\mu\nu\rho} = {} & D_{31} p_1^{\mu} p_1^{\nu} p_1^{\rho} + D_{32} p_2^{\mu} p_2^{\nu} p_2^{\rho} + D_{33} p_3^{\mu} p_3^{\nu} p_3^{\rho} \\ & + D_{34} p_1^{[\mu} p_1^{\nu} p_2^{\rho]} + D_{35} p_1^{[\mu} p_1^{\nu} p_3^{\rho]} + D_{36} p_2^{[\mu} p_2^{\nu} p_1^{\rho]} \\ & + D_{37} p_2^{[\mu} p_2^{\nu} p_3^{\rho]} + D_{38} p_3^{[\mu} p_3^{\nu} p_1^{\rho]} + D_{39} p_3^{[\mu} p_3^{\nu} p_2^{\rho]} \\ & + D_{310} p_1^{[\mu} p_2^{\nu} p_3^{\rho]} + D_{311} g^{[\mu\nu} p_1^{\rho]} + D_{312} g^{[\mu\nu} p_2^{\rho]} \\ & + D_{313} g^{[\mu\nu} p_3^{\rho]}, \end{aligned} \tag{A.13c}$$

$$\begin{aligned} D^{\mu\nu\rho\sigma} = {} & D_{41} p_1^{\mu} p_1^{\nu} p_1^{\rho} p_1^{\sigma} + D_{42} p_2^{\mu} p_2^{\nu} p_2^{\rho} p_2^{\sigma} + D_{43} p_3^{\mu} p_3^{\nu} p_3^{\rho} p_3^{\sigma} \\ & + D_{44} p_1^{[\mu} p_1^{\nu} p_1^{\rho} p_2^{\sigma]} + D_{45} p_1^{[\mu} p_1^{\nu} p_1^{\rho} p_3^{\sigma]} + D_{46} p_2^{[\mu} p_2^{\nu} p_2^{\rho} p_1^{\sigma]} \\ & + D_{47} p_2^{[\mu} p_2^{\nu} p_2^{\rho} p_3^{\sigma]} + D_{48} p_3^{[\mu} p_3^{\nu} p_3^{\rho} p_1^{\sigma]} + D_{49} p_3^{[\mu} p_3^{\nu} p_3^{\rho} p_2^{\sigma]} \\ & + D_{410} p_1^{[\mu} p_1^{\nu} p_2^{\rho} p_2^{\sigma]} + D_{411} p_1^{[\mu} p_1^{\nu} p_3^{\rho} p_3^{\sigma]} + D_{412} p_2^{[\mu} p_2^{\nu} p_3^{\rho} p_3^{\sigma]} \\ & + D_{413} p_1^{[\mu} p_1^{\nu} p_2^{\rho} p_3^{\sigma]} + D_{414} p_2^{[\mu} p_2^{\nu} p_1^{\rho} p_3^{\sigma]} + D_{415} p_3^{[\mu} p_3^{\nu} p_1^{\rho} p_2^{\sigma]} \\ & + D_{416} g^{[\mu\nu} p_1^{\rho} p_1^{\sigma]} + D_{417} g^{[\mu\nu} p_2^{\rho} p_2^{\sigma]} + D_{418} g^{[\mu\nu} p_3^{\rho} p_3^{\sigma]} \\ & + D_{419} g^{[\mu\nu} p_1^{\rho} p_2^{\sigma]} + D_{420} g^{[\mu\nu} p_1^{\rho} p_3^{\sigma]} + D_{421} g^{[\mu\nu} p_2^{\rho} p_3^{\sigma]} \\ & + D_{422} g^{[\mu\nu} g^{\rho\sigma]}. \end{aligned} \tag{A.13d}$$

A.2 PHASE-SPACE PARAMETRIZATION

In this section we present the phase-space parametrization used in the calculation of NLO QCD corrections to $gg \to HZ$ presented in Chapter 4, i.e. for the cases of two massive and two massive plus one massless particles.[1] Thanks to the subtraction method[2], the phase-space integration can be carried out in four dimensions. Nevertheless we present the expressions in $d = 4 - 2\epsilon$ dimension here.

A.2.1 *Phase Space for Two Massive Particles*

Let p_1 and p_2 denote the four-momenta of the incoming particles, which are assumed to be massless, and p_3 and p_4 those of the outgoing ones, which have masses m_3 and m_4, respectively. The two-particle phase-space factor in d dimensions in the center-of-mass frame

[1] This section is mostly taken from the appendix of Ref. [106]. The derivation given there was in turn based on Ref. [107], where the case of one massive and two massless particles was treated.

[2] cf. Section 2.4.2

of p_1 and p_2 (or p_3 and p_4), which we simply quote here, can be written as

$$\mathrm{dPS}_2 = \frac{1}{8\pi}\frac{(4\pi)^\epsilon}{\Gamma(1-\epsilon)}\frac{1}{s^{1-\epsilon}}\lambda^{1/2-\epsilon}(m_3^2, m_4^2, s)\; y^{-\epsilon}(1-y)^{-\epsilon}\mathrm{d}y\,, \tag{A.14}$$

where $s = (p_1 + p_2)^2$ and

$$\lambda(x, y, z) = x^2 + y^2 + z^2 - 2xy - 2xz - 2xy. \tag{A.15}$$

The variable y can have values between 0 and 1 and is connected to the angle θ between the two final state particles by

$$y \equiv \frac{1}{2}(1 - \cos\theta). \tag{A.16}$$

Finally we give expressions for the Mandelstam varibles $t := (p_1 - p_3)^2$ and $u := (p_2 - p_3)^2$ in terms of the integration variable y:

$$t = -\frac{1}{2}\left(s - m_3^2 - m_4^2 + (2y-1)\lambda^{\frac{1}{2}}(m_3^2, m_4^2, s)\right), \tag{A.17a}$$

$$u = -\frac{1}{2}\left(s - m_3^2 - m_4^2 - (2y-1)\lambda^{\frac{1}{2}}(m_3^2, m_4^2, s)\right). \tag{A.17b}$$

A.2.2 *Phase Space for Two Massive and One Massless Particle*

The parametrization of the three-particle phase space has been slightly improved compared to Ref. [106] and will be re-derived in the following. Let again p_1 and p_2 denote the momenta of the massless incoming and p_3, p_4 and p_5 those of the outgoing particles, where $m_3 = 0$ and $m_4, m_5 \neq 0$. In the center of mass frame the phase-space element is given by

$$\begin{aligned}\mathrm{dPS}_3 &= \frac{\mathrm{d}^{d-1}p_3}{(2\pi)^{d-1}2E_3}\frac{\mathrm{d}^{d-1}p_4}{(2\pi)^{d-1}2E_4}\frac{\mathrm{d}^{d-1}p_5}{(2\pi)^{d-1}2E_5} \\ &\quad\cdot(2\pi)^d\,\delta^{(d)}(p_1 + p_2 - p_3 - p_4 - p_5) \\ &= \frac{\mathrm{d}^{d-1}p_3\,\mathrm{d}^{d-1}p_4}{(2\pi)^{2d-3}8E_3E_4E_5}\,\delta(\sqrt{s} - E_3 - E_4 - E_5),\end{aligned} \tag{A.18}$$

where $\vec{p}_i$ denotes the $(d-1)$-dimensional spatial part of p_i, and the energy components are given by

$$E_3 = |\vec{p}_3|, \tag{A.19a}$$

$$E_4 = \sqrt{m_4^2 + |\vec{p}_4|^2}, \tag{A.19b}$$

$$E_5 = \sqrt{m_5^2 + |\vec{p}_3 + \vec{p}_4|^2}, \tag{A.19c}$$

since momentum conservation has been used to eliminate $\vec{p}_5$.

Next we choose coordinates for p_1, p_2, and p_3 in the center-of-mass system of p_1 and p_2 as follows:

$$p_1 = \frac{\sqrt{s}}{2}(1, 0, \cdots, 0, 1), \tag{A.20}$$

$$p_2 = \frac{\sqrt{s}}{2}(1, 0, \cdots, 0, -1), \tag{A.21}$$

$$p_3 = |\vec{p}_3|(1, 0, \cdots, 0, \sin\theta, \cos\theta). \tag{A.22}$$

To determine the direction of $\vec{p}_4$ two more angles are required. It is useful to define them with respect to $\vec{p}_3$. Spherical coordinates in a system whose $(d-1)$-axis points in the direction of $\vec{p}_3$, read

$$\vec{p}_4{}' = |\vec{p}_4|(0, \cdots, \sin\chi\sin\phi, \sin\chi\cos\phi, \cos\chi). \tag{A.23}$$

Rotating into a system with $(d-1)$-axis in direction of $\vec{p}_1$,

$$\vec{p}_4 = R\,\vec{p}_4{}' \quad \text{with} \quad R = \begin{pmatrix} \mathbb{1}_{d-3} & 0 & 0 \\ 0 & \cos\theta & \sin\theta \\ 0 & -\sin\theta & \cos\theta \end{pmatrix}, \tag{A.24}$$

yields

$$\begin{aligned} p_4 = (E_4, 0, \cdots, |\vec{p}_4|\sin\chi\sin\phi, |\vec{p}_4|(\sin\theta\cos\chi + \cos\theta\sin\chi\cos\phi), \\ |\vec{p}_4|(\cos\theta\cos\chi - \sin\theta\sin\chi\cos\phi)). \end{aligned} \tag{A.25}$$

For the elements of integration one obtains

$$d^{d-1}p_3 = E_3^{d-2}\sin^{d-3}\theta\, dE_3\, d\theta\, d\Omega^{d-2}, \tag{A.26a}$$

$$\begin{aligned} d^{d-1}p_4 &= \underbrace{|\det R|}_{=1} d^{d-1}p_4' \\ &= |\vec{p}_4|^{d-2}\sin^{d-3}\chi\sin^{d-4}\phi\, d|\vec{p}_4|\, d\chi\, d\phi\, d\Omega^{d-3} \\ &= |\vec{p}_4|^{d-3}E_4\sin^{d-3}\chi\sin^{d-4}\phi\, dE_4\, d\chi\, d\phi\, d\Omega^{d-3}, \end{aligned} \tag{A.26b}$$

where Ω^n denotes the solid angle in n dimensions. Thus one has

$$\begin{aligned} dPS_3 = \frac{E_3^{d-3}|\vec{p}_4|^{d-3}}{(2\pi)^{2d-3}8E_5}\sin^{d-3}\theta\sin^{d-3}\chi\sin^{d-4}\phi \\ \cdot dE_3\, dE_4\, d\theta\, d\chi\, d\phi\, d\Omega^{d-2}\, d\Omega^{d-3}\, \delta\left(\sqrt{s} - E_3 - E_4 - E_5\right). \end{aligned} \tag{A.27}$$

In order to make use of the remaining delta function, an expression for E_5 is required. Note that E_5 is fixed if E_3, E_4, and the angle χ between $\vec{p}_3$ and $\vec{p}_4$ are known, which can be seen from relation (A.19c):

$$E_5^2 = m_5^2 + |\vec{p}_3 + \vec{p}_4|^2 = m_5^2 + E_3^2 + |\vec{p}_4|^2 + 2E_3|\vec{p}_4|\cos\chi. \tag{A.28}$$

By substituting

$$\cos\chi = \frac{E_5^2 - m_5^2 - E_3^2 - |\vec{p}_4|^2}{2E_3|\vec{p}_4|}, \tag{A.29a}$$

$$\mathrm{d}\cos\chi = \frac{E_5}{E_3|\vec{p}_4|}\mathrm{d}E_5\,, \tag{A.29b}$$

the delta function can be integrated. Performing the trivial integrations over the solid angles using $\int \mathrm{d}\Omega^n = \frac{2\pi^{n/2}}{\Gamma(n/2)}$ as well, one obtains

$$\begin{aligned}\mathrm{dPS}_3 = {} & \frac{E_3^{d-4}|\vec{p}_4|^{d-4}}{8(2\pi)^{2d-3}} \sin^{d-3}\theta \sin^{d-4}\chi \sin^{d-4}\phi \,\mathrm{d}E_3\,\mathrm{d}E_4\,\mathrm{d}E_5 \\ & \cdot \mathrm{d}\theta\,\mathrm{d}\phi\,\mathrm{d}\Omega^{d-2}\,\mathrm{d}\Omega^{d-3}\;\delta\left(\sqrt{s} - E_3 - E_4 - E_5\right) \\ = {} & \frac{E_3^{d-4}|\vec{p}_4|^{d-4}}{4(2\pi)^d\Gamma(d-3)} \sin^{d-3}\theta \sin^{d-4}\chi \sin^{d-4}\phi \\ & \cdot \mathrm{d}E_3\,\mathrm{d}E_4\,\mathrm{d}\theta\,\mathrm{d}\phi\,. \end{aligned} \tag{A.30}$$

In addition it is useful to introduce the following invariants:

$$s \equiv (p_1 + p_2)^2 = 2p_1 \cdot p_2, \tag{A.31a}$$

$$t_3 \equiv (p_1 - p_3)^2 = -2p_1 \cdot p_3, \tag{A.31b}$$

$$u_3 \equiv (p_2 - p_3)^2 = -2p_2 \cdot p_3, \tag{A.31c}$$

$$t_4 \equiv (p_1 - p_4)^2 = m_4^2 - 2p_1 \cdot p_4, \tag{A.31d}$$

$$u_4 \equiv (p_2 - p_4)^2 = m_4^2 - 2p_2 \cdot p_4, \tag{A.31e}$$

$$s_{34} \equiv (p_3 + p_4)^2 = m_4^2 + 2p_3 \cdot p_4, \tag{A.31f}$$

$$s_{35} \equiv (p_3 + p_5)^2, \tag{A.31g}$$

$$s_{45} \equiv (p_4 + p_5)^2. \tag{A.31h}$$

Only five of them are independent. Using momentum conservation it is easy to show that

$$s + t_3 + u_3 = s_{45}, \tag{A.32a}$$

$$s + t_4 + u_4 = m_4^2 + s_{35}, \tag{A.32b}$$

$$s_{34} + s_{35} + s_{45} = s + m_3^2 + m_5^2. \tag{A.32c}$$

With the choice of coordinates introduced above one obtains

$$t_3 = -\sqrt{s}E_3\,(1 - \cos\theta)\,, \tag{A.33a}$$

$$u_3 = -\sqrt{s}E_3\,(1 + \cos\theta)\,, \tag{A.33b}$$

$$t_4 = m_4^2 - \sqrt{s}\left(E_4 - \sqrt{E_4^2 - m_4^2}(\cos\theta\cos\chi - \sin\theta\sin\chi\cos\phi)\right), \tag{A.33c}$$

$$u_4 = m_4^2 - \sqrt{s}\left(E_4 + \sqrt{E_4^2 - m_4^2}(\cos\theta\cos\chi - \sin\theta\sin\chi\cos\phi)\right). \tag{A.33d}$$

Adding the first two and the last two of these relations make it possible to express the energies E_3 and E_4 in the center of mass frame in terms of invariants:

$$E_3 = \frac{1}{2\sqrt{s}}\,(-t_3 - u_3) = \frac{1}{2\sqrt{s}}\,(s - s_{45})\,, \tag{A.34a}$$

$$E_4 = \frac{1}{2\sqrt{s}}\,\left(2m_4^2 - t_4 - u_4\right) = \frac{1}{2\sqrt{s}}\,\left(m_4^2 + s - s_{35}\right). \tag{A.34b}$$

Since $E_5 = \sqrt{s} - E_3 - E_4$, inserting these relations into Eq. (A.29a) yields $\cos\chi$ in terms of invariants:

$$\cos\chi = \frac{(m_4^2 + s - s_{35})(s - s_{45}) - 2s(s + m_5^2 - s_{35} - s_{45})}{(s - s_{45})\lambda^{\frac{1}{2}}(s_{35}, m_4^2, s)}, \tag{A.35}$$

with λ as in Eq. (A.15).

Substituting E_3 and E_4 by s_{45} and s_{35} in (A.30) according to Eqs. (A.34) and using (A.35), the phase-space element can be expressed in terms of invariants and angles:

$$\begin{aligned} \mathrm{dPS}_3 = \Big(&\lambda(m_4^2, s_{35}, s)(s - s_{45})^2 \\ &- \left[(m_4^2 + s - s_{35})(s - s_{45}) - 2s(s + m_5^2 - s_{35} - s_{45})\right]^2\Big)^{-\epsilon} \\ &\cdot \frac{1}{(4\pi)^d \Gamma(d-3) s^{1-2\epsilon}} \mathrm{d}s_{35}\,\mathrm{d}s_{45}\,\sin^{d-3}\theta\,\sin^{d-4}\phi\,\mathrm{d}\theta\,\mathrm{d}\phi\,. \end{aligned} \tag{A.36}$$

From trivial conditions like $E_3 \geqslant 0$ or $E_4 \geqslant m_4$ one has

$$m_5^2 \leqslant s_{35} \leqslant (\sqrt{s} - m_4)^2, \tag{A.37a}$$

$$(m_4 + m_5)^2 \leqslant s_{45} \leqslant s. \tag{A.37b}$$

Actually, the limits of integration for s_{35} and s_{45} are coupled. Since there may be poles in $s - s_{45}$, when the massless particle becomes soft, it makes sense to choose the simpler limits for s_{45}. The limits for s_{35} then follow from $|\cos\chi| \leqslant 1$. Solving a quadratic equation one obtains

$$s_{35}^- \leqslant s_{35} \leqslant s_{35}^+, \tag{A.38}$$

where

$$\begin{aligned} s_{35}^{\pm} = \frac{1}{2s_{45}}\,&\big[(s + s_{45})m_5^2 + (s_{45} - m_3^2)(s - s_{45}) \\ &\pm (s - s_{45})\lambda^{\frac{1}{2}}(m_4^2, m_5^2, s_{45})\big]\,. \end{aligned} \tag{A.39}$$

Thus one is lead to substitute

$$\begin{aligned} s_{35} = \frac{1}{2s_{45}}\,&\Big[(s + s_{45})m_5^2 + (s_{45} - m_3^2)(s - s_{45}) \\ &- (1 - 2x)(s - s_{45})\lambda^{\frac{1}{2}}(m_4^2, m_5^2, s_{45})\Big], \end{aligned} \tag{A.40}$$

in order to arrive at limits 0 and 1. This also casts the expression for $\cos\chi$ into a simpler form. It seems to appear mostly in the following combination:

$$\lambda^{\frac{1}{2}}(m_4, s_{35}, s)\cos\chi = -\frac{1}{2s_{45}}\Big[(m_4^2 - m_5^2 + s_{45})(s - s_{45}) + (1-2x)(s+s_{45})\lambda^{\frac{1}{2}}(m_4^2, m_5^2, s)\Big]. \tag{A.41}$$

The awkward first factor on the right hand side of Eq. (A.36) is simplified as well and can be factorized:

$$\begin{aligned} &\lambda s^2(s-s_{45})^2 \\ &- \left[(m_4^2 + s - s_{35})(s-s_{45}) - 2s(s + m_5^2 - s_{35} - s_{45})\right]^2 \\ &= 4s(s-s_{45})^2 s_{45}^{-1}\lambda(m_4^2, m_5^2, s_{45})(1-x)x. \end{aligned} \tag{A.42}$$

Substituting $s_{45} = zs$ the phase-space factor finally becomes

$$\begin{aligned} \mathrm{dPS}_3 = \frac{4^{-\epsilon}\lambda^{\frac{1}{2}-\epsilon}(m_4^2, m_5^2, zs)}{(4\pi)^d\Gamma(d-3)}(1-x)^{-\epsilon}x^{-\epsilon}(1-z)^{1-2\epsilon}z^{-1+\epsilon} \\ \cdot dx\,dz\,\sin^{d-3}\theta\,\sin^{d-4}\phi\,d\theta\,d\phi\,. \end{aligned} \tag{A.43}$$

The boundaries for z are $z_{min} = \frac{(m_4+m_5)^2}{s}$ and 1, where $z \to 1$ corresponds to the soft limit. The angular integrations run from 0 to π for both θ and ϕ and may produce collinear divergencies.

B

FDR INTEGRALS

B.1 PARAMETRIZATION OF FDR-REGULATED INTEGRALS

B.1.1 *Scalar Integrals*

Let us start from a scalar integral[1] that has been made convergent with FDR and is thus at most logarithmically divergent in μ^2:

$$\mathcal{I} = \prod_{i=1}^{L} \int d^4 l_i \prod_{j=1}^{N_x} \frac{1}{\left((p_j + q_j)^2 - m_j^2 - \mu^2\right)^{\alpha_j}} \prod_{k=1}^{N_y} \frac{1}{\left(p_k^2 - \mu^2\right)^{\beta_k}}, \tag{B.1}$$

where the p_i are combinations of the loop momenta l_i, the q_i are combinations of the external momenta, and $\alpha_i, \beta_i \in \mathbb{N}$. By introducing Schwinger parameters using the relation

$$\frac{1}{A^\alpha} = \frac{(-1)^\alpha}{(-A)^\alpha} = \frac{(-1)^\alpha}{\Gamma(\alpha)} \int_0^\infty dx x^{\alpha-1} e^{xA} \tag{B.2}$$

for each propagator, one obtains

$$\begin{aligned} \mathcal{I} = (-1)^N \prod_{j=1}^{N_x} \int_0^\infty dx_j \, \frac{x_j^{\alpha_j - 1}}{\Gamma(\alpha_j)} \prod_{k=1}^{N_y} \int_0^\infty dy_k \, \frac{y_k^{\beta_k - 1}}{\Gamma(\beta_k)} \\ \cdot \prod_{i=1}^{L} \int d^4 l_i \, \exp(D), \end{aligned} \tag{B.3}$$

where we have defined

$$N := \sum_{i=1}^{N_x} \alpha_i + \sum_{j=1}^{N_y} \beta_j, \tag{B.4}$$

and the argument of the exponential can be written as

$$\begin{aligned} D &= \sum_{i=1}^{N_x} x_i ((p_i + q_i)^2 - m_i^2 - \mu^2) + \sum_{j=1}^{N_y} y_j (p_j^2 - \mu^2) \\ &= \sum_{i=1}^{N_x} (x_i p_i^2 + 2 x_i p_i \cdot q_i) + \sum_{j=1}^{N_y} y_j p_j^2 \\ &\quad - \sum_{i=1}^{N_x} x_i (m_i^2 - q_i^2) - \left(\sum_{i=1}^{N_x} x_i + \sum_{j=1}^{N_y} y_j \right) \mu^2. \end{aligned} \tag{B.5}$$

[1] By scalar integral we mean that the numerator of the integrand is equal to one.

$x = (x_1, \cdots, x_{N_x})$ are the parameters for the propagators that do not diverge at small loop momentum because they have a non-zero mass or non-zero scalar product of external momenta[2] and $y = (y_1, \cdots, y_{N_y})$ are the parameters for the remaining, possibly infrared-divergent propagators.

Before completing the square, D has to be expressed in terms of an linearly independent set of l_i, which we write as an L-dimensional vector $l = (l_1, \cdots, l_L)$.[3] Then we collect the coefficients of the scalar products, which are determined by the topology of the graph:

$$D = \sum_{i,j=1}^{L} a_{ij} l_i l_j + \sum_{i=1}^{L} 2 b_i l_i - c, \tag{B.6}$$

with

$$a_{ij} = \sum_{k \in \mathcal{X}_{ij}} x_k + \sum_{k \in \mathcal{Y}_{ij}} y_k, \tag{B.7a}$$

$$b_i = \sum_{k \in \mathcal{X}_{ii}} x_k p_k, \tag{B.7b}$$

$$c = \sum_{j=1}^{N_x} x_j (m_j^2 - q_j^2) + \left(\sum_{i=1}^{N_x} x_i + \sum_{j=1}^{N_y} y_j \right) \mu^2, \tag{B.7c}$$

where $\mathcal{X}_{ij}$ and $\mathcal{Y}_{ij}$ are empty or non-empty index sets. Obviously it is $a_{ji} = a_{ij}$.

Now we diagonalize the symmetric matrix $A := (a_{ij})$ by an orthogonal matrix O, so that $OAO^T = \operatorname{diag}(\tilde{a}_1, \cdots, \tilde{a}_L)$, and change the integration momenta to $\tilde{l} := Ol$. Making use of the orthogonality of O, the exponential can be rewritten as

$$\begin{aligned}
D &= l^T A l + 2b \cdot l - c \\
&= (Ol)^T OAO^T (Ol) + 2(Ob) \cdot (Ol) - c \\
&= \sum_{i=1}^{L} \left(\tilde{a}_i \tilde{l}_i^2 + 2(Ob)_i \cdot \tilde{l}_i \right) - c \\
&= \sum_{i=1}^{L} \tilde{a}_i \left(\tilde{l}_i + \frac{1}{\tilde{a}_i} (Ob)_i \right)^2 - \sum_{i=1}^{L} \frac{1}{\tilde{a}_i} (Ob)_i^2 - c \\
&= \sum_{i=1}^{L} \tilde{a}_i \left(\tilde{l}_i + \frac{1}{\tilde{a}_i} (Ob)_i \right)^2 - (Ob)^T \underbrace{\operatorname{diag}\left(\frac{1}{\tilde{a}_1}, \cdots, \frac{1}{\tilde{a}_L}\right)}_{=(OAO)^{-1} = OA^{-1}O^T} (Ob) - c \\
&= \sum_{i=1}^{L} \tilde{a}_i \left(\tilde{l}_i + \frac{1}{\tilde{a}_i} (Ob)_i \right)^2 - b^T A^{-1} b - c.
\end{aligned} \tag{B.8}$$

[2] At the moment, it is assumed that no thresholds are crossed, which requires in particular $q_i^2 < m_i^2$ for all i.

[3] This should be done in a way that all the p_i are positive sums of the l_i.

For the integration measure one obtains

$$\prod_{i=1}^{L} d^4\tilde{l}_i = \underbrace{\det(O)^4}_{=1} \prod_{i=1}^{L} d^4 l_i \,. \tag{B.9}$$

The next step is to shift and rescale the $\tilde{l}_i$ as

$$\tilde{l}_i \to \frac{1}{\sqrt{\tilde{a}_i}} \tilde{l}_i - \frac{1}{\tilde{a}_i} (Ob)_i \tag{B.10}$$

to obtain

$$\begin{aligned} D &= \sum_{i=1}^{L} \tilde{l}_i^2 - (Ob)^T \operatorname{diag}\left(\frac{1}{\tilde{a}_1}, \cdots, \frac{1}{\tilde{a}_L}\right)(Ob) - c \\ &= \sum_{i=1}^{L} \tilde{l}_i^2 - b^T A^{-1} b - c \end{aligned} \tag{B.11}$$

and

$$\prod_{i=1}^{L} d^4\tilde{l}_i \to \prod_{i=1}^{L} \frac{1}{\tilde{a}_i^2} d^4\tilde{l}_i = \frac{1}{\det A^2} \prod_{i=1}^{L} d^4\tilde{l}_i \,. \tag{B.12}$$

So the Schwinger-parametrized integral now reads

$$\begin{aligned} \mathcal{I} = (-1)^N \prod_{j=1}^{N_x} \int_0^\infty dx_j \, \frac{x_j^{\alpha_j - 1}}{\Gamma(\alpha_j)} \prod_{k=1}^{N_y} \int_0^\infty dy_k \, \frac{y_k^{\beta_k - 1}}{\Gamma(\beta_k)} \\ \cdot \frac{1}{\det A^2} \exp\left(-b^T A^{-1} b - c\right) \prod_{i=1}^{L} \underbrace{\int d^4 l_i \, \exp\left(\sum_{i=1}^{L} \tilde{l}_i^2\right)}_{=i\pi^2} . \end{aligned} \tag{B.13}$$

We have chosen Schwinger parameters because this allows for factors in the numerator to be taken into account in a convenient way, which will be explained in the next subsection. For further analyses, however, Feynman parameters turn out to be more useful. The integral (B.13) can be transformed to Feynman parameters[4] by inserting

$$1 = \int_0^\infty dr \, \delta\left(r - \sum_{i=1}^{N_x} x_i - \sum_{j=1}^{N_y} y_j\right) \tag{B.14}$$

and substituting

$$x_i \to r x_i, \tag{B.15a}$$

$$y_i \to r y_i \tag{B.15b}$$

[4] cf. Section 3.4 of Ref. [108]

so that

$$b \to rb, \tag{B.16a}$$
$$A \to rA, \tag{B.16b}$$
$$\det A \to r^L \det A, \tag{B.16c}$$
$$c \to rc, \tag{B.16d}$$

and thus

$$\begin{aligned}\mathcal{I} = (-1)^N (i\pi^2)^L \prod_{j=1}^{N_x} \int_0^\infty dx_j \, \frac{x_j^{\alpha_j - 1}}{\Gamma(\alpha_j)} \prod_{k=1}^{N_y} \int_0^\infty dy_k \, \frac{y_k^{\beta_k - 1}}{\Gamma(\beta_k)} \\ \cdot \delta \left(1 - \sum_{i=1}^{N_x} x_i - \sum_{j=1}^{N_y} y_j \right) \\ \cdot \frac{1}{\det(A)^2} \int_0^\infty dr \, \exp\left(-r(b^T A^{-1} b + c)\right) \cdot r^{N-2L-1}.\end{aligned} \tag{B.17}$$

Integrating out r using the relation

$$\int_0^\infty dr \, \exp(-rc) r^{n-1} = \frac{\Gamma[n]}{c^n}, \tag{B.18}$$

we arrive at the Feynman parameter integral:

$$\begin{aligned}\mathcal{I} = (-1)^N (i\pi^2)^L \Gamma(N - 2L) \prod_{i=1}^{N_x} \int_0^1 dx_i \, \frac{x_i^{\alpha_i - 1}}{\Gamma(\alpha_i)} \prod_{j=1}^{N_y} \int_0^1 dy_j \, \frac{y_j^{\beta_j - 1}}{\Gamma(\beta_j)} \\ \cdot \delta \left(1 - \sum_{k=1}^{N_x} x_k - \sum_{l=1}^{N_y} y_l \right) \frac{\det(A)^{N-2L-2}}{\left(b^T \operatorname{adj}(A) b + \det(A) c\right)^{N-2L}},\end{aligned} \tag{B.19}$$

where we have written $\det(A) A^{-1} = \operatorname{adj} A$ for the adjugate of the matrix A, whose elements are polynomials in x and y. The expression for c can now be simplified using the delta function:

$$c = \sum_{j=1}^{N_x} x_j (m_j^2 - q_j^2) + \mu^2. \tag{B.20}$$

Note that the delta function also allows to restrict the upper integration limit to one.

B.1.2 *Tensor Integrals*

If we allow for non-trivial numerators, we assume they have the form of an inverse, massless propagator and include them in the argument of the exponential,[5] making use of

$$A^\alpha = \frac{\partial^\alpha}{\partial x^\alpha} e^{xA} \Big|_{x=0}. \tag{B.21}$$

[5] cf. Section 2.3 of Ref. [108]

Thus the inverse propagators are taken into account when completing the square, and the transformations of the loop momenta (B.10) never have to be performed explicitly. The coefficients a_{ij} and b_i then involve additional summands with parameters with respect to which a derivative has to be performed instead of an integral. To distinguish them from the regular x_i or y_i, we label them z_i.

Assuming N_z inverse propagators with powers γ_i, we obtain instead of (B.13) the more general form

$$\begin{aligned}\mathcal{I} = (-1)^N (i\pi^2)^L \prod_{i=1}^{N_x} \int_0^\infty dx_i \, \frac{x_i^{\alpha_i - 1}}{\Gamma(\alpha_j)} \prod_{j=1}^{N_y} \int_0^\infty dy_j \, \frac{y_j^{\beta_j - 1}}{\Gamma(\beta_k)} \\ \cdot \prod_{k=1}^{N_z} \frac{\partial^{\gamma_k}}{\partial z_k^{\gamma_k}} \frac{1}{\det(A)^2} \exp\left(-b^T A^{-1} b - c\right) \Big|_{z_1 = \cdots z_{N_z} = 0} . \end{aligned} \tag{B.22}$$

So we have to evaluate

$$\begin{aligned}&\prod_{k=1}^{N_z} \frac{\partial^{\gamma_k}}{\partial z_k^{\gamma_k}} \frac{1}{\det(A)^2} \exp\left(-b^T A^{-1} b - c\right) \Big|_{z_k = 0} \\ &= \exp(-c) \prod_{k=1}^{N_z} \frac{\partial^{\gamma_k}}{\partial z_k^{\gamma_k}} \frac{1}{\det(A)^2} \exp\left(-\frac{b^T \operatorname{adj}(A) b}{\det(A)}\right) \Big|_{z_1 = \cdots z_{N_z} = 0} \end{aligned} \tag{B.23}$$

before we can introduce Feynman parameters analogously to the scalar case in the previous section. Structurally, the result will be similar to (B.19), but with additional powers of $\det(A)$ in the denominator and additional factors involving x_i and y_i in the numerator.

B.2 TWO-LOOP COUNTERTERMS: THE SPECIAL CASES

The transformation (7.43) is only valid if $N_1 \geqslant 1$, $N_x - N_1 \geqslant 1$, and $N_y \geqslant 2$. The idea how to proceed otherwise is apparent tough. Since Eq. (7.43) has been motivated by applying the scaling relation (7.12) repeatedly to different subsets of parameters, the scaling is simply not done if it were to be applied to an empty set. In general, this leads to simpler integrals but quite a few cases that have to be distinguished. In the following, the cases where either t or s or both are absent are discussed. By construction, r is always present except for trivial cases. If an integral can be written as the product of two one-loop integrals, they can be treated separately with one one-loop transformation each.

B.2.1 *The Case* $N_1 = 0$

If $N_1 = 0$, all the x_i are scaled by rs and the variable t need not be introduced. The transformation then reduces to

$$x_i \to rsx_i \qquad i \in \{1, \cdots, N_x\}, \tag{B.24a}$$
$$y_1 \to 1 - r, \tag{B.24b}$$
$$y_i \to r(1-s)y_i \qquad i \in \{2, \cdots, N_y\}, \tag{B.24c}$$

which yields

$$\begin{aligned}
&\frac{\mathcal{J}^{(2l)}}{(i\pi^2)^2} \\
&= \frac{(-1)^N \Gamma(N-4)}{\Gamma(\beta_1)} \left(\prod_{i=1}^{N_x} \int_0^1 dx_i \, \frac{x_i^{\alpha_i - 1}}{\Gamma(\alpha_i)} \right) \left(\prod_{j=2}^{N_y} \int_0^1 dy_j \, \frac{y_j^{\beta_j - 1}}{\Gamma(\beta_j)} \right) \\
&\quad \cdot \delta \left(1 - \sum_{l=1}^{N_x} x_l \right) \delta \left(1 - \sum_{n=2}^{N_y} y_n \right) \\
&\quad \cdot \int_0^1 dr \int_0^1 ds \, I^{(2l)}_{N_1=0}(r,s),
\end{aligned} \tag{B.25}$$

where

$$\begin{aligned}
&I^{(2l)}_{N_1=0}(r,s) \\
&= r^{-2+\sum_{j=2}^{N_y} \beta_j} (rs)^{-1+\sum_{i=N_1+1}^{N_x} \alpha_i} \\
&\quad \cdot \frac{(1 - r + r\,d(s))^{N-6} (1-r)^{\beta_1} (1-s)^{-1+\sum_{j=2}^{N_y} \beta_j}}{\left[(1 - r + r\,d(s)) (\mu^2 + c_1 rs) + e(r,s,0) \right]^{N-4}}.
\end{aligned} \tag{B.26}$$

Since t did not enter $d(s)$ anyway, nothing has changed in the first factor of the denominator. From the second factor we conclude that the region where the logarithmic dependence on μ^2 originates from is determined only by rs being small.

B.2.2 *The Cases* $N_y < 2$

The case $N_y = 0$ is trivial. Since each propagator is massive or has a non-zero momentum squared, the integral must be finite for $\mu^2 = 0$ and can be evaluated as is. If $N_y = 1$, the only y parameter disappears after using the overall delta function. Thus there cannot be overlapping divergencies leading to a $\ln(\mu^2)$ behavior. In principle they could be treated like one-loop integrals. Nevertheless it might be advantageous to cancel a factor of r from the $\det(A)$ factors. To do

so, one can use the two-loop transformation without introducing the parameter s:

$$x_i \to (1-r)t x_i \qquad i \in \{1, \cdots, N_1\}, \tag{B.27a}$$

$$x_i \to r x_i \qquad i \in \{N_1+1, \cdots, N_x\}, \tag{B.27b}$$

$$y_1 \to (1-r)(1-t). \tag{B.27c}$$

Then one obtains

$$\frac{\mathcal{J}^{(2l)}}{(i\pi^2)^2} = \frac{(-1)^N \Gamma(N-4)}{\Gamma(\beta_1)} \left(\prod_{i=1}^{N_x} \int_0^1 dx_i \, \frac{x_i^{\alpha_i - 1}}{\Gamma(\alpha_i)} \right) \delta \left(1 - \sum_{l=N_1+1}^{N_x} x_l \right) \cdot \delta \left(1 - \sum_{m=1}^{N_1} x_m \right) \int_0^1 dr \int_0^1 dt \, I^{(2l)}_{N_y=1}(r,t), \tag{B.28}$$

where

$$I^{(2l)}_{N_y=1}(r,t) = r^{-3+\sum_{i=N_1+1}^{N_x} \alpha_i} [(1-r)t]^{-1+\sum_{i=1}^{N_1} \alpha_i} \cdot \frac{(1-r+r\,d(1))^{N-6} (1-r)^{\beta_1} (1-t)^{\beta_1 - 1}}{[(1-r+r\,d(1))(\mu^2 + c_1 r + c_2(1-r)t) + e(r,1,t)]^{N-4}}. \tag{B.29}$$

The appearance of a logarithmic dependence on μ^2 is then associated with the vanishing of r and t only.

B.2.3 *The Case* $N_1 = 0$ *and* $N_y = 1$

A combination of the cases discussed above is possible as well. The transformation is even simpler then and identical to the one-loop case:

$$x_i \to r x_i \qquad i \in \{1, \cdots, N_x\}, \tag{B.30a}$$

$$y_1 \to 1 - r. \tag{B.30b}$$

This yields

$$\frac{\mathcal{J}^{(2l)}}{(i\pi^2)^2} = \frac{(-1)^N \Gamma(N-4)}{\Gamma(\beta_1)} \left(\prod_{i=1}^{N_x} \int_0^1 dx_i \, \frac{x_i^{\alpha_i - 1}}{\Gamma(\alpha_i)} \right) \delta \left(1 - \sum_{l=0+1}^{N_x} x_l \right) \cdot \int_0^1 dr \, I^{(2l)}_{N_y=1;\, N_1=0}(r), \tag{B.31}$$

where

$$I^{(2l)}_{N_y=1;\, N_1=0}(r) = r^{-3+\sum_{i=N_1+1}^{N_x} \alpha_i} [(1-r)t]^{-1+\sum_{i=1}^{N_1} \alpha_i} \cdot \frac{(1-r+r\,d(1))^{N-6} (1-r)^{\beta_1}}{[(1-r+r\,d(1))(\mu^2 + c_1 r) + e(r,1,0)]^{N-4}}. \tag{B.32}$$

The most important structural difference to the one-loop case is the factor of $1-r+rd(1)$, which can be neglected in the auxiliary integral, though. However, $e(r,1,0)$ still might have to be taken into account.

B.3 STANDARD INTEGRALS

In this section we define generic integrands I to which the actually occurring integrands are matched and discuss the corresponding auxiliary integrand A as well.

B.3.1 *One Loop*

All IR-finite integrands can be matched to

$$I^{(1l)}_{N_1,n_1,n_2}(r) = \frac{r^{N_1-1+n_1}(1-r)^{n_2}(f_0+f_1(r)r)}{(a+c_1r+c_2r^2)^{N_1}}. \tag{B.33}$$

The correct asymptotic behavior for small a is reproduced by

$$A^{(1l)}_{N_1,n_1}(r) = \frac{r^{N_1-1+n_1}f_0}{(a+c_1r)^{N_1}}, \tag{B.34}$$

which is needed if $n_1 \leqslant 0$.

B.3.2 *Two Loop*

In this subsection all the generic integrands needed in the context of the applications presented in Chapter 8 are listed, including their approximations to obtain the expansion for small a.

B.3.2.1 *One-Parameter Integrals*

Whereas the two-loop version of the r integral,

$$\begin{aligned} &I_{N_1,N_2,n_1,n_3,n_6}(r) \\ &= \frac{r^{n_1+N_1-1}(1-r)^{n_3}(f_0+\sum_{n=1}^{N_{pow}} f_n r^n)a^{n_6}}{(a+c_1r+c_2r^2)^{N_1}(1-r+r(d_0+d_1s+d_2s^2))^{N_2}}, \end{aligned} \tag{B.35}$$

has a richer structure than the one-loop integral, the approximative integral is basically the same:

$$A_{N_1,n_1,n_6}(r) = \frac{r^{n_1+N_1-1}f_0a^{n_6}}{(a+c_1r)^{N_1}}. \tag{B.36}$$

The only difference is that we allow for additional powers of a in the numerator. In case $n_1 = n_6 = 0$ there will be a $\ln(a)$ dependence. If $n_1 < 0$ (and $N_1 > 1-n_1$), the integral behaves like powers of $\frac{1}{a}$,

which can be compensated by large enough n_6 to produce a finite result.[6]

B.3.2.2 *Two-Parameter Integrals*

The rs integral,

$$\begin{aligned}
&I_{N_1,N_2,n_1,n_2,n_3,n_4,n_6}(r,s) \\
&= \frac{r^{n_1+N_1-1}s^{n_2+N_1-1}(1-r)^{n_3}(1-s)^{n_4}a^{n_6}}{(a+c_1rs)^{N_1}} \\
&\quad \cdot \frac{(f_0+\sum_{n=1}^{N_{pow}} f_{r,n}r^n+\sum_{n=1}^{N_{pow}} f_{s,n}s^n+f_{rs}(r,s)rs)}{(1-r+r(d_0+d_1s+d_2s^2))^{N_2}},
\end{aligned} \tag{B.37}$$

is the simplest one that can have a $\ln^2(a)$ dependence. This occurs if $n_1 = n_2 = n_6 = 0$ (and $f_0 \neq 0$). To reproduce this dependence correctly, only terms suppressed by rs may be neglected in the auxiliary integral:

$$\begin{aligned}
&A^{(1)}_{N_1,N_2,n_1,n_2,n_3,n_4,n_6}(r,s) \\
&= \frac{r^{n_1+N_1-1}s^{n_2+N_1-1}(1-r)^{n_3}(1-s)^{n_4}a^{n_6}}{(a+c_1rs)^{N_1}} \\
&\quad \cdot \frac{\left(f_0+\sum_{n=1}^{N_{pow}} f_{r,n}r^n+(1-r)^{\max(N_2-n_3,0)}\sum_{n=1}^{N_{pow}} f_{s,n}s^n\right)}{(1-r+d_0r)^{N_2}}.
\end{aligned} \tag{B.38}$$

A problem may arise if $N_2 > n_3$. Then the denominator will be proportional to d_0 in the limit $r \to 1$, and d_0 might have a zero. At $(r,s) = (1,0)$, the auxiliary integral behaves exactly like the original one, which must be integrable. Thus this point should not cause any problems. The point $(r,s) = (1,1)$ is more dangerous, however. There, the numerator of the original integrand tends towards $f_0 + \sum_{n=1}^{N_{pow}} f_{r,n} + \sum_{n=1}^{N_{pow}} f_{s,n} + f_{rs}(1,1)$. In case there are delicate cancellations to balance the vanishing of $d(1)$, this is disturbed by neglecting the $f_{rs}(r,s)$ term in the auxiliary integral. To compensate for that, we introduce the additional factor $(1-r)^{\max(N_2-n_3,0)}$ in front of the s dependent terms in the enumerator, which is allowed because it only alters terms of order rs. As a consequence, the auxiliary integral now tends to $f_0 + \sum_{n=1}^{N_{pow}} f_{r,n}$ in the numerator and to d_0 in the denominator both at $(r,s) = (1,0)$ and $(r,s) = (1,1)$ even if $N_2 > n_3$, and thus be integrable at both points.

Sometimes the powers of r and s that can be factorized in the enumerator are not the same. Suppose for example that $n_1 = n_6 = 0$ and

[6] Of course, one could allow this in the one-loop case as well. As explained in Section 8.2, these integrals appear from canceling scalar products of loop momenta against propagators to obtain better behaved integrals, which is only required for two-loop integrals.

$n_2 > 0$. Then an extra factor of r would make the integral convergent and one should choose a simplified auxiliary integral, where all terms suppressed by a factor of r are dropped as well:

$$\begin{aligned} &A^{(2)}_{N_1,n_1,n_2,n_4,n_6}(r,s) \\ &= \frac{r^{n_1+N_1-1} s^{n_2+N_1-1} (1-s)^{n_4} a^{n_6} \left(f_0 + \sum_{n=1}^{N_{pow}} f_{s,n} s^n\right)}{(a + c_1 rs)^{N_1}} \end{aligned} \tag{B.39}$$

This choice is also suited for the case $n_1 < 0$, $n_2 \geqslant 0$, and $n_6 > 0$. Under analogous conditions with $n_1 \leftrightarrow n_2$, we define

$$\begin{aligned} &A^{(3)}_{N_1,N_2,n_1,n_2,n_3,n_6}(r,s) \\ &= \frac{r^{n_1+N_1-1} s^{n_2+N_1-1} (1-r)^{n_3} a^{n_6} \left(f_0 + \sum_{n=1}^{N_{pow}} f_{r,n} r^n\right)}{(a + c_1 rs)^{N_1} (1 - r + d_0 r))^{N_2}}. \end{aligned} \tag{B.40}$$

B.3.2.3 *Three-Parameter Integrals*

The most complicated integrand is the one dependent on r, s, and t:

$$\begin{aligned} &I_{N_1,N_2,n_1,n_2,n_3,n_4,n_5,n_6}(r,s,t) \\ &= \frac{r^{n_1+N_1-2+n_5} s^{n_2+N_1-2+n_5} (1-r)^{n_3} (1-s)^{n_4} t^{n_5} a^{n_6}}{(a + c_1 rs + c_2(1-r)t)^{N_1}} \\ &\cdot \frac{f_0 + \sum_{n=1}^{N_{pow}} f_{r,n} r^n + \sum_{n=1}^{N_{pow}} f_{s,n} s^n + f_{rs}(r,s,t) rs + f_t(r,s,t) t}{(1 - r + r(d_0 + d_1 s + d_2 s^2))^{N_2}}. \end{aligned} \tag{B.41}$$

The parameters n_1 and n_2 are defined so that there is a $\ln^2(a)$ behavior if $n_1 = n_2 = n_6 = 0$. The corresponding auxiliary integral reads:

$$\begin{aligned} &A^{(1)}_{N_1,N_2,n_1,n_2,n_3,n_4,n_5,n_6}(r,s,t) \\ &= \frac{r^{n_1+N_1-2+n_5} s^{n_2+N_1-2+n_5} (1-r)^{n_3} (1-s)^{n_4} t^{n_5} a^{n_6}}{(a + c_1 rs + c_2(1-r)t)^{N_1}} \\ &\quad \cdot \frac{f_0 + \sum_{n=1}^{N_{pow}} f_{r,n} r^n + (1-r)^{\max(N_2-n_3,0)} \sum_{n=1}^{N_{pow}} f_{s,n} s^n}{(1 - r + d_0 r))^{N_2}}, \end{aligned} \tag{B.42}$$

where we have neglected all terms of order rs and t and introduced a factor of $(1-r)^{\max(N_2-n_3,0)}$ to stabilize the integrand in the region where $(r,s) = (1,1)$. The conditions when to use a simplified auxiliary

integral discussed in the previous paragraph apply as well. For the sake of completeness we print these as well:

$$\begin{aligned} &A^{(2)}_{N_1,n_1,n_2,n_4,n_5,n_6}(r,s,t) \\ &= \frac{r^{n_1+N_1-2+n_5} s^{n_2+N_1-2+n_5} (1-s)^{n_4} t^{n_5} a^{n_6}}{(a+c_1 rs+c_2(1-r)t)^{N_1}} \\ &\quad \cdot \left(f_0 + \sum_{n=1}^{N_{pow}} f_{s,n} s^n \right), \end{aligned} \tag{B.43a}$$

$$\begin{aligned} &A^{(3)}_{N_1,N_2,n_1,n_2,n_3,n_5,n_6}(r,s,t) \\ &= \frac{r^{n_1+N_1-2+n_5} s^{n_2+N_1-2+n_5} (1-r)^{n_3} t^{n_5} a^{n_6}}{(a+c_1 rs+c_2(1-r)t)^{N_1}} \\ &\quad \cdot \frac{f_0 + \sum_{n=1}^{N_{pow}} f_{r,n} r^n}{(1-r+d_0 r)^{N_2}}. \end{aligned} \tag{B.43b}$$

There is one particularity in the analytical integration compared to the cases where t is absent. The integration over t is performed first. The denominator of the primitive contains a factor of

$$(1-r)(a+c_1 rs+c_2(1-r)t)^{N_1-1-n_5}.$$

As we assume again that the integral is integrable at $r=1$, the factor of $(1-r)$ must cancel. The two terms that arise from inserting the integration boundaries 0 and 1 are handled separately. Whereas the former has just the form of Eq. (B.38), the integral over r and s of the latter must be finite and will be evaluated numerically later.

B.4 MISCELLANEOUS

Here we present a proof of the "scaling relation", which helps to analyze the limit where a set of parameters vanishes simultaneously.[7] The following lines should be self-explanatory:

$$\begin{aligned}
&\prod_{i=1}^{n}\int_0^1 dx_i\, f(x_1,\cdots,x_n)\,\theta\left(1-\sum_{k=1}^{n}x_k\right)\\
&=\prod_{i=1}^{n}\int_0^\infty dx_i\, f(x_1,\cdots,x_n)\,\theta\left(1-\sum_{k=1}^{n}x_k\right)\\
&=\int_0^\infty dr\prod_{i=1}^{n}\int_0^\infty dx_i\, f(x_1,\cdots,x_n)\,\theta(1-r)\;\delta\left(r-\sum_{k=1}^{n}x_k\right)\\
&=\int_0^\infty dr\prod_{i=1}^{n}\int_0^\infty d(rx_i)\, f(rx_1,\cdots,rx_n)\,\theta(1-r)\;\delta\left(r-r\sum_{k=1}^{n}x_k\right)\\
&=\int_0^\infty dr\prod_{i=1}^{n}\int_0^\infty dx_i\;\; r^{n-1} f(rx_1,\cdots,rx_n)\,\theta(1-r)\;\delta\left(1-\sum_{k=1}^{n}x_k\right)\\
&=\prod_{i=1}^{n}\int_0^1 dx_i\;\delta\left(1-\sum_{k=1}^{n}x_k\right)\int_0^1 dr\;\; r^{n-1} f(rx_1,\cdots,rx_n). \qquad \text{(B.44)}
\end{aligned}$$

[7] A similar relation is used to transform from Schwinger to Feynman parameters, see Eqs. (B.14) and (B.15).

BIBLIOGRAPHY

[1] F. Halzen and A. D. Martin. *Quarks and Leptons: An Introductory Course in Modern Particle Physics*. Wiley, 1984.

[2] M. E. Peskin and D. V. Schroeder. *An Introduction to Quantum Field Theory*. Westview, 1995.

[3] S. Weinberg. A Model of Leptons. *Phys. Rev. Lett.*, 19:1264–1266, 1967.

[4] R. K. Ellis, W. J. Stirling, and B. R. Webber. QCD and Collider Physics. *Camb. Monogr. Part. Phys. Nucl. Phys. Cosmol.*, 8:1–435, 1996.

[5] T. Sjöstrand. Monte Carlo Generators. 2006, hep-ph/0611247.

[6] LHC Higgs Cross Section Working Group, S. Heinemeyer et al. Handbook of LHC Higgs Cross Sections: 3. Higgs Properties. 2013, 1307.1347.

[7] LHC Higgs Cross Section Working Group. `https://twiki.cern.ch/twiki/bin/view/LHCPhysics/CrossSections`, 2014. [Online; accessed 08-April-2014].

[8] F. Englert and R. Brout. Broken Symmetry and the Mass of Gauge Vector Mesons. *Phys. Rev. Lett.*, 13:321–323, 1964.

[9] P. W. Higgs. Broken Symmetries, Massless Particles and Gauge Fields. *Phys. Lett.*, 12:132–133, 1964.

[10] P. W. Higgs. Broken Symmetries and the Masses of Gauge Bosons. *Phys. Rev. Lett.*, 13:508–509, 1964.

[11] G. S. Guralnik, C. R. Hagen, and T. W. B. Kibble. Global Conservation Laws and Massless Particles. *Phys. Rev. Lett.*, 13:585–587, 1964.

[12] LEP Working Group for Higgs Boson Searches, ALEPH Collaboration, DELPHI Collaboration, L3 Collaboration, OPAL Collaboration, G. Abbiendi et al. Search for the Standard Model Higgs Boson at LEP. *Phys. Lett.*, B565:61–75, 2003, hep-ex/0306033.

[13] ATLAS Collaboration, G. Aad et al. Observation of a New Particle in the Search for the Standard Model Higgs Boson with the ATLAS Detector at the LHC. *Phys. Lett.*, B716:1–29, 2012, 1207.7214.

[14] CMS Collaboration, S. Chatrchyan et al. Observation of a New Boson at a Mass of 125 GeV with the CMS Experiment at the LHC. *Phys. Lett.*, B716:30–61, 2012, 1207.7235.

[15] CMS Collaboration, S. Chatrchyan et al. Study of the Mass and Spin-Parity of the Higgs Boson Candidate via its Decays to Z Boson Pairs. *Phys. Rev. Lett.*, 110:081803, 2013, 1212.6639.

[16] ATLAS Collaboration. Study of the Spin of the New Boson with up to 25 fb^{-1} of ATLAS Data. ATLAS-CONF-2013-040, ATLAS-COM-CONF-2013-048, 2013.

[17] ATLAS Collaboration, G. Aad et al. Measurement of the Higgs Boson Mass from the $H \to \gamma\gamma$ and $H \to ZZ^* \to 4\ell$ Channels with the ATLAS Detector using 25 fb^{-1} of pp Collision Data. 2014, 1406.3827.

[18] CMS Collaboration. Precise Determination of the Mass of the Higgs Boson and Studies of the Compatibility of its Couplings with the Standard Model. CMS-PAS-HIG-14-009, 2014.

[19] LEP Collaboration, ALEPH Collaboration, DELPHI Collaboration, L3 Collaboration, OPAL Collaboration, LEP Electroweak Working Group, SLD Electroweak Group, SLD Heavy Flavor Group. A Combination of Preliminary Electroweak Measurements and Constraints on the Standard Model. 2003, hep-ex/0312023.

[20] ATLAS Collaboration. Updated Coupling Measurements of the Higgs Boson with the ATLAS Detector Using up to 25 fb^{-1} of Proton-Proton Collision Data. ATLAS-CONF-2014-009, ATLAS-COM-CONF-2014-013, 2014.

[21] CMS Collaboration. Combination of Standard Model Higgs Boson Searches and Measurements of the Properties of the New Boson with a Mass near 125 GeV. CMS-PAS-HIG-13-005, 2013.

[22] S. P. Martin. A Supersymmetry Primer. *Adv. Ser. Direct. High Energy Phys.*, 21:1–153, 2010, hep-ph/9709356.

[23] H. Baer and X. Tata. *Weak Scale Supersymmetry: From Superfields to Scattering Events*. Cambridge, 2006.

[24] G. Degrassi, S. Di Vita, J. Elias-Miró, J. R. Espinosa, G. F. Giudice, et al. Higgs Mass and Vacuum Stability in the Standard Model at NNLO. *JHEP*, 1208:098, 2012, 1205.6497.

[25] D. A. Ross and M. J. G. Veltman. Neutral Currents in Neutrino Experiments. *Nucl. Phys.*, B95:135, 1975.

[26] G. 't Hooft and M. J. G. Veltman. Regularization and Renormalization of Gauge Fields. *Nucl. Phys.*, B44:189–213, 1972.

[27] S. L. Adler. Axial Vector Vertex in Spinor Electrodynamics. *Phys. Rev.*, 177:2426–2438, 1969.

[28] S. A. Larin. The Renormalization of the Axial Anomaly in Dimensional Regularization. *Phys. Lett.*, B303:113–118, 1993, hep-ph/9302240.

[29] J. C. Collins, D. E. Soper, and G. F. Sterman. Factorization of Hard Processes in QCD. *Adv. Ser. Direct. High Energy Phys.*, 5:1–91, 1988, hep-ph/0409313.

[30] G. Altarelli and G. Parisi. Asymptotic Freedom in Parton Language. *Nucl. Phys.*, B126:298, 1977.

[31] S. Catani and M. H. Seymour. A General Algorithm for Calculating Jet Cross Sections in NLO QCD. *Nucl. Phys.*, B485:291–419, 1997, hep-ph/9605323. Erratum: ibid., B510:504, 1998.

[32] V. A. Smirnov. Applied Asymptotic Expansions in Momenta and Masses. *Springer Tracts Mod. Phys.*, 177:1–262, 2002.

[33] V. A. Smirnov. Asymptotic Expansions in Momenta and Masses and Calculation of Feynman Diagrams. *Mod. Phys. Lett.*, A10:1485–1500, 1995, hep-th/9412063.

[34] R. Harlander. Asymptotic Expansions: Methods and Applications. *Acta Phys. Polon.*, B30:3443–3462, 1999, hep-ph/9910496.

[35] P. Nogueira. Automatic Feynman Graph Generation. *J. Comput. Phys.*, 105:279–289, 1993.

[36] R. Harlander, T. Seidensticker, and M. Steinhauser. Complete Corrections of $\mathcal{O}(\alpha\alpha_s)$ to the Decay of the Z Boson into Bottom Quarks. *Phys. Lett.*, B426:125–132, 1998, hep-ph/9712228.

[37] T. Seidensticker. Automatic Application of Successive Asymptotic Expansions of Feynman Diagrams. 1999, hep-ph/9905298.

[38] J. Vermaseren. New Features of FORM. 2000, math-ph/0010025.

[39] M. Steinhauser. `MATAD`: A Program Package for the Computation of Massive Tadpoles. *Comput. Phys. Commun.*, 134:335–364, 2001, hep-ph/0009029.

[40] R. V. Harlander. Virtual Corrections to $gg \to H$ to Two Loops in the Heavy Top Limit. *Phys. Lett.*, B492:74–80, 2000, hep-ph/0007289.

[41] CDF Collaboration, Do Collaboration, T. Aaltonen et al. Evidence for a Particle Produced in Association with Weak Bosons

and Decaying to a Bottom-Antibottom Quark Pair in Higgs Boson Searches at the Tevatron. *Phys. Rev. Lett.*, 109:071804, 2012, 1207.6436.

[42] CDF Collaboration, Do Collaboration, T. Aaltonen et al. Higgs Boson Studies at the Tevatron. *Phys. Rev.*, D88(5):052014, 2013, 1303.6346.

[43] J. M. Butterworth, A. R. Davison, M. Rubin, and G. P. Salam. Jet Substructure as a New Higgs Search Channel at the LHC. *Phys. Rev. Lett.*, 100:242001, 2008, 0802.2470.

[44] ATLAS Collaboration. Search for Invisible Decays of a Higgs Boson Produced in Association with a Z Boson in ATLAS. ATLAS-CONF-2013-011, ATLAS-COM-CONF-2013-013, 2013.

[45] CMS Collaboration. Search for the Higgs boson Decaying to Invisible Particles Produced in Association with Z bosons Decaying to Bottom Quarks. CMS-PAS-HIG-13-028, 2013.

[46] CMS Collaboration, S. Chatrchyan et al. Search for the Standard Model Higgs Boson Produced in Association with a W or a Z Boson and Decaying to Bottom Quarks. *Phys. Rev.*, D89:012003, 2014, 1310.3687.

[47] The ATLAS Collaboration. Search for the $b\bar{b}$ Decay of the Standard Model Higgs Boson in Associated $(W/Z)H$ Production with the ATLAS Detector. ATLAS-CONF-2013-079, ATLAS-COM-CONF-2013-080, 2013.

[48] T. Han and S. Willenbrock. QCD Correction to the $pp \to WH$ and ZH Total Cross Sections. *Phys. Lett.*, B273:167–172, 1991.

[49] O. Brein, A. Djouadi, and R. Harlander. NNLO QCD Corrections to the Higgs-Strahlung Processes at Hadron Colliders. *Phys. Lett.*, B579:149–156, 2004, hep-ph/0307206.

[50] R. Hamberg, W. L. van Neerven, and T. Matsuura. A Complete Calculation of the Order α_s^2 Correction to the Drell-Yan K-Factor. *Nucl. Phys.*, B359:343–405, 1991. Erratum: ibid., B644:403-404, 1991.

[51] R. V. Harlander and W. B. Kilgore. Next-to-Next-to-Leading Order Higgs Production at Hadron Colliders. *Phys. Rev. Lett.*, 88:201801, 2002, hep-ph/0201206.

[52] B. A. Kniehl. Associated Production of Higgs and Z Bosons from Gluon Fusion in Hadron Collisions. *Phys. Rev.*, D42:2253–2258, 1990.

[53] LHC Higgs Cross Section Working Group, S. Dittmaier et al. Handbook of LHC Higgs Cross Sections: 1. Inclusive Observables. 2011, 1101.0593.

[54] L. Altenkamp, S. Dittmaier, R. V. Harlander, H. Rzehak, and T. J. E. Zirke. Gluon-Induced Higgs-Strahlung at Next-to-Leading Order QCD. *JHEP*, 1302:078, 2013, 1211.5015.

[55] O. Brein, R. Harlander, M. Wiesemann, and T. Zirke. Top-Quark Mediated Effects in Hadronic Higgs-Strahlung. *Eur. Phys. J.*, C72:1868, 2012, 1111.0761.

[56] M. L. Ciccolini, S. Dittmaier, and M. Krämer. Electroweak Radiative Corrections to Associated WH and ZH Production at Hadron Colliders. *Phys. Rev.*, D68:073003, 2003, hep-ph/0306234.

[57] O. Brein, M. Ciccolini, S. Dittmaier, A. Djouadi, R. Harlander, and M. Krämer. Precision Calculations for Associated WH and ZH Production at Hadron Colliders. 2004, hep-ph/0402003.

[58] O. Brein, R. V. Harlander, and T. J. E. Zirke. `vh@nnlo` – Higgs Strahlung at Hadron Colliders. *Comput. Phys. Commun.*, 184:998–1003, 2013, 1210.5347.

[59] S. Dawson, T. Han, W. K. Lai, A. K. Leibovich, and I. Lewis. Resummation Effects in Vector-Boson and Higgs Associated Production. *Phys. Rev.*, D86:074007, 2012, 1207.4207.

[60] G. Ferrera, M. Grazzini, and F. Tramontano. Associated WH Production at Hadron Colliders: A Fully Exclusive QCD Calculation at NNLO. *Phys. Rev. Lett.*, 107:152003, 2011, 1107.1164.

[61] G. Ferrera, M. Grazzini, and F. Tramontano. Associated ZH Production at Hadron Colliders: The Fully Differential NNLO QCD Calculation. 2014, 1407.4747.

[62] A. Denner, S. Dittmaier, S. Kallweit, and A. Mück. Electroweak Corrections to Higgs-Strahlung off W/Z Bosons at the Tevatron and the LHC with `HAWK`. *JHEP*, 1203:075, 2012, 1112.5142.

[63] R. V. Harlander, S. Liebler, and T. Zirke. Higgs Strahlung at the Large Hadron Collider in the 2-Higgs-Doublet Model. *JHEP*, 1402:023, 2014, 1307.8122.

[64] M. Spira, A. Djouadi, D. Graudenz, and P. M. Zerwas. Higgs Boson Production at the LHC. *Nucl. Phys.*, B453:17–82, 1995, hep-ph/9504378.

[65] W. H. Furry. A Symmetry Theorem in the Positron Theory. *Phys. Rev.*, 51:125–129, 1937.

[66] L. D. Landau. The Moment of a 2-Photon System. *Dokl. Akad. Nawk.*, 60:207, 1948.

[67] C.-N. Yang. Selection Rules for the Dematerialization of a Particle into Two Photons. *Phys. Rev.*, 77:242–245, 1950.

[68] P. Baikov and K. Chetyrkin. Top Quark Mediated Higgs Boson Decay into Hadrons to Order α_s^5. *Phys. Rev. Lett.*, 97:061803, 2006, hep-ph/0604194.

[69] A. D. Martin, W. J. Stirling, R. S. Thorne, and G. Watt. Parton Distributions for the LHC. *Eur. Phys. J.*, C63:189–285, 2009, 0901.0002.

[70] R. V. Harlander, H. Mantler, S. Marzani, and K. J. Ozeren. Higgs Production in Gluon Fusion at Next-to-Next-to-Leading Order QCD for Finite Top Mass. *Eur. Phys. J.*, C66:359–372, 2010, 0912.2104.

[71] R. V. Harlander, T. Neumann, K. J. Ozeren, and M. Wiesemann. Top-Mass Effects in Differential Higgs Production through Gluon Fusion at Order α_S^4. *JHEP*, 1208:139, 2012, 1206.0157.

[72] T. Neumann and M. Wiesemann. Finite Top-Mass Effects in Gluon-Induced Higgs Production with a Jet-Veto at NNLO. 2014, 1408.6836.

[73] S. Dawson, S. Dittmaier, and M. Spira. Neutral Higgs-Boson Pair Production at Hadron Colliders: QCD Corrections. *Phys. Rev.*, D58:115012, 1998, hep-ph/9805244.

[74] G. P. Lepage. A New Algorithm for Adaptive Multidimensional Integration. *J. Comput. Phys.*, 27:192, 1978.

[75] K. G. Chetyrkin, J. H. Kühn, and M. Steinhauser. `RunDec`: A `Mathematica` Package for Running and Decoupling of the Strong Coupling and Quark Masses. *Comput. Phys. Commun.*, 133:43–65, 2000, hep-ph/0004189.

[76] J. F. Gunion, H. E. Haber, G. L. Kane, and S. Dawson. The Higgs Hunter's Guide. *Front. Phys.*, 80:1–448, 2000.

[77] G. C. Branco, P. M. Ferreira, L. Lavoura, M. N. Rebelo, M. Sher, and J. P. Silva. Theory and Phenomenology of Two-Higgs-Doublet Models. *Phys. Rept.*, 516:1–102, 2012, 1106.0034.

[78] A. Celis, V. Ilisie, and A. Pich. LHC Constraints on Two-Higgs Doublet Models. *JHEP*, 1307:053, 2013, 1302.4022.

[79] C.-Y. Chen and S. Dawson. Exploring Two Higgs Doublet Models through Higgs Production. *Phys. Rev.*, D87(5):055016, 2013, 1301.0309.

[80] O. Eberhardt, U. Nierste, and M. Wiebusch. Status of the Two-Higgs-Doublet Model of Type II. *JHEP*, 1307:118, 2013, 1305.1649.

[81] L. L. Yang, C. S. Li, J. J. Liu, and L. G. Jin. Production of Scalar Higgs Bosons Associated with Z^0 Boson at the CERN LHC in the MSSM. *J.Phys.*, G30:1821–1835, 2004, hep-ph/0312179.

[82] B. A. Kniehl and C. P. Palisoc. Associated Production of Z and Neutral Higgs Bosons at the CERN Large Hadron Collider. *Phys. Rev.*, D85:075027, 2012, 1112.1575.

[83] C. Kao. Production of a Pseudoscalar Higgs with a Z Boson from Gluon Fusion. *Phys. Rev.*, D46:4907–4913, 1992.

[84] J. Yin, W.-G. Ma, R.-Y. Zhang, and H.-S. Hou. A^0Z^0 Associated Production at the CERN Large Hadron Collider in the Minimal Supersymmetric Standard Model. *Phys. Rev.*, D66:095008, 2002.

[85] C. Kao, G. Lovelace, and L. H. Orr. Detecting a Higgs Pseudoscalar with a Z Boson at the LHC. *Phys. Lett.*, B567:259–264, 2003, hep-ph/0305028.

[86] Q. Li, C. S. Li, J. J. Liu, L. G. Jin, and C.-P. Yuan. Next-to-Leading Order QCD Predictions for A^0Z^0 Associated Production at the CERN Large Hadron Collider. *Phys. Rev.*, D72:034032, 2005, hep-ph/0501070.

[87] T. Hahn. Generating Feynman Diagrams and Amplitudes with `FeynArts` 3. *Comput. Phys. Commun.*, 140:418–431, 2001, hep-ph/0012260.

[88] T. Hahn and M. Perez-Victoria. Automatized One-Loop Calculations in Four and D Dimensions. *Comput. Phys. Commun.*, 118:153–165, 1999, hep-ph/9807565.

[89] T. Hahn. `CUBA`: A Library for Multidimensional Numerical Integration. *Comput. Phys. Commun.*, 168:78–95, 2005, hep-ph/0404043.

[90] D. Eriksson, J. Rathsman, and O. Stål. `2HDMC`: Two-Higgs-Doublet Model Calculator. *Comput. Phys. Commun.*, 181:189–205, 2010, 0902.0851.

[91] D. Eriksson, J. Rathsman, and O. Stål. `2HDMC`: Two-Higgs-Doublet Model Calculator. *Comput. Phys. Commun.*, 181:833–834, 2010.

[92] C. Englert, M. McCullough, and M. Spannowsky. Gluon-Initiated Associated Production Boosts Higgs Physics. *Phys. Rev.*, D89(1):013013, 2014, 1310.4828.

[93] R. Pittau. A Four-Dimensional Approach to Quantum Field Theories. *JHEP*, 1211:151, 2012, 1208.5457.

[94] A. M. Donati and R. Pittau. FDR, an Easier Way to NNLO Calculations: A Two-Loop Case Study. *Eur. Phys. J.*, C74:2864, 2014, 1311.3551.

[95] A. M. Donati and R. Pittau. Gauge Invariance at Work in FDR: $H \to \gamma\gamma$. *JHEP*, 1304:167, 2013, 1302.5668.

[96] R. Pittau. QCD Corrections to $H \to gg$ in FDR. *Eur. Phys. J.*, C74:2686, 2014, 1307.0705.

[97] Z. Nagy and D. E. Soper. Numerical Integration of One-Loop Feynman Diagrams for N-Photon Amplitudes. *Phys. Rev.*, D74:093006, 2006, hep-ph/0610028.

[98] S. Borowka, J. Carter, and G. Heinrich. Numerical Evaluation of Multi-Loop Integrals for Arbitrary Kinematics with `SecDec` 2.0. *Comput. Phys. Commun.*, 184:396–408, 2013, 1204.4152.

[99] A. Djouadi, M. Spira, J. J. van der Bij, and P. M. Zerwas. QCD Corrections to $\gamma\gamma$ Decays of Higgs Particles in the Intermediate Mass Range. *Phys. Lett.*, B257:187–190, 1991.

[100] S. Dawson and R. P. Kauffman. QCD corrections to $H \to \gamma\gamma$. *Phys. Rev.*, D47:1264–1267, 1993.

[101] A. Djouadi, M. Spira, and P. M. Zerwas. Two Photon Decay Widths of Higgs Particles. *Phys. Lett.*, B311:255–260, 1993, hep-ph/9305335.

[102] K. G. Chetyrkin, J. H. Kühn, and M. Steinhauser. Corrections of Order $\mathcal{O}(G_F M_t^2 \alpha_s^2)$ to the ρ Parameter. *Phys. Lett.*, B351:331–338, 1995, hep-ph/9502291.

[103] R. Pittau. Integration-by-Parts Identities in FDR. 2014, 1408.5345.

[104] R. K. Ellis and G. Zanderighi. Scalar One-Loop Integrals for QCD. *JHEP*, 0802:002, 2008, 0712.1851.

[105] G. Passarino and M. Veltman. One-Loop Corrections for e^+e^- Annihilation into $\mu^+\mu^-$ in the Weinberg Model. *Nucl. Phys.*, B160:151, 1979.

[106] T. J. E. Zirke. Higgs-Strahlung am Large Hadron Collider. Diploma thesis, University of Wuppertal, 2011. Unpublished.

[107] W. B. Kilgore. Private Notes, 2000. Unpublished.

[108] V. A. Smirnov. *Feynman Integral Calculus*. Springer, 2006.

DANKSAGUNG

Zu allererst möchte ich mich bei Prof. Dr. Robert Harlander bedanken, der mir die Promotion in seiner Gruppe an der Bergischen Universität ermöglicht hat. Seine hervorragende Betreuung und die wissenschaftliche Zusammenarbeit auf Augenhöhe haben mich stets motiviert und inspiriert.

Prof. Dr. Stefan Dittmaier danke ich sehr für die Übernahme des Zweitgutachtens und auch noch einmal ausdrücklich für sein Empfehlungsschreiben zur Unterstützung meiner Postdoc-Bewerbung.

Des Weiteren danke ich den gegenwärtigen und den schon weitergezogenen Mitgliedern der Arbeitsgruppe für die gute Atmosphäre, viele Diskussionen und gute Zusammenarbeit, insbesondere meinen beiden langjährigen Büronachbarn Dr. Marius Wiesemann und Dipl.-Phys. Tobias Neumann sowie Dr. Stefan Liebler. Tobias und Dipl.-Phys. Mario Prausa bin ich außerdem zu großem Dank für das Korrekturlesen dieser Arbeit verpflichtet.

Zu guter Letzt bedanke ich mich bei meinen Verwandten und Freunden für die moralische Unterstützung.